Available online at www.sciencedirect.com
SCIENCE DIRECT®
International Journal of Mass Spectrometry 240 (2005) 37–99
International Journal of Mass Spectrometry
www.elsevier.com/locate/ijms

Review

Theoretical methods that help understanding the structure and reactivity of gas phase ions

J.M. Mercero[a], J.M. Matxain[a], X. Lopez[a], D.M. York[b], A. Largo[c], L.A. Eriksson[d,e], J.M. Ugalde[a,*]

[a] *Kimika Fakultatea, Euskal Herriko Unibertsitatea, P.K. 1072, 20080 Donostia, Euskadi, Spain*
[b] *Department of Chemistry, University of Minnesota, 207 Pleasant St. SE, Minneapolis, MN 55455-0431, USA*
[c] *Departamento de Química-Física, Universidad de Valladolid, Prado de la Magdalena, 47005 Valladolid, Spain*
[d] *Department of Cell and Molecular Biology, Box 596, Uppsala University, 751 24 Uppsala, Sweden*
[e] *Department of Natural Sciences, Örebro University, 701 82 Örebro, Sweden*

Received 27 May 2004; accepted 14 September 2004
Available online 25 November 2004

Abstract

The methods of the quantum electronic structure theory are reviewed and their implementation for the gas phase chemistry emphasized. Ab initio molecular orbital theory, density functional theory, quantum Monte Carlo theory and the methods to calculate the rate of complex chemical reactions in the gas phase are considered. Relativistic effects, other than the spin–orbit coupling effects, have not been considered. Rather than write down the main equations without further comments on how they were obtained, we provide the reader with essentials of the background on which the theory has been developed and the equations derived. We committed ourselves to place equations in their own proper perspective, so that the reader can appreciate more profoundly the subtleties of the theory underlying the equations themselves. Finally, a number of examples that illustrate the application of the theory are presented and discussed.

Keywords: Ab initio molecular orbital electronic structure theory; Density functional theory; Time dependent density functional theory; Quantum Monte Carlo theory; Surface hopping; Two-state reactivity

Contents

* Corresponding author. Tel.: +34 430 18190; fax: +34 943 212236.
E-mail address: ugalde@sq.ehu.es (J.M. Ugalde).

1387-3806/$ – see front matter © 2004 Elsevier B.V. All rights reserved.
doi:10.1016/j.ijms.2004.09.018

1. Introduction

Quantum chemistry and computer modeling nowadays has a major impact on the chemist's ways of thinking and working, as the role of both theoretical understanding and computational modeling is becoming increasingly important in chemical research.

Quantum chemistry has enjoyed the benefits of the remarkable achievements in computer technology over the past decades. Technological advances include increasingly more powerful and lower-cost microprocessors, memory devices, disk drives, and affordable computer clusters with advanced visualization capabilities. Indeed, the availability of powerful computers has succeeded in changing the face of theoretical chemistry in general and quantum chemistry in particular [1]. In some areas, of which gas-phase ion chemistry is most prominent [2], quantum chemistry can provide results with an accuracy approaching that of the experiments and with a freedom to consider rare or even "*impossible*" species and configurations which are hardly accessible for experimental observation.

In spite of its great usability, quantum chemistry is more than a collection of practical rules and recipies. It lies on strong foundations. The theory is based on the study of *practical* solutions to the Schrödinger equation. It is well known that the Schrödinger equation is easily solved exactly for one-electron atoms, but the exact solution for any other system was not found possible, which lead to the famous remark by Dirac:

- The fundamental laws necessary for the mathematical treatment of a *large part* of physics and the *whole* chemistry are thus completely known, and the difficulty lies only in the fact that application of these laws leads to equations that are too complex to be solved.

For many, this statement represented the end of chemistry in that it marked the end of the process of fundamental discoveries. However, it was not so. The quest for practical approaches to the unknown exact solution of the Schrödinger equation has enriched chemistry with a number of new concepts and interpretations that help in rationalizing the vast land of chemical knowledge. Concepts like electronic configuration, valence orbitals, σ/π separation, electron charge-transfer, electron correlation, etc., have been created in the coarse of quantum chemical research and many of them have been pivotal to development of the field.

As pointed out by Pople [3], given the hopelessness of attaining the exact solutions, quantum chemistry faces the task of assisting in the qualitative interpretation of chemical phenomena and providing predictive capability. In order to achieve these targets, quantum chemistry has developed a number of methods and procedures of various levels of sophistication that can operate at different levels of accuracy. Both free-ware and commercial software packages have been also produced. Some of them have been interfaced with *user-friendly* appliances which provide a sense of beauty and perfection to the layman practitioner. Often used terms, like ab initio or *highly accurate calculation*, reinforce this feeling.

However, it is worth pointing out that in some sense, this emphasis on computation has weakened the connection with the theories that make the calculations possible. The possibilities for chemical interpretations of the calculations are enormous nowadays, but have ironically been seen to decrease just at the time when the volume and reliability of numerical information available from computational work increases. In addition, whether all chemically relevant information can be obtained directly from the principles of quantum mechanics (i.e., ab initio or not) is a question that requires, at least, a second thought, as recently pointed out by Scerri [4]. Indeed, he has argued that quantum mechanics cannot *deduce* the details of the periodic table without the input of some empirical data at a level well beyond the rules of quantum mechanics.

Quantum chemistry has changed our view of the molecular entities, and in some sense of the whole of chemistry. Regarding molecular entities as dynamic elements in an electronic system and appropriately conducting calculations, can yield useful insight to understand properties and behavior. As recently stated by Schwarz [5], that despite its omnipresence the question "*Have you already tried your reaction in isopropanol*?" is not what chemistry is about. First and foremost chemistry is about the understanding of how atoms and molecules behave, why they do so, and, of course, how to affect their behavior in a desired way. This emphasis on processes rather that on substances has recently been addressed also by others [6,7] who argue that it is molecular change that should be viewed as the basis of increasing chemical complexity and hence substances can be defined according to their characteristic reactions. Quantum chemistry can contribute to this debate as it offers the possibility of viewing molecular change without the limitations of an experimental system. This has the advantage of allowing us to explore a very large region of reaction space—in many cases also regions never attainable by experiments, and thereby draw more general conclusions.

In this review, we try to provide a comprehensive presentation of the most widely used methods in quantum chemistry. We will not derive all the equations but will certainly provide the most important ones, for the reader to appreciate their meaning more clearly. In Section 5, we then discuss some examples to illustrate the application of the theoretical methods. We do not claim that these examples are the best ones, not even, that they are good ones. However, as they all come from our own work they are consequently problems that we know in more detail. Finally, we emphasize that this review can be read starting either from Section 2 or from Section 5, depending on the taste of the reader.

2. Molecular orbital theory

The land-mark paper of Hitler and London [8] on the ground state of H_2 opened the way to a theoretical understanding of the chemical bond and marked the birth of quantum chemistry. Their wave function reflects the long standing idea that chemical bonds between atoms in molecules, are formed by pairs of electrons belonging to each of the participant two atoms. Therefore, their trial wave function for the ground state of H_2 includes only bonding *covalent* contributions. Namely, being $\psi_X(\mathbf{r})$ the orbital centered on nucleus X, the Heitler and London ansatz is:

$$\Psi_{\mathrm{HL}}(\mathbf{x}_1, \mathbf{x}_2) = \frac{1}{\sqrt{2}}[\psi_A(\mathbf{r}_1)\psi_B(\mathbf{r}_2) + \psi_A(\mathbf{r}_2)\psi_B(\mathbf{r}_1)] \times \Theta(s_1, s_2) \quad (1)$$

where $\mathbf{x} = (\mathbf{r}, s)$ is the composite spatial plus spin coordinate of the electrons and $\Theta(s_1, s_2)$ is the normalized singlet spin wave function:

$$\Theta(s_1, s_2) = \frac{1}{\sqrt{2}}[\alpha(s_1)\beta(s_2) - \alpha(s_2)\beta(s_1)] \quad (2)$$

The *Valence Bond* theory elaborated afterwards by Pauling [9], Slater [10] and van Vleck [11] was a refinement of the

original idea of Heitler and London. The generalized many electron *Valence Bond* wave function [12] is built up from electron pairs occupying hybridized orbitals that are spatially localized in the directions associated with the chemical bonds of the molecule.

Almost at once a rival theory of molecular structure was developed by Hund [13] and Mulliken [14] which became known as the *Molecular Orbital* theory. In contrast to the *Valence Bond* approach, the many electron wave function in the Molecular Orbital theory is built up from one-electron orbitals extending over the whole molecule, which are occupied in accordance with the Aufbau principle and Fermi statistics. Within this model, the ground state wave function of H_2 is:

$$\Psi_{\mathrm{MO}}(1,2) = \frac{1}{\sqrt{2}} \begin{vmatrix} \sigma_{\mathrm{g}}(1) & \bar{\sigma}_{\mathrm{g}}(1) \\ \sigma_{\mathrm{g}}(2) & \bar{\sigma}_{\mathrm{g}}(2) \end{vmatrix} \tag{3}$$

which constitutes a single determinant constructed with the molecular spin-orbitals

$$\sigma_{\mathrm{g}}(1) = \frac{1}{\sqrt{2}}[\psi_A(1) + \psi_B(1)]\alpha(1)$$

$$\bar{\sigma}_{\mathrm{g}}(1) = \frac{1}{\sqrt{2}}[\psi_A(1) + \psi_B(1)]\beta(1)$$

expressed as a normalized linear combination of the atomic orbitals (LCAO-MO approximation).

If we expand the determinant of Eq. (3), the resulting expression for the wave function:

$$\Psi_{\mathrm{MO}}(\mathbf{x}_1, \mathbf{x}_2) = \frac{1}{2}[\psi_A(\mathbf{r}_1)\psi_B(\mathbf{r}_2) + \psi_A(\mathbf{r}_2)\psi_B(\mathbf{r}_1) + \psi_A(\mathbf{r}_1)\psi_A(\mathbf{r}_2) + \psi_B(\mathbf{r}_1)\psi_B(\mathbf{r}_2)]\Theta(s_1, s_2) \tag{4}$$

contains, in addition to the bonding *covalent* contributions of Eq. (1), the non-bonding *ionic* contributions $\psi_A(\mathbf{r}_1)\psi_A(\mathbf{r}_2)$ and $\psi_B(\mathbf{r}_1)\psi_B(\mathbf{r}_2)$, which enter in the wave function with the same weight as the covalent contributions.

However, it was soon established by Slater [15] that both *Valence Bond* and *Molecular Orbital* approaches could be extended to give ultimately the same description of the electronic structure of the hydrogen molecule. Later, this proof was extended by Longuet-Higgins [16] to cover polyatomic molecules. Consequently, the choice of the method could be said to rest on *convenience* rather than principle.

Actually, it has been found that the molecular orbital wave functions, which are *conveniently* written in terms of antisymmetrized products of orthonormal molecular orbitals, as in Eq. (3), are easier to handle. In particular, after Roothaan [17] introduced the concept of the *basis functions*. These are sets of known one-electron functions which are used to represent all the electrons in the molecule as a linear combination of the functions of the set. This has the virtue of transforming the integro-differential equations of the molecular Hamiltonian problem into algebraic ones, which can be conveniently handled by computers. Hence, ultimately, the quality of the wave functions is lend over the selected basis functions set. Needless to say, the choice of the basis function set should thus be carried out with extreme care.

Two broad categories of basis functions may be used for molecular calculations, *numerical* or *analytical*. Numerical basis sets are appreciated by their great accuracy, although they are computationally *less* tractable than analytical basis sets. Indeed, numerical basis sets are generally used only for atoms [18] or molecules with high symmetry [19,20], due to the large number of grid points required to estimate the basic molecular integrals.

For most molecular systems, therefore, we are forced to use analytic basis functions to expand the molecular orbitals. This poses the question as to what functions are suitable for the expansions. Three requirements have been identified [21] as the most important ones that proper basis functions sets should meet:

1. The basis should be designed in such a way that it allows for a systematic saturation of increasingly higher angular momentum functions.
2. The basis should yield a fast convergence of the self-consistent cycles.
3. The basis should provide for an easy manipulation and efficient implementation of all the basic molecular integrals required. Also, the basis should not cause numerical instability problems.

Basis sets that fulfill all the three requirements are scarce. The most popular basis sets are based on the so-called *Gaussian basis functions*. They have been found to combine satisfactorily short expansions with efficient algorithms for fast integral evaluation, although they require considerable self-consistent cycles for molecular properties to converge [22].

However, Gaussian basis sets can hardly be considered as a *panacea*. Indeed, the huge number of calculations, performed over the years with a large number of Gaussian basis sets, have established beyond any reasonable doubt that, nowadays, it is essentially impossible to construct one universal molecular basis set which is applicable under all circumstances. This points to the fact that selecting properly an appropriate basis set for a given calculation is a tricky business, which often receives less attention than it deserves.

Given the basis set, the unknown coefficients of the molecular orbital expansions are determined such that the total electronic energy calculated from the wave functions, constructed as an antisymmetrized product of the molecular orbitals, is minimized and, according to the variational theorem [23], is as close as possible to the energy of the exact solution. This energy and its associated wave function is the best that we can obtain with the *Hartree–Fock approximation*, that is, the best result under the following constraints: (i) a finite expansion of the molecular orbitals made in the finite basis function set (the orbital space) and (ii) the use of a single assignment of electrons to orbitals, i.e. a single configuration of the Fock

space. For an exact representation of the true wave function both expansions must be complete.

The Hartree–Fock approximation constitutes, therefore, the simplest of the possible models that we can construct within the *Molecular Orbital* theory. At this simplest level, the wave function is made of one single configuration. At the most complex level, the wave function will contain a variationally energy minimized superposition of all the configurations of the Fock space. Between these two extremes computational chemistry has developed a hierarchy of models, which provide approximate solutions to the electronic structure problem of known quality at a given computational cost.

The remainder of this section will be devoted to summarizing these approaches succinctly. We will not derive all the equations, but will certainly present the basic equations to assist the reader to appreciate the advantages and the potential shortcomings of each approximation.

2.1. The Hartree–Fock approximation

The most commonly applied ab initio electronic structure methods are based on the time independent, nonrelativistic Born-Oppenheimer approximation. Extensions to time-dependent electronic structure will be discussed in later sections of this review. However, although proper accounting of relativistic effects is an area of intense research effort, and important for heavy elements (e.g., atomic number greater than 54), this aspect will not be treated in this review. The interested reader may consult the recent compilation of Schwarz [24].

The Born-Oppenheimer approximation allows the separation of electronic and nuclear degrees of freedom, and is valid in the limit that the ratio of electronic to nuclear masses are small. The mathematical consequence of the Born-Oppenheimer approximation is that the total molecular wave function can be treated as a product of the form:

$$\Psi(\mathbf{x}_N, \mathbf{Q}_M) = \Psi_{\text{nuc}}(\mathbf{Q}_M)\Psi_{\text{elec}}(\mathbf{x}_N; \mathbf{Q}_M) \tag{5}$$

where Ψ_{nuc} and Ψ_{elec} are the nuclear and electronic wave functions, respectively, and $\mathbf{x}_N = \mathbf{x}_1, \mathbf{x}_2, \ldots, \mathbf{x}_N$ and $\mathbf{Q}_M = \mathbf{Q}_1, \mathbf{Q}_2, \ldots, \mathbf{Q}_M$ are the generalized spatial/spin coordinates for the N electrons and M nuclei, respectively. *Note*: The electronic wave function depends *parametrically* on the generalized nuclear coordinates $\mathbf{Q}_M$. The Born-Oppenheimer approximation is valid when $(m_e/m_\alpha)^{1/4} \ll 1$, where m_e and m_α are the mass of the electron and of a particular nucleus, respectively, and is generally more accurate for ground state energies. For most chemical applications, the error introduced by the Born-Oppenheimer approximation is considerably less than that of other approximations introduced to arrive at a practical solution.

The problem that we have at hand is, therefore, to find the best solution of the Schrödinger equation:

$$\hat{\mathcal{H}}\Phi = E\Phi \tag{6}$$

where Φ represents the total electronic wave function, E its energy and $\hat{\mathcal{H}}$ is the well-known molecular Hamiltonian operator:

$$\hat{\mathcal{H}} = \sum_{i=1}^{N}\left[\frac{-\nabla_i^2}{2} + \sum_{A=1}^{M}\frac{-Z_A}{|\mathbf{r}_i - \mathbf{R}_A|}\right] + \sum_{i>j}^{N}\frac{1}{|\mathbf{r}_i - \mathbf{r}_j|} + \sum_{A=1}^{M}\frac{-\nabla_A^2}{2m_A} + \sum_{A>B}^{M}\frac{Z_A Z_B}{|\mathbf{R}_A - \mathbf{R}_B|} \tag{7}$$

in atomic units, namely: $e = m_e = \hbar = c = 1$.

We shall adopt the Born-Oppenheimer "clamped-nuclei" approximation, which underlies nearly all electronic structure calculations. Under this approximation, nuclei are assumed to be fixed relative to the electrons, that move in the potential field exerted by the nuclei. Hence, the penultimate term of Eq. (7), which accounts for the kinetic energy of the nuclei, is zero and the last one contributes a constant depending on the nuclear arrangement, that is simply added at the end of the calculation.

Hence, a regular molecular calculation has normally two parts. Firstly, we wish to calculate the electronic energy for a given fixed nuclei arrangement and, secondly to find which nuclear arrangement has the lowest total energy, i.e., electronic energy plus nuclear repulsion energy. We shall describe in detail the former step. The latter consists of a minimization of a multivariant function.

Recall that once we have omitted the last two terms of Eq. (7) the resulting electronic Hamiltonian, $\hat{H}$, can be factorized into one term containing exclusively the one-electron operators:

$$h(i) = \sum_{i=1}^{N}\left[\frac{-\nabla_i^2}{2} + \sum_{A=1}^{M}\frac{-Z_A}{|\mathbf{r}_i - \mathbf{R}_A|}\right] \tag{8}$$

and a second which consists of the bielectronic electron–electron repulsion term. Then

$$\hat{H} = \sum_{i=1}^{N} h(i) + \sum_{i<j}^{N}\frac{1}{r_{ij}} \tag{9}$$

Consider, for the time being the following approximate wave function: the Hartree–Fock electronic wave function which is constructed as an antisymmetrized product of a set of molecular orbitals $\{\psi_i\}_{i=1}^{N}$. Namely:

$$\Psi_{\text{HF}} = \frac{1}{\sqrt{N!}}\begin{vmatrix} \psi_1(1) & \psi_1(2) & \cdots & \psi_1(N) \\ \psi_2(1) & \psi_2(2) & \cdots & \psi_2(N) \\ \cdots & \cdots & \cdots & \cdots \\ \psi_N(1) & \psi_N(2) & \cdots & \psi_N(N) \end{vmatrix} \tag{10}$$

The Hartree–Fock method is aimed at obtaining the best such single determinant approximation to the exact wave function Φ, of Eq. (6). To do this we use the variational principle:

$$E_{\text{HF}} = \langle\Psi_{\text{HF}}|\hat{H}|\Psi_{\text{HF}}\rangle \geq E \tag{11}$$

where we have adopted, for convenience, the Dirac's *bra* "⟨|" and *ket*"|⟩" notation [25]. The variations are carried out varying the form of the N molecular orbitals keeping their orthonormality $\langle\psi_i|\psi_j\rangle = \delta_{ij}$ until the lowest possible energy is reached. The resulting equations that yield the best molecular orbitals are:

$$\hat{f}(1)\psi_i(1) = [\hat{h}(1) + \hat{u}(1)]\psi_i(1) = \epsilon_i\psi_i(1), \quad i = 1, N \tag{12}$$

where the operator $\hat{u}$ is defined as:

$$\hat{u}(\mathbf{r}_1) = \sum_{j=1}^{N} \int \psi_j^*(\mathbf{r}_2)\frac{1}{r_{12}}(1 - \hat{\mathcal{P}}_{12})\psi_j(\mathbf{r}_2)\,\mathrm{d}\mathbf{r}_2 \tag{13}$$

with $\hat{\mathcal{P}}_{12}$ being the operator that replaces electron 1 by electron 2 and vice versa. Hence, an iterative self-consistent procedure must be set up for the solution of Eq. (12), since the operator $\hat{f}$ depends on its eigenfunctions ψ_i via $\hat{u}$.

These eigenfunctions, $\{\psi_i\}_{i=1}^N$, are the *Molecular Orbitals*. A molecular orbital is an eigenfunction of a *fictitious* one-electron operator $\hat{f}$, which accounts for the kinetic energy plus the attraction by all the nuclei ($\hat{h}$) and, an approximate *averaged* repulsion ($\hat{u}$) exerted by the rest of the electrons. The latter term is clearly an approximation. An electron in the molecular orbital ψ_i is considered to have the orbital energy ϵ_i.

Once the molecular orbitals have been obtained, we wish to estimate the total electronic energy of the molecule [26]. That is

$$\begin{aligned} E_{\mathrm{HF}} &= \langle\Psi_{\mathrm{HF}}|\hat{H}|\Psi_{\mathrm{HF}}\rangle \\ &= \sum_{i=1}^{N}\langle\psi_i|\hat{h}(1)|\psi_i\rangle + \frac{1}{2}\sum_{i,j}^{N}\langle ij||ij\rangle \end{aligned} \tag{14}$$

where we have used the following notation:

$$\langle ij||ij\rangle = \int \mathrm{d}\mathbf{r}_1\,\mathrm{d}\mathbf{r}_2\,\psi_i^*(1)\psi_j^*(2)\frac{1}{r_{12}}(1 - \hat{\mathcal{P}}_{12})\psi_i(1)\psi_j \tag{2}$$

This equation can be seen a sum of the following two terms:

$$\begin{aligned} \langle ij||ij\rangle &= \int \mathrm{d}\mathbf{r}_1\,\mathrm{d}\mathbf{r}_2\frac{|\psi_i(1)|^2 \times |\psi_j(2)|^2}{r_{12}} \\ &\quad - \int \mathrm{d}\mathbf{r}_1\,\mathrm{d}\mathbf{r}_2\frac{\psi_i^*(1)\psi_j\psi_j^*(2)\psi_i(2)}{r_{12}} \end{aligned} \tag{15}$$

The former represents the Coulomb repulsion of the electron 1 in molecular orbital ψ_i with the electron 2 in molecular orbital ψ_j and, the latter term, the exchange term, arises form the antisymmetry of the Hartree–Fock wave function Eq. (10). Note that:

$$\langle ii||ii\rangle = 0 \tag{16}$$

Hence, the Hartree–Fock method is *self interaction* free by construction, since the exchange term cancels out exactly the Coulomb repulsion of molecular orbital ψ_i with itself, included in Eq. (14) under $i = j$ in the second summatory of the right hand side. That is, the Hartree–Fock approximation describes the electron–electron repulsion by one electron moving in the average field of the remaining $N - 1$ electrons.

Let us now write the Hartree–Fock energy of Eq. (14) in a slightly different form. Rearranging the electronic Hamiltonian operator as:

$$\hat{H} = \underbrace{\sum_{i=1}^{N}\hat{f}(i)\overbrace{[\hat{h}(i) + \hat{u}(i)]}}_{\hat{H}_0} + \underbrace{\left[\sum_{i<j}^{N}\frac{1}{r_{ij}} - \sum_{i=1}^{N}\hat{u}(i)\right]}_{\hat{\mathcal{V}}} \tag{17}$$

and consider the energy associated with the one-electron operator $\hat{H}_0$. Taking into account Eqs. (12) and (17) we have:

$$\langle\Psi_{\mathrm{HF}}|\hat{H}_0|\Psi_{\mathrm{HF}}\rangle = \sum_{i=1}^{N}\langle\psi_i|\hat{f}|\psi_i\rangle = \sum_{i=1}^{N}\epsilon_i = E_0 \tag{18}$$

Consequently, using the form of Eq. (17) for $\hat{H}$ the molecular Hartree–Fock energy can be cast as:

$$E_{\mathrm{HF}} = E_0 + \langle\Psi_{\mathrm{HF}}|\hat{\mathcal{V}}|\Psi_{\mathrm{HF}}\rangle \tag{19}$$

That is, the Hartree–Fock energy is not simply the sum of the molecular orbitals energies, E_0. It contains an additional term:

$$\langle\Psi_{\mathrm{HF}}|\hat{\mathcal{V}}|\Psi_{\mathrm{HF}}\rangle = -\sum_{i<j}^{N}\langle ij||ij\rangle \tag{20}$$

to correct for over-counting of the electron–electron repulsion terms in E_0.

Recall that so far we have not restricted the molecular orbitals to be doubly occupied. Indeed, we may have $\psi_i\alpha$ and $\psi_{i+1}\beta$ with $\psi_i \neq \psi_{i+1}$. This is the unrestricted Hartree–Fock (UHF) method, which as detailed above applies for both closed-shell and open-shell systems. However, for closed-shell systems we can impose $\psi_i = \psi_{i+1}$. This defines the so-called restricted Hartree–Fock (RHF) procedure. Finally, for open shells, we may wish to obtain the best molecular orbitals with *maximum* double occupancy. This yields the restricted open-shell Hartree–Fock (ROHF). The foregoing approaches are collectively referred to as *Self Consistent Field* (SCF) methods [27].

2.2. The symmetry breaking problem

The SCF approximation determines an optimal set of molecular orbitals $\{\psi_i\}_{i=1}^N$ from the condition that the energy expression, Eq. (14), is stationary with respect to the variations of the orbitals themselves. However, neither of the SCF methods guarantees that this optimal set constitutes a *stable* solution. To verify this, a *stability analysis* must be carried out in order to analyze the behavior of the energy with respect to the second-order variations of the molecular

orbitals. This allows us to find it out whether the optimal set of molecular orbitals corresponds to a true (although local) minimum or a saddle point. For the latter case, there exists a number of variations of the molecular orbitals that lead to a lowering of the electronic energy [28].

Therefore, an additional condition that a particular Hartree–Fock solution must satisfy in order to be considered as the best solution, is that *no* infinitesimal change of the molecular orbitals will decrease the expectation value of the electronic Hamiltonian with respect to the determinant built from the occupied molecular orbitals.

At this point, it might be worth to indicate that all the SCF formalisms are approximate methods which, opposite to the *exact* solution, may eventually achieve lower energy by relaxing some of the constrains imposed by the commutation rules of the Hamiltonian. That is, the *exact* wave function must also be an eigenfunction of all the operators that commute with the Hamiltonian, in particular, the spin and space symmetry operators. Approximate wave functions may fail to fulfill this requirement.

The occurrence of eigenfunctions of the Hamiltonian $\hat{H}_0$ that do not conform to the symmetry of the Hamiltonian $\hat{H}$ is one of the weak points of the SCF formalisms. This instability of the Hartree–Fock is often referred to as the *symmetry broken dilemma* [29]: Which wave function should be regarded as the best solution?: (i) The one with the correct symmetry but higher energy or (ii) the one with the lower energy but the incorrect symmetry.

Dunietz and Head-Gordon [30] have indicated that, although symmetry breaking appears only for systems with point group symmetry, it is a signature of problems associated with the restricted Hartree–Fock (RHF) wave functions. Thus, they have identified the symmetry broken problem as arising from the comparison of the energy of the symmetry preserving SCF solution along the relevant coordinate with its value at the extreme of such coordinate. Whenever the symmetry preserving energy is greater than the expected energy of the system at the asymptotic region, a lower energy solution, with symmetry constrains relaxed, must exist.

Finally, we wish to mention one more interesting paper that has recently appeared, related to the symmetry broken problem, in which Marañón [31] claims that both the σ–π separation and the π-ring current in benzene can be viewed as a direct consequence of the broken global symmetry in SCF formalisms.

2.3. The electron correlation

The SCF formalism as shown in the previous section, represents one of the most successful examples of modern computational quantum chemistry. Many of the chemical regularities of the periodic table can be well accounted for, at least qualitatively, within the Hartree–Fock approximation. However, detailed quantitative comparison with experimental data almost always points to the need of going beyond such approximation. For instance, it is well-known that the Hartree–Fock approximation fails to predict the existence of both, the hydrogen anion, H^- and the F_2 molecule. In the former case it is found that the energy of H^- is higher than the energy of the neutral hydrogen atom. For the latter case, the Hartree–Fock approximation predicts that two separated F atoms have lower energy than the F_2 molecule, as the potential energy curve monotonically decreases with respect to the internuclear separation.

The correction to the energy to bring cases like these in agreement with reality, is vaguely referred to as the *correlation energy* and, it is ascribed to the fact that the motion of an electron is *correlated* with those of the remaining electrons and, these effects are by construction no accounted for within the Hartree–Fock approximation, where electrons move in the *average* field of all the other electrons. The correlation energy is not huge; normally it is only of the order of 1% of the total energy of the system, but the truth of the matter is that (unfortunately) most chemically interesting properties, such as bond dissociation energies, ionization potentials, electron affinities, excitation energies, etc., often lie within this narrow energy interval.

To improve on the Hartree–Fock approximation we must develop, therefore, a superior treatment of the electron–electron interaction term. However, if we wish retain the use of molecular orbitals (which in essence are anything else but one-particle functions), electron correlation can only be introduced by constructing wave functions flexible enough to push electrons apart from each other. Namely, we need molecular orbitals that expand over regions of space not covered by the Hartree–Fock wave function. Since the Hartree–Fock wave function spans only on the *occupied* molecular orbitals, the obvious way is to admit *virtual* molecular orbitals into the wave function. Thereby, the wave function now, can take into account the long-range interactions, which are poorly represented by the wave functions spanned only in terms of the occupied molecular orbitals.

Moreover, allowing *virtual* molecular orbitals into the wave function, we add flexibility to the wave function also in the regions already spanned by the *occupied* molecular orbitals. This improves the description of the short-range electron–electron interactions.

These two types of electron correlation, i.e., long-range and short-range, are not mutually exclusive. The former, arising from long-range electron–electron interactions is called *non-dynamical* correlation and is related to the degeneracy of bonding and antibonding configurations. If nearly degenerate, they will interact strongly and hence cannot be treated separately. The non-dynamical electron correlation is consequently system-specific, since it depends on the system of study which configurations get nearly degenerate.

The latter, due to short range interactions between the electrons, stems from the failure of the Hartree–Fock representation to describe the detailed correlated motion of the electrons as induced by their instantaneous mutual repulsion. This type of electron correlation is customarily referred to

Table 1
Energies (a.u.) and occupations of a number of selected natural orbitals of H_2 for selected internuclear distances R, in a.u.

E_{H_2}	$R = 1.4$	$R = 4.0$	$R = 15.0$
	−1.173796	−1.015724	−0.999891
$n(1\sigma_g)$	1.9643	1.5162	1.0000
$n(2\sigma_g)$	0.0061	0.0015	0.0000
$n(1\sigma_u)$	0.0199	0.4804	1.0000
$n(2\sigma_u)$	0.0002	0.0000	0.0000
$n(1\pi_u)$	0.0043	0.0000	0.0000

as *dynamical* correlation and is, since it is nonspecific, in a sense, universal.

Unfortunately, the field is plagued with a number of terms to denote the same concept. This is perhaps best illustrated by the energies and occupation numbers of the orbitals of H_2 at three internuclear distances. As shown in Table 1, at the equilibrium distance, 1.4 a.u., the $1\sigma_g$ orbital with an occupation of 1.9643 should provide a reasonable representation of the exact wave function. Nevertheless, the $1\sigma_u$ orbital with an occupation of 0.0199 is the second largest populated orbital. This orbital has a nodal plane which bisects the molecular axis. Its occupation, therefore, increases the probability of finding the two electrons on one nucleus each. This, which is non-dynamical correlation, is often referred to as *left–right correlation* [32]. The $1\pi_u$ orbital, which has an occupation of 0.0043 at the equilibrium distance, possesses a nodal plane which contains the molecular axis. Then its occupation increases the probability of finding the electrons on opposite sides of the molecular axis. This is normally referred to as *angular correlation* [33]. Notice finally that the $2\sigma_g$ orbital belongs to the same irreducible representation as the most populated orbital $1\sigma_g$, but it has a radial node. Occupation of this orbital introduces *radial correlation*, increasing the probability of locating electrons at different distances along the molecular axis.

At long internuclear distances, $R = 15.0$ a.u., where electrons do not interact, the $1\sigma_g$ and $1\sigma_u$ molecular orbitals became degenerate and their occupation numbers are 1. Hence, we need two configurations to properly represent the wave function. Indeed, at the stretched limit, $R \to \infty$, the exact wave function, Eq. (1), is cast as:

$$\psi_{HL}(1,2) = \begin{vmatrix} \sigma_g(1) & \bar{\sigma}_g(1) \\ \sigma_g(2) & \bar{\sigma}_g(2) \end{vmatrix} + c \begin{vmatrix} \sigma_u(1) & \bar{\sigma}_u(1) \\ \sigma_u(2) & \bar{\sigma}_u(2) \end{vmatrix} \quad (21)$$

where the *virtual* molecular orbitals

$$\sigma_u(1) = \frac{1}{\sqrt{2}}[\psi_A(1) - \psi_B(1)]\alpha(1)$$

$$\bar{\sigma}_u(1) = \frac{1}{\sqrt{2}}[\psi_A(1) - \psi_B(1)]\beta(1)$$

account for the long-range effects aimed at eliminating the ionic configurations from the Hartree–Fock wave function.

Table 2
Comparison of different electronic structure methods

Method	VE	SE	DEC	NDEC	CS	Size
HF	√	√			N^3–N^4	50–100
MP2		√	*		N^5	20–30
MP4		√	**		N^7	10–20
DFT/LDA		√	*		N^3–N^4	50–200
DFT/GGA		√	*		N^3–N^4	50–0
DFT/mGGA		√	*		N^3–N^4	50–100
CCSD		√	**		N^6	10–30
CCSD(T)		√	***		N^7	10–30
CCSDT		√	***		‘8	5–15
CIS	√				N^4	50–100
CISD	√		**		N^6	<10
CISDT	√		**	*	N^7	<10
CISDTQ	√		***	***	N^8	<10
MRCI	√		***	***	$n \times N^6$	<10
MCSCF	√	√	*	***	$n \times N^6$	15–25
QMC	√	√	***	***	N^3	<250
full CI	√	√	Exact	Exact	$N!$	<5

The properties/characteristics compared include: the presence/absence of a variationally bounded energy (VE), size extensivity/size consistency (SE), reliable treatment of dynamic electron correlation (DEC) and non-dynamic electron correlation (NDEC). The latter electron correlation categories are marked with 0–3 asterisks to indicate successively improved treatment, whether the method generally performs poorly, moderately well or satisfactorily. Also shown is the order of the formal computational scaling (CS) with the number of basis functions (N), the dimension of the multireference space (n) and the typical atomic size range (size) for which the methods are typically applied in the current literature.

Nevertheless, note that this configuration also contributes to the improved description of the short-range electron–electron interaction at the equilibrium distance $R = 1.4$ a.u.

The relative weights of these effects vary with the internuclear distance, which supports the previous statement that the nondynamical and dynamical electron correlations are not mutually exclusive. In fact, they interplay in an intricate manner.

Consideration of electron correlation effects is subtle and in fact, there are a number of procedures that have been developed over the years to account for the subtleties of the electron–electron interaction. In Table 2 we have compiled the advantages and disadvantages of some of the most used procedures.

Basically, there are two ways to perform correlation or post-HF calculations: the variational approach the perturbational approach. We shall describe them in turn.

2.4. (Multi)configuration interaction

As outlined above, the problem with HF theory is that it only includes an average interaction between the electrons. The theory thus fails to account for the fact that electrons, being charged particles, exhibit instantaneous Coulomb repulsion that separate them. Since the motion of one electron will affect the motion of all others, a correct description of the system leads to a complex many-body problem. Several post-HF approaches have been proposed in order to treat the electron correlation, varying significantly in complexity, accuracy and applicability.

The inclusion of electron correlation can essentially be divided into two sub-categories: those focusing on the dynamical correlation problem and those where we aim for the non-dynamical correlation. In the first class, we find methods based on expanding a single reference wave function (typically the HF solution), such as truncated configuration interaction (CI), many-body perturbation theory (MBPT), coupled cluster methods (CC) and quadratic CI (QCI). In the second category, where we aim to solve problems where excited states have a comparatively high weight, we find the multi-reference (MR) approaches such as MRCI, multiconfiguration SCF (MCSCF), complete active space SCF (CASSCF) and generalized valence bond (GVB) methods.

Within the non-relativistic Born-Oppenheimer approximation, the main source of error that arise in the Hartree–Fock method include

- Incompleteness of the *basis set* used to represent the electronic degrees of freedom.
- Incomplete treatment of *electron correlation*.

These errors as "theoretical errors" inherent to a particular quantum method, to distinguish them from "numerical errors" introduced by the specific hardware and software used in actual calculations. Numerical errors can arise from a variety of sources such as the hardware precision, to the convergence criteria and stability of solutions of complex linear and non-linear algebraic equations, and the accuracy of analytic and numerical integration techniques.

The present section begins the discussion of improved treatment of electron correlation beyond the Hartree–Fock approximation. Recall, the Hartree–Fock approximation modeled the molecular electronic wave function as a single determinant of occupied spin–orbitals. The spatial orbitals are expanded as a linear combination of basis functions, and the variational principle on the electronic energy is applied to determine the expansion coefficients. The single determinant form of the wave function is the simplest mathematical construct that enforces the antisymmetry requirement for a system of identical Fermions (i.e., the Pauli exclusion principle). The antisymmetry, in a sense, builds in a certain degree of electron correlation; however, it does not include the dynamical and non-dynamical correlation described in Section 2.1. The end result is that, in the Hartree–Fock method, each electron moves in the mean electrostatic field of the other electrons, within the constrains of the Pauli principle.

An obvious extension of the Hartree–Fock method is to generalize the form of the wave function to include multiple determinants, or more specifically multiple configuration state functions (CSFs):

$$\Psi = \sum_{k=0} c_k \Psi_k \tag{22}$$

where the Ψ_k are the CSFs used in the expansion and the c_k are the corresponding coefficients. Only CSFs that satisfy the same symmetry and spin conditions of the state being modeled in the expansion will contribute to the wave function (hence considerable advantage can be taken if such symmetry is known a priori). For closed-shell singlet states, CSFs can always be represented by a single determinant. However, for certain open-shell systems, CSFs may require multiple determinants for proper representation. The coefficients c_k are determined variationally (see below).

A wave function of the form shown in Eq. (22) is said to be a *multi-reference* wave function. As will be seen below, often such expansions may contain a very large number of terms, and solution of the resulting equations requires computational effort that scales highly non-linearly such that practical applications are limited to fairly small systems. Indeed part of the art of multi-reference electronic structure calculations is to devise strategies whereby the expansion is more rapidly convergent such that methods can be extended to larger molecular systems. Multi-reference calculations are perhaps the best modern computational tools to reliably treat problems that involve a high degree of non-dynamical correlation, and hence are important for the study of reactions that involve formation/cleavage of bonds, electron transfer, and even conformational events (for example, in many conjugated systems) that are concerted with changes in the nature of diabatic states on the potential energy surface (PES).

In this section, the basic method of configuration interaction will be discussed. The basic CI method will form the basis of more advanced multi-reference methods, and hence is deserving of initial focus. The essential difference between all CI-type methods involves the precise way in which the CSFs that enter the expansion of Eq. (22) are constructed.

The most common way in which to construct a CSF is from a set of orthonormal molecular orbitals. Note that the orthonormality of the molecular orbitals is not a requirement: determinantal wave functions are invariant with respect to unitary transformation of the molecular orbitals. However, the expressions for the calculation of quantum mechanical observables derived from determinantal waves functions that use non-orthogonal molecular orbitals quickly become extremely complex. Nonetheless, some research has been directed at the use of non-orthogonal localized orbitals that, in certain circumstances, might afford computational advantage. These methods are beyond the scope of this review.

In conventional CI-based methods, the orthonormal set of molecular orbitals are taken to be the occupied and virtual orbitals derived from a Hartree–Fock calculation. The occupied orbitals are thus the best orbitals (in a variational sense) for the Hartree–Fock wave function. With this choice of orbitals, the leading term (CSF) in the CI expansion, Ψ_0, is the Hartree–Fock wave function ($\Psi_0 = \Psi_{\mathrm{HF}}$). Additional CSFs are constructed through excitations from the occupied to the virtual orbitals. It is often useful to rewrite Eq. (22) in a more descriptive notation as:

$$\Psi = c_0 \Psi_{\mathrm{HF}} + \sum_{i}^{\mathrm{occ}} \sum_{r}^{\mathrm{vir}} a_i^r \Psi_i^r + \sum_{i<j}^{\mathrm{occ}} \sum_{r<s}^{\mathrm{vir}} a_{ij}^{rs} \Psi_{ij}^{rs} + \cdots \tag{23}$$

where the indices i and j sum over occupied MOs and the indices r and s sum over virtual MOs, Ψ_i^r denotes a CSF arising from single excitation from the ith occupied MO to the rth virtual MO, and Ψ_{ij}^{rs} denotes a CSF arising from double excitation from the i and j occupied MOs to the r and s virtual MOs. The first term on the right hand side of the equation, therefore, is simply the Hartree–Fock CSF, the term is a summation over all singly electronic excitations, the third term is a summation over all double electronic excitations, etc.

The coefficients c_k are determined variationally (under the normalization constraint). This leads to the CI secular equation:

$$\det(\mathbf{H} - E1) = \begin{vmatrix} H_{11} - E & H_{12} & \dots & H_{1N} \\ H_{21} & H_{22} - E & \dots & H_{2N} \\ \vdots & \vdots & \ddots & \vdots \\ H_{N1} & H_{N2} & \dots & H_{NN} - E \end{vmatrix} = 0 \quad (24)$$

where H_{ij} is the matrix element

$$H_{ij} = \langle \Psi_i | \hat{H} | \Psi_j \rangle \quad (25)$$

and Ψ_i is the CSF of Eq. (22). The roots of the secular equation that involve the determinant in Eq. (24) give the ground and excited state energies (i.e., the energy eigenvalues), and the corresponding eigenvectors provide the coefficients in the CI expansion (Eq. (22)). In order to solve for the CI expansion coefficients requires evaluation of matrix elements in Eq. (25). The construction of the CSFs from excitations using an orthonormal set of MOs (Eq. (23)) produces an orthonormal set of CSFs and greatly simplifies the evaluation of matrix elements. Since the electronic Hamiltonian consists only of one- and two-electron operators, matrix elements that involve CSFs that differ by more than two of their occupied MOs vanish, leading to a CI matrix that is very sparse, and ammenable to solution using sparse-matrix linear-algebraic techniques. The non-vanishing matrix elements that involve CSFs that differ by 0, 1 or 2 MOs can be calculated using Slater-Condon rules.

2.4.1. Full CI

The result of a (closed shell) Hartree–Fock SCF procedure for a molecule is to produce $N/2$ occupied MOs and $N_b - N/2$ virtual MOs, where N_b is the number of basis functions used in the variational procedure. If a CI calculation is performed where the wave function is expanded is a set of CSFs that represent *all possible*excitations from occupied to virtual orbitals, the result is called a *full CI*calculation and represents the best possible calculation for a given basis set. In the basis set limit, a full CI calculation provides and exact solution to the Schrodinger equation within the time-independent non-relativistic Born-Oppenheimer approximations. Alternately stated, the set of CSFs, in the basis set limit, represents a *complete orthonormal basis*that spans the appropriate Hilbert space of the N-electron wave function. A full CI calculation within a given basis provides a variational energy, treats reliably both dynamical and non-dynamical correlation and is *size consistent*, that is to say, the energy of two infinitely separated molecules will be the same as the sum of the energies obtained from two individual calculations at the same theory and basis set level.

Moreover, the choice of a particular set of molecular orbitals is arbitrary since the wave function is invariant to unitary transformation, although, as mentioned earlier, the traditional orthonormal Hartree–Fock orbitals offer particular computational advantages.

Unfortunately, full CI calculations are almost useless as a practical computational tool for all but the smallest of chemical problems. The reason is that the number of CSFs grows factorially with the system size. For a closed shell system of N electrons, the number of CSFs for a full CI calculation (no spatial symmetry) of the ground state is given by:

$$\#\text{CSFs} = \frac{N_b!(N_b+1)!}{(N/2)!((N/2)+1)!(N_b-(N/2))!(N_b-(N/2)+1)!} \quad (26)$$

with N_b being the number of basis set functions. This makes full CI calculations the most costly considered here, and almost always, one can obtain more highly accurate solutions for comparable computational cost from other methods (perhaps at higher basis set levels).

2.4.2. Truncated CI methods

A more practical, computationally tractable application of the CI method is to use a *truncated expansion*. The most common way of systematically specifying truncation schemes is to consider in Eq. (23) all single excitations (CIS), single + double excitations (CISD), single + double + triple excitations (CISDT), etc. The number of CSFs grows very rapidly with successive number of excitations, and applications of CISDTQ (up to quadruple excitations) are very expensive and fairly rare. As a particular case of the Slater-Condon rules for evaluating CI matrix elements, consider the matrix elements that involve the Hartree–Fock determinant with all singly excited CFSs:

$$\langle \Psi_{HF} | \hat{H} | \Psi_i^r \rangle = \langle \psi_r | \hat{F} | \psi_i \rangle = \epsilon_i \delta_{ij} \quad (27)$$

where $\hat{F}$ is the Fock operator, and ψ_i and ϵ_i are the ith HF molecular orbital and eigenvalue, respectively. *Note*: This quantity is always zero for a CIS calculation where the indices i and r correspond to occupied and virtual orbitals, respectively, and hence never coincide. This indicates that there is no direct mixing between the Hartree–Fock determinant and any singly excited CSF constructed from the HF molecular orbitals, and consequently inclusion of only single excitations does not alter the *ground state* properties from the Hartree–Fock values. This observation is known as Brillouin's theorem. The CIS method, however, is routinely used

to approximate the wave function for low-lying excited states. Inclusion of double excitations do couple with the HF determinant, and hence the CISD method is the first truncated CI method that corrects the HF reference state. The single and double excitations are also coupled (their matrix elements are not all zero), and hence inclusion of single excitations couple indirectly with the HF reference and influence the wave function in a CISD calculation. The CISD method is variational, and provides a reasonable reliable description of the non-dynamical correlation for a few systems.

The method, however, is fairly expensive and scales as order N^6. A problem with the CISD method is that it is not *size consistent*. The lack of size consistency, also referred to as *size extensivity*, of the CISD method results in reduced accuracy for dissociation processes and a systematic reduction in the percentage of the correlation energy that is recovered as the molecular system size increases. The main reason for the size consistency problem in CISD methods derived from the lack of quadruple excitations corresponding to two non-interacting pairs of interacting electrons; e.g., simultaneous double excitations on two molecules that are far apart from one another. Inclusion of these quadruple excitations corrects for the principle deficiency of the CISD method in terms of size consistency.

There have been several procedures proposed to address the problem of size consistency in CISD calculations, perhaps the most widely applied being the so-called *Davidson correction*. The Davidson correction approximates the contributions from quadruple excitations as the additive term

$$\Delta E_Q = (1 - a_0^2)(E_{\mathrm{CISD}} - E_{\mathrm{HF}}) \tag{28}$$

Sometimes this is abbreviated as CISD + Q(Davidson), or on some references simply CISD(Q). A variation of the correction that takes into account the wave function normalization, referred to as the *renormalized Davidson correction*, includes a multiplicative factor $1/a_0^2$. A shortcoming of the Davidson correction term is that does not vanish for two-electron systems where CISD and full CI are equivalent, and by induction, the term tends to similarly overestimate the contribution of higher-order excitations for systems with few electrons.

In cases where non-dynamical correlation is small, the Hartree–Fock wave function is a reasonable reference state, and the c_0 coefficient usually dominates the expansion in Eq. (23) (i.e., is the largest in magnitude). However, this expansion is often slowly convergent, which limits the overall accuracy of the truncated CI calculations. Recall, a full CI calculation, the result is invariant to any unitary transformation of the molecular orbitals. However, for a truncated CI method, this is no longer true. This begs the question as to how to accelerate the convergence of the CI expansion in order to obtain the highest accuracy possible for the least number of CSFs. One strategy involves altering the choice of the orthonormal molecular orbitals for which, as we just alluded, the Hartree–Fock orbitals typically lead to rather slowly convergent CI expansion. A better set of molecular orbitals, first introduced by Löwdin [34], are the so-called *natural orbitals* taken to be the eigenfunctions of the first-order reduced density matrix (see Eq. (138)). Another strategy is to choose a reference state, other than the Hartree–Fock reference state, that is better suited to the problem of interest. This becomes important when we have a high degree of non-dynamical correlation, and in particular in applications to potential energy surfaces where there may be crossings of diabatic states and the truncated CI methods may lead to discontinuities.

2.5. Coupled cluster theory

The coupled-cluster (CC) methods represent some of the most advanced correlated ab initio approaches in use today. The original formulations date back to the work of Čižek [35,36] and Paldus [37,38], and later pursued extensively by several workers, and in particular by the group of R.J. Bartlett. Due to the scaling of the methods, discussed in more detail below, the methods are extensively used when exploring the properties of small molecules, and yield results of very high accuracy.

As the name implies, CC theory is based on the idea of describing the electron correlation in terms of interacting clusters of electrons. The formalism is based on the exponential wavefunction ansatz:

$$\Psi_{\mathrm{cc}} = \mathrm{e}^{\hat{T}}\Phi_0 = \left(1 + \hat{T} + \frac{1}{2}\hat{T}^2 + \frac{1}{3!}\hat{T}^3 + \cdots\right)\Phi_0 \tag{29}$$

where $\hat{T} = \hat{T}_1 + \hat{T}_2 + \cdots$ and each operator $\hat{T}_i$ generates the i-fold excitations. In analogy with CI theory, we speak of CCD, CCSD, CCSDT and so forth; in each case we include the appropriate $\hat{T}$ operators in the wavefunction expansion. As in CI theory, the double excitations—the coupling of electrons into two-electron clusters—lie at the very basis of the method, and the corresponding wavefunction for the CCD method is expanded as:

$$\begin{aligned}\Psi_{\mathrm{CCD}} &= \mathrm{e}^{\hat{T}_2}\Phi_0 \\ &= \Phi_0 + \sum_{i<j}^{r<s} t_{ij}^{rs}\Phi_{ij}^{rs} + \sum_{i<j<k<l}^{r<s<t<u} t_{ijkl}^{rstu}\Phi_{ijkl}^{rstu} + \cdots\end{aligned} \tag{30}$$

in which the number of coupling coefficients t_{ij}^{rs} is identical to that in CID. As opposed to CID, however, we note that in CCD we also include the quadruple, hexuple, etc., excitations (up to N-tuples for a system with N electrons). The CCD approach does not only cover the major part of the correlation energy though the double excitations, in addition the components of the higher excitations included in CCD form the major components of these excitations. Taking the expansion one step further and including also the single excitations (CCSD), provides exact results for two-electron correlation for any given choice of orbitals [39]. The inclusion of singles also provides great advantages in terms of orbital choice, and in the treatment of other properties than the energy [40,41].

Adding the triple excitations to the expansion increases the computational requirements considerably, albeit at the same time yielding results for small systems that are frequently used for benchmarking of other, less accurate, methods. Besides the full implementation of triple excitations, CCSDT [42–46] a number of simpler (less computationally demanding) approximations to the inclusion of triples also exist, such as CCSD(T) [47,48], CCSD + T(CCSD) [49] and CCSDT-N [50]. Higher excitations such as quadruples (CCSDTQ) [51] have also been developed and implemented, but are due to very unfavourable scaling mainly though of as reference methods for the lower expansions—i.e. to check the validity of CCSDT and similar for very difficult systems, or to explore the need for multi-reference solutions.

We now return to the simplest case, the CCD approximation, for an illustration of the Schrödinger equation and energy expressions in coupled cluster theory. We begin by defining the Hamiltonian for the electron correlation as:

$$\hat{H}_N = \hat{H} - \langle \Phi_0 | \hat{H} | \Phi_0 \rangle \tag{31}$$

Using Eq. (30) for the wavefunction, the Schrödinger equation then takes the form:

$$\hat{H}_N e^{\hat{T}_2} | \Phi_0 \rangle = \Delta E e^{\hat{T}_2} | \Phi_0 \rangle \tag{32}$$

and

$$\begin{aligned} &\langle \Phi_0 | \hat{H}_N e^{\hat{T}_2} | \Phi_0 \rangle = \Delta E \\ &\langle \Phi_{ij}^{rs} | \hat{H}_N e^{\hat{T}_2} | \Phi_0 \rangle = \Delta E \langle \Phi_{ij}^{rs} | e^{\hat{T}_2} | \Phi_0 \rangle = \Delta E t_{ij}^{rs} \end{aligned} \tag{33}$$

Inserting the projections of Eq. (29) in Eq. (33), we obtain:

$$\begin{aligned} \Delta E = \langle \Phi_0 | \hat{H}_N \hat{T}_2 | \Phi_0 \rangle &= \sum_{i<j}^{r<s} t_{ij}^{rs} \langle \Phi_{ij} | \hat{H}_N | \Phi_0 \rangle \\ &= \sum_{i<j}^{r<s} t_{ij}^{rs} \langle ij || rs \rangle, \\ \Delta E t_{ij}^{rs} = \langle \Phi_{ij}^{rs} | \hat{H}_N | \Phi_0 \rangle &+ \langle \Phi_{ij}^{rs} | \hat{H}_N \hat{T}_2 | \Phi_0 \rangle \\ &+ \langle \Phi_{ij}^{rs} | \hat{H}_N \hat{T}_2^2 | \Phi_0 \rangle \end{aligned} \tag{34}$$

No higher terms than $\hat{T}_2^2$ will contribute due to higher excitations giving vanishing matrix elements. Eq. (34) can be simplified further in terms of canonical orbital equations, yielding expressions involving two-electron integrals of the type above multiplied by various coupling coefficients t_{ij}^{rs} (for a detailed outline, see Refs. [52,53]).

As mentioned above, the CC methods in general are very computationally demanding, both in terms of large storage needed for the large number of integrals and coefficients and, in particular, in terms of the scaling with number of basis functions. The CCSD approach scales as N^6, CCSD + approximately T as N^7, and full CCSDT as N^8. In addition, the methods are—like the MBPT methods described below—non-variational. They are, however, size-extensive, as opposed to truncated CI expansions, and provide results of an accuracy very close to Full CI for a number of molecular (ground state) properties [52,54]. Furthermore, systematic improvements can be made by increasing the series expansion. For example, for a set of small (di- and tri-atomic) molecules, the series CCD, CCSD, CCSD(T), CCSDT and CCSDTQ provide mean absolute errors in energy compared with Full CI results, of 12.8, 7.06, 1.15, 0.78 and 0.03 mhartree [52].

The CC approaches can also be employed in treatments of excited states, through the equation-of-motion (EOM) formalism. This has been used in studies of small system (atoms, di- and tri-atomics) at the EOM-CCSD, EOM-CCSD + approximately *T*, and EOM-CCSDT levels (see Ref. [55], and references therein). For the latter method, an accuracy of between 0.1 and 0.2 eV has been reported. These excited state treatments normally scale as the corresponding parent method.

2.6. Many body perturbation theory (MBPT)

Many body perturbation theory applied in the computational quantum chemistry context, is also referred to as Moller-Plesset perturbation theory (MPPT) [56]. The method is based on applying Rayleigh–Schrödinger perturbation theory [57] on the HF Hamiltonian, and treating the non-HF part (the electron correlation) as a perturbation. The level of the perturbation theory expansion employed in the computation enters as an index; e.g., MP2 for second-order perturbation theory.

The derivation of the main equations is straightforward. Consider $\hat{H}_0$, the zeroth order Hamiltonian formed by summing the one-electron Fock-operators $\hat{f}(i)$ of Eq. (17), and define $\hat{H}_\lambda$ as a generalized electronic Hamiltonian given by the expression:

$$\hat{H}_\lambda = \hat{H}_0 + \lambda \hat{\mathcal{V}} \tag{35}$$

The corresponding total energy to zeroth order, E_0, is given by the Schrödinger equation:

$$\hat{H}_0 | \Psi \rangle = E_0 | \Psi \rangle \tag{36}$$

and is the sum of the one-electron energies ϵ_i, as shown in Eq. (18). The perturbation, $\lambda\hat{\mathcal{V}}$, of Eq. (35) is by definition the electron–electron interation term $\hat{\mathcal{V}}$ multiplied by an order parameter (λ). The order parameter will, after the correct expansions have been made, be set to unity.

The next step is to expand the total wave function and energy corresponding to the generalized Hamiltonian (Eq. (35)) as a Taylor series. This gives

$$E_\lambda = E^{(0)} + \lambda E^{(1)} + \lambda^2 E^{(2)} + \cdots \tag{37}$$

$$|\Psi_\lambda\rangle = |\Psi^{(0)}\rangle + \lambda |\Psi^{(1)}\rangle + \lambda^2 |\Psi^{(2)}| + \cdots \tag{38}$$

We then insert these expansions in the Schrödinger equation of $\hat{H}_\lambda$, and collect terms of equal order in λ. We thereby

obtain a new set of equations:

$$\begin{aligned}
&\lambda^0 : \hat{H}_0|\Psi^{(0)}\rangle = E^{(0)}|\Psi^{(0)}\rangle \\
&\lambda^1 : \hat{H}_0|\Psi^{(1)}\rangle + \hat{\mathcal{V}}|\Psi^{(0)}\rangle = E^{(0)}|\Psi^{(1)}\rangle + E^{(1)}|\Psi^{(0)}\rangle \\
&\lambda^2 : \hat{H}_0|\Psi^{(2)}\rangle + \hat{\mathcal{V}}|\Psi^{(1)}\rangle = E^{(0)}|\Psi^{(2)}\rangle + E^{(1)}|\Psi^{(1)}\rangle \\
&\qquad\qquad + E^{(2)}|\Psi^{(0)}\rangle \\
&\cdots
\end{aligned} \tag{39}$$

If we assume the energies to be non-degenerate, the zeroth-order equation of Eq. (39) becomes identical to the unperturbed equation Eq. (36). The first-order equation of Eq. (39) can then be rewritten as:

$$(\hat{H}_0 - E^{(0)})|\Psi^{(1)}\rangle + (\hat{\mathcal{V}} - E^{(1)})|\Psi^{(0)}\rangle = 0 \tag{40}$$

Multiplying with $\langle\Psi^{(0)}|$ we have

$$\langle\Psi_0|\hat{H}_0 - E^{(0)}|\Psi^{(1)}\rangle + \langle\Psi^{(0)}|\hat{\mathcal{V}} - E^{(1)}|\Psi^{(0)}\rangle = 0 \tag{41}$$

Using the Hermiticity of the Hamiltonian operator, it can be shown after some manipulation that the left integral of Eq. (41) is equal to zero, and hence

$$\langle\Psi^{(0)}|\hat{\mathcal{V}}|\Psi^{(0)}\rangle = \langle\Psi^{(0)}|E^{(1)}|\Psi^{(0)}\rangle \tag{42}$$

or

$$E^{(1)} = \frac{\langle\Psi^{(0)}|\hat{\mathcal{V}}|\Psi^{(0)}\rangle}{\langle\Psi^{(0)}|\Psi^{(0)}\rangle} \tag{43}$$

Thus, $E^{(1)}$ is the expectation value of the electron–electron repulsion term, using the unperturbed wave function. This allows us to identify the HF-energy as:

$$E_{\mathrm{HF}} = E^{(0)} + E^{(1)} \tag{44}$$

i.e., the HF energy is given by the MPPT energy to the first order, in accordance with our earlier result of Eq. (19).

The first-order correction to the wave function is obtained by assuming that each element $|\Psi_j^{(1)}\rangle$ of the total first order wave function $|\Psi^{(1)}\rangle$ can be expanded in a basis of the unperturbed wave functions:

$$|\Psi_j^{(1)}\rangle = \sum_i c_{ij}|\Psi_j^{(0)}\rangle \tag{45}$$

Inserting Eq. (45) into the one-particle form of the first order expression Eq. (40), we get

$$\sum_i c_{ij}(\hat{H}_0 - E_j^{(0)})|\Psi_j^{(0)}\rangle + (\hat{\mathcal{V}} - E_j^{(1)})|\Psi_j^{(0)}\rangle = 0 \tag{46}$$

Multiplying from the left with the bra $|\Psi_j^{(0)}\rangle$ gives, after a procedure analogous to that of Eqs. (41)–(43):

$$c_{ij} = \frac{\langle\Psi_i^{(0)}|\hat{\mathcal{V}}|\Psi_j^{(1)}\rangle}{E_j^{(0)} - E_i^{(0)}} = \frac{\mathcal{V}_{ij}}{E_j^{(0)} - E_i^{(0)}} \tag{47}$$

and thus

$$|\Psi_j^{(1)}\rangle = \sum_{i<j} \frac{\mathcal{V}_{ij}}{E_j^{(0)} - E_i^{(0)}}|\Psi_i^{(0)}\rangle \tag{48}$$

Turning now to the equations for the second order energy correction $E^{(2)}$ we start off by multiplying the corresponding second order expression in λ of Eq. (39) by $|\Psi_j^{(0)}\rangle$:

$$\begin{aligned}
&\langle\Psi^{(0)}|\hat{H}_0 - E^{(0)}|\Psi^{(2)}\rangle + \langle\Psi^{(0)}|\hat{\mathcal{V}} - E^{(0)}|\Psi^{(1)}\rangle \\
&= E^{(2)}\langle\Psi^{(0)}|\Psi^{(0)}\rangle
\end{aligned} \tag{49}$$

In analogy with the derivation of the expression for $E^{(1)}$ the first integral on the LHS is zero. The integral on the RHS is from normalization equal to unity. Eq. (49) thus becomes:

$$\begin{aligned}
E^{(2)} &= \langle\Psi^{(0)}|\hat{\mathcal{V}} - E^{(1)}|\Psi^{(1)}\rangle \\
&= \langle\Psi^{(0)}|\hat{\mathcal{V}}|\Psi^{(1)}\rangle + E^{(1)}\langle\Psi^{(0)}|\Psi^{(1)}\rangle
\end{aligned} \tag{50}$$

Using the orthogonality of $|\Psi^{(0)}\rangle$ and $|\Psi^{(1)}\rangle$ together with the expression for the first order wave function, Eq. (48), we can rewrite Eq. (50) as:

$$E^{(2)} = \sum_{i<j} \frac{\mathcal{V}_{ij}\mathcal{V}_{ji}}{E_j^0 - E_i^0} \tag{51}$$

This is the first correction to the HF energy, and hence provides a first estimate of the correlation energy, i.e.

$$E^{(0)} + E^{(1)} + E^{(2)} = E_{\mathrm{HF}} + E^{(2)} = E_{\mathrm{MP2}} \tag{52}$$

Inserting the one-electron HF-equations explicitly into the perturbation expansions we note that (recall Eq. (17))

$$\hat{H}_0 = \sum_i \hat{f}(i) = \sum_i (\hat{h}(i) + u(i)) \tag{53}$$

and

$$\hat{\mathcal{V}} = \sum_{ij} \frac{1}{r_{ij}} - \sum_i u(i) \tag{54}$$

Letting $\lambda = 1$, the total Hamiltonian thus takes the form:

$$\hat{H} = \hat{H}_0 + \mathcal{V} = \sum_i \hat{h}(i) + \sum_{ij} \frac{1}{r_{ij}} \tag{55}$$

As noted above (Eq. (36)), the energy of the unperturbed system is the sum of the single-particle energies:

$$E^{(0)} = \sum_a \epsilon_a \tag{56}$$

and since the first order correction to the energy is the expectation value of the electron–electron repulsion operator r_{ij}^{-1}, we can thus write the HF energy as:

$$E^{\mathrm{HF}} = E^{(0)} + E^{(1)} = \sum_a \epsilon_a - \frac{1}{2}\sum_{a,b}\langle ab||ab\rangle \tag{57}$$

The integral of Eq. (57) is shorthand notation for Coulomb-exchange (a and b denoting occupied orbitals ψ_a and ψ_b, respectively), in analogy with Eq. (15).

From the above equations, the observation can now be made that in order to find the first-order corrections to the wave function, and thus the second-order correction to the energy, we must find a good representation of the excited states Ψ_j, assuming the unperturbed manifold Ψ_i to be the HF wave functions. Using Brillouin's theorem, it can readily be shown that the Ψ_j cannot be the singly excited states. Furthermore, due to the two-electron nature of the potential operators, the integrals between ground state and triply or higher excited states also vanish. The natural choice for the expansions of the Ψ_j is hence the doubly excited states. Assuming the excitations to have occurred from orbitals a and b to virtual orbitals r and s, the expression for the second-order correction to the energy can thus be written as:

$$E^{(2)} = \frac{1}{4}\sum_{a,b,r,s}\frac{|\langle ab||rs\rangle|^2}{(\epsilon_a+\epsilon_b)-(\epsilon_r+\epsilon_s)} = \frac{1}{2}\sum_{a,b,r,s}\frac{\langle ab|rs\rangle\langle rs|ab\rangle}{(\epsilon_a+\epsilon_b)-(\epsilon_r+\epsilon_s)} - \frac{1}{2}\sum_{a,b,r,s}\frac{\langle ab|rs\rangle\langle rs|ba\rangle}{(\epsilon_a+\epsilon_b)-(\epsilon_r+\epsilon_s)} \quad (58)$$

Following the above schemes, the third and higher order perturbation corrections can also readily be derived, although the expressions quickly become very complex. In terms of computational applications, MP2 and MP4(SDTQ) are the most commonly used MPPT corrections. MP3, on the other hand, albeit giving a lower total energy than does MP2, it provides very little improvement to the wave functions and properties.

The MPPT methods have the advantage of being size consistent, i.e., the correlation energy per particle scales linearly as the number of particles increases. This means that results of calculations on different systems using the same level of MPPT are comparable. This is a great advantage over systems based on, e.g., a truncated configuration interaction expansion, which are not size consistent. On the other hand the latter methods obey the variational principle, whereas MPPT methods do not. As a consequence, MPPT (and in particular MP2) calculations have been shown to overestimate the correlation energy.

In terms of computational time, the estimated CPU time for MP2 calculations are approximately 1.5 times the corresponding HF calculations, whereas for MP3 and MP4 factors 3.6 and 5.8 have been reported, respectively.

2.7. Quantum Monte Carlo

A wide range of methods is included in the general name of Quantum Monte Carlo. The name comes from the fact that the Monte Carlo technique is used for the evaluation of the integrals, where the functions involved are quantum wave functions. Nowadays the most widely used QMC methods are Variational Quantum Monte Carlo (VMC) and Diffusion Quantum Monte Carlo (DMC), although other methods such as Auxiliary Field Quantum Monte Carlo or Path-integral Quantum Monte Carlo have also been developed. In this report we focus on VMC and DMC.

Quantum Monte Carlo methods are powerful tools in order to calculate the correlation energy in a very accurate way. In previous sections of this review other accurate methods for the calculation of correlation energy have been shown.

2.7.1. Trial wave functions

The importance of accurate trial wavefunctions has been mentioned above. This accuracy is crucial in the case of VMC, while it is not so crucial for DMC as we will see later. However, since the calculation of the trial wave function is quite time consuming, it is necessary to use of wavefunctions that are both accurate and easy to evaluate. A common form employed in QMC calculations are the so-called Slater–Jastrow [58] wavefuntions:

$$\Psi(X) = D(X)\mathrm{e}^{J(X)} \quad (59)$$

where $D(X)$ is a Slater-type determinant and $J(X)$ is the Jastrow correlation factor. $X = (x_1, x_2, \ldots, X_N)$ contains the spatial and spin coordinates of all electrons, being $x_i = (r_i, \sigma_i)$. The spin is usually removed from the Slater–Jastrow wavefunction, which is rewritten in the following way:

$$\Psi(R) = D^{\uparrow}(r_1, \ldots, r_n)D^{\downarrow}(r_{n+1}, \ldots, r_N)\mathrm{e}^{J(R)} \quad (60)$$

The Slater determinant has been divided into two smaller ones, one containing the spin-up electrons and the other the spin-down electrons. In addition no sum over the spin coordinates has to be performed. However, the wave-function of Eq. (60) is not antisymmetric with respect to exchange of electrons of different spin, and is therefore different from that of Eq. (59). Nevertheless, the expectation values for spin independent operators are the same in both cases, and therefore the energies obtained with both wavefunctions are the same.

Usually, mono-determinantal wavefunctions are used, and the orbitals are generally calculated using HF or DFT methods, which are described elsewhere in this work. The HF orbitals give the lowest energy, and combined with a good Jastrow factor usually gives accurate results. Some attempts have been done in order to improve the determinantal part of the wave function. Direct numerical optimization of single-particle orbitals [59–63], the use of natural orbitals [64–66], backflow correlation [67], three-body terms within the Jastrow factor [67–70], or multideterminantal Slater–Jastrow wavefunctions [59,71] are some of these attempts.

The Jastrow factor may contain many-body terms, but is usually limited to one- and two-body terms.

$$J(X) = \sum_{i=1}^{N}\chi(x_i) - \frac{1}{2}\sum_{i=1}^{N}\sum_{i=1,\, j\neq i}^{N}u(x_i, x_j)$$

The one-body term contains the electron–nuclear correlation, while the electron–electron correlation is contained in the two-body term. The shape of these terms depends on the system under study. In solids, χ may be represented by plane waves, while in the case of molecules atom-centered functions are more convenient. The shape of u is more complicated. The physics underlying the Jastrow factor is not well understood yet and much effort is being done in this field. We refer the reader to more specialized papers for further details.

We have mentioned above the importance of the quality of the trial wavefunction for the efficiency of the VMC and DMC calculations. In this type of calculations we usually use Slater–Jastrow wave functions, where the Slater determinant is built from Hartree–Fock orbitals. This wave function is on one hand accurate and on the other easy to evaluate. Ideally, one would like to optimize the orbitals and the Jastrow factor at the same time, but usually the Slater determinant is optimized during the HF calculation, and only the Jastrow factor is optimized during the minimization. Depending on the property we want to calculate, different functions can be minimized. For instance, if one wants to calculate the best variational bound on the energy in a VMC calculation, one should minimize the variational energy. It has been suggested that minimizing the energy the efficiency of a DMC calculation is maximized [72]. Another option is to optimize the variance of the energy, which minimizes the error bar of the VMC calculations. Usually the variance of the energy is minimized instead of the energy itself, due to the fact that this is more stable in large systems.

2.7.2. Variational Monte Carlo

This is one of the simplest QMC method. It is based on the variational principle, where the integrals are evaluated according to the Monte Carlo procedure. The reliability of the method depends on the quality of the trial wave function, which has to be a good approximation to the exact solution. In this work, we will deal with Slater–Jastrow type trial wavefunctions, introduced above.

The expectation value of $\hat{H}$ using a trial wavefunction of the type described above gives an upper-bound to the exact energy, as it is known from the variational principle:

$$E_{\text{var}} = \frac{\langle \Psi_{\text{T}}(R)|\hat{H}|\Psi_{\text{T}}(R)\rangle}{\langle \Psi_{\text{T}}(R)|\Psi_{\text{T}}(R)\rangle} \geq E_0 \tag{61}$$

where E_{var} is the variational energy and E_0 is the true energy. In order to perform a VMC calculation Eq. (61) is rewritten as follows:

$$\begin{aligned} E_{\text{var}} &= \frac{\langle (\Psi_{\text{T}}(R)/\Psi_{\text{T}}(R))\Psi_{\text{T}}(R)|\hat{H}|\Psi_{\text{T}}(R)\rangle}{\langle \Psi_{\text{T}}(R)|\Psi_{\text{T}}(R)\rangle} \\ &= \frac{\langle |\Psi_{\text{T}}(R)|^2[\Psi_{\text{T}}^{-1}(R)|\hat{H}|\Psi_{\text{T}}(R)]\rangle}{\langle |\Psi_{\text{T}}(R)|^2\rangle} \end{aligned} \tag{62}$$

The Metropolis algorithm is used to sample a set of points R_m, where $m = 1, \ldots, M$ from the configuration-space probability density. In each of these points the local energy $E_{\text{L}} = \Psi_{\text{T}}^{-1}(R)\hat{H}\Psi_{\text{T}}(R)$ is evaluated and the average accumulated, thereby yielding the VMC energy:

$$E_{\text{VMC}} \approx \frac{1}{M}\sum_{m=1}^{M} E_{\text{L}}(R_m) \tag{63}$$

Usually the moves are sampled from a Gaussian centered on the position of R_m. The variance of the Gaussian is chosen so that the average acceptance probability is roughly 50%.

2.7.3. Diffusion Monte Carlo

The DMC method [73–75] is a stochastic projector method for solving the imaginary-time many-body Schrödinger equation. It is based on the similarity between the Schrödinger equation in imaginary time $\tau = it$

$$\frac{\partial \Phi(r,\tau)}{\partial \tau} = \frac{1}{2m}\nabla^2\Phi(r,\tau) - V(r)\Phi(r,\tau) \tag{64}$$

and the generalized diffusion equation

$$\frac{\partial f(r,t)}{\partial t} = D\nabla^2 f(r,\tau) - k(r)f(r,t) \tag{65}$$

where D is the diffusion constant in Fick's second law, and $k(r)$ is the position-dependent rate constant of a first-order rate equation. Fermi suggested that a random walk in which a particle diffuses and simultaneously multiplies based on the rate constant would eventually give the ground-state wave function. Starting from the formal solution of Eq. (64)

$$\Phi(r,\tau) = \mathrm{e}^{-\tau H}\Phi(r,0)$$

with

$$H = -\frac{1}{2m}\nabla^2 + V(r)$$

and expanding the initial wave function in eigenfunctions of H:

$$\Phi(r,0) = \sum_i a_i\psi_i$$

we obtain the time-dependent solution in terms of the eigenfunctions:

$$\Phi(r,\tau) = \sum_i a_i \mathrm{e}^{-E_i\tau}\psi_i$$

The contributions from excited states decay exponentially compared with the ground state. When a random walk that satisfies the diffusion equation is performed, the exact ground state wave function will be, after sufficient time, obtained. Hence, exact imaginary-time evolution would lead to the exact ground state wave function, provided it has a non-zero overlap with the initial state. This is a fundamental property of the projector $\mathrm{e}^{-\tau H}$, which is the basis of Diffusion Monte Carlo methods.

Let us rewrite Eq. (64) in a different manner

$$-\partial_t\Phi(R,t) = (\hat{H} - E_{\text{T}})\Phi(R,t) \tag{66}$$

where t measures the progress in imaginary time, R is a $3N$-dimensional vector specifying all electronic coordinates and E_T is an energy offset. The importance of E_T will appear below. In order to rewrite Eq. (66) in the integral form we introduce a Green's function:

$$G(R \leftarrow R', \tau) = \langle R|e^{-\tau(\hat{H}-E_T)}|R'\rangle \quad (67)$$

that satisfies the same equation as the wave function with initial condition $G(R \leftarrow R', 0) = \delta(R - R')$. In this way, Eq. (66) is recast into the integral form as follows:

$$\Phi(R, t+\tau) = \int G(R \leftarrow R', \tau)\Phi(R', t)\,dR' \quad (68)$$

The explicit expression for the exact Green's function is not known for the case of the full Hamiltonian with interacting particles. Instead, an approximate expression may be obtained using the Trotter–Suzuki formula for the exponential of a sum of operators. That is

$$G(R \leftarrow R', \tau) = \langle R|e^{-\tau(\hat{T}+\hat{V}-E_T)}|R'\rangle \approx e^{-\tau[V(R)-E_T]/2} \times \langle R|e^{-\tau\hat{T}}|R'\rangle e^{-\tau[V(R')-E_T]/2} \quad (69)$$

For small τ Eq. (69) becomes (76)

$$G(R \leftarrow R', \tau) \approx (2\pi\tau)^{-3N/2} e^{-(R-R')^2/2\tau} e^{-\tau[V(R)+V(R')-2E_T]/2} \quad (70)$$

The factor $P = e^{-\tau[V(R)+V(R')-2E_T]/2}$ is a time-dependent re-weighting of the Green's function. In the branching, or birth–death algorithm, it is used to determine the number of walkers that survive to the next step [76]. If $P < 1$, the walker continues the evolution with probability P. However, if $P \geq 1$ the walker continues, and in addition to it, a new walker with probability $P - 1$ is created. In regions of high potential energy, the walkers disappear, while they proliferate in low potential regions. E_T is used to control the total number of walkers, which is maintained roughly constant through the calculation.

We have been assuming that the wave function is positive everywhere. However, due to the antisymmetry of the wave function, it has positive and negative regions. Unfortunately, DMC can only handle positive values. There are several ways in order to overcome this so-called sign problem, the fixed-node approximation [73,76–78] being the most common one. This method is not exact, but provides a variational upper bound on the ground state energy, and usually is very accurate. The fixed-node variational principle was proved by Moskowitz et al. [78] and Reynolds et al. [76], and the reader is referred to those references for the derivation. Hereafter, we assume that we are dealing with a real Hamiltonian. The idea of the fixed-node approximation is to use a trial wave function to define a trial nodal surface. In an N-electron system the trial wave function is $3N$-dimensional, while the trial nodal surface is the $(3N-1)$-dimensional surface where the wave function is zero. In this way the wave function can be separated into regions with the same sign. Absorbing barriers are placed between different regions, causing the simulation to progress independently in all regions. If a walker changes sign, it is automatically rejected. Within each region the fixed-node DMC method projects out the lowest-energy nodeless wave function satisfying zero boundary conditions on the corresponding nodal surface.

Due to Coulomb singularities in the electronic Hamiltonian, which make the renormalization factor P fluctuate, the described DMC algorithm is inefficient. This is overcome by a procedure called importance-sampling [76,79,80]. In this procedure a guide or trial function (Ψ_T) is used in the calculation, which guides the random walk to regions where the trial function is large. Let us multiply Eq. (66) by $\Psi_T(R)$ and define the new function $f(R, t) = \Phi(R, t)\Psi_T(R)$.

$$-\partial_t f(R,t) = -\frac{1}{2}\nabla^2 f(R,t) + \nabla\cdot[\upsilon_D(R)f(R,t)] + [E_L(R) - E_T]f(R,t) \quad (71)$$

In this equation, we introduce the drift velocity $\upsilon_D(R)$, defined as:

$$\upsilon_D(R) = \nabla \ln|\Psi_T(R)| = \Psi_T(R)^{-1}\nabla\Psi_T(R) \quad (72)$$

and the local energy (as in VMC)

$$E_L(R) = \Psi_T(R)^{-1}\hat{H}\Psi_T(R) \quad (73)$$

We then write the equation in its integral form:

$$f(R, t+t) = \int \bar{G}(R \leftarrow R', \tau)f(R', t)\,dR'$$

where

$$\bar{G}(R \leftarrow R', \tau) = \Psi_T(R)G(R \leftarrow R', \tau)\Psi_T(R')^{-1}$$

For $\bar{G}$ we can form a short-time approximation, as in Eq. (70). Thus

$$\bar{G}(R \leftarrow R', \tau) \approx G_d(R \leftarrow R', \tau)G_b(R \leftarrow R', \tau) \quad (74)$$

where

$$G_d(R \leftarrow R', \tau) = (2\pi r)^{-3N/2} e^{-[R-R'-\tau\upsilon_D(R)^2]/2r} \quad (75)$$

and

$$G_b(R \leftarrow R', \tau) = e^{-\tau[E_L(R)+E_L(R')-2E_T]/2} \quad (76)$$

The consequence of introducing the drift velocity is that the density of walkers is increased in the regions where $\Psi_T(R)$ is large. Moreover, the reweighting factor G_b now contains the local energy instead of the potential energy. The local energy is close to the ground-state energy if the trial wave function is good, and it maintains roughly constant, which drastically reduces the fluctuations. Using importance-sampling DMC simulations can be carried out in systems with hundreds or thousands of electrons.

The result of the process that we have described above is a set of walker positions representing the distribution $f(R, t) = \Phi(R, t)\Psi_T(R)$. Given this distribution, the expectation

value of the energy can be calculated. Normally the so-called mixed estimator is used.

$$E_{\mathrm{d}} = \lim_{\tau\to\infty} \frac{\langle \mathrm{e}^{-\tau\hat{H}/2}\Psi_{\mathrm{T}}|\hat{H}|\mathrm{e}^{-\tau\hat{H}/2}\Psi_{\mathrm{T}}\rangle}{\langle \mathrm{e}^{-\tau\hat{H}/2}\Psi_{\mathrm{T}}|\mathrm{e}^{-\tau\hat{H}/2}\Psi_{\mathrm{T}}\rangle}$$
$$= \lim_{\tau\to\infty} \frac{\langle \mathrm{e}^{-\tau\hat{H}}\Psi_{\mathrm{T}}|\hat{H}|\Psi_{\mathrm{T}}\rangle}{\langle \mathrm{e}^{-\tau\hat{H}}\Psi_{\mathrm{T}}|\Psi_{\mathrm{T}}\rangle} = \frac{\langle \Psi_0|\hat{H}|\Psi_{\mathrm{T}}\rangle}{\langle \Psi_0|\Psi_{\mathrm{T}}\rangle}$$
$$= \lim_{\tau\to\infty} \frac{\int f(R,\tau)E_{\mathrm{L}}(R)\,\mathrm{d}R}{\int f(R,\tau)\,\mathrm{d}R} \approx \frac{1}{M}\sum_m E_{\mathrm{L}}(R_m)$$

where $\{R_m\}$ is the set of M samples of $f(R,\infty)$ resulting from the DMC run. We emphasize that the DMC energies are not limited by the basis set or the detailed form of the orbitals, the DMC energy is fixed only by the nodal surface of the guiding wave function.

2.7.4. Pseudopotentials

Although the computational effort of a DMC calculations scales as the cube of the number of electrons, the scaling [81,82] with the atomic number, Z, of the atoms is approximately $Z^{5.5–6.5}$. Many properties such as the interatomic bonding and low-energy excitations are determined by the behavior of the valence electrons. It is therefore very advantageous to use pseudopotentials in DMC calculations, which reduces the effective value of Z. Errors are introduced, but the gain in computational efficiency is huge and makes applications to heavy atoms possible. The idea of pseudopotentials is to create an effective potential (pseudopotential) in order to reproduce the effect of both the nucleus and the core electrons on the valence electrons. For each angular momentum state this is done separately, and hence the pseudopotential contains angular momentum projectors which are nonlocal operators. Conventionally the pseudopotential $V_l^{\mathrm{ps}}(r)$ is divided into a local part, $V_{\mathrm{loc}}^{\mathrm{ps}}(r)$, common to all angular momenta, and a nonlocal part, $V_{nl,l}^{\mathrm{ps}}(r)$, different for each angular momentum l.

The use of pseudopotentials in VMC is straightforward, and we will not elaborate on this here. In DMC, however, the use of pseudopotentials is more problematic. If the Hamiltonian contains the nonlocal operator $V_{nl,l}^{\mathrm{ps}}(r)$, the propagator contains matrix elements of the form $\langle R|\mathrm{e}^{-\tau\hat{V}_{nl}}|R'\rangle$ which may be positive or negative for any R, R', τ. Therefore, as the population of walkers evolve according to

$$\partial_t f = \frac{1}{2}\nabla^2 f - \nabla\cdot(\upsilon_{\mathrm{D}} f) - \frac{(\hat{H}-E_{\mathrm{T}})\Psi_{\mathrm{T}}}{\Psi_{\mathrm{T}}} f + \left\{\frac{\hat{V}_{nl}\Psi_{\mathrm{T}}}{\Psi_{\mathrm{T}}} - \frac{\hat{V}_{nl}\Phi}{\Phi}\right\} f \qquad (77)$$

the sign of a walker can change as time evolves. This is a problem similar to the sign problem presented before. In order to overcome this problem, the terms containing $V_{nl,l}^{\mathrm{ps}}(r)$ are neglected, making Eq. (77) formally equivalent to an imaginary-time Schrödinger equation with local potentials. This procedure is called the pseudopotential localization approximation. If the trial wave function is a good approximation to the exact wave function, the error is proportional to $(\Psi_{\mathrm{T}}-\Psi_0)^2$, [83]. It is thus important to use accurate trial wave functions such as the Slater–Jastrow type wave functions introduced earlier. Hartree–Fock pseudopotentials have been shown to give better results than density functional theory (DFT) ones when used DMC calculations [84]. Unfortunately the Hartree–Fock pseudopotentials available within the quantum chemistry literature usually diverge at the origin, normally like $1/r^2$ or $1/r$. These divergences lead to large “time-step" errors and even instabilities in DMC calculations [85].

3. Density functional methods

In the field of applied computational chemistry, density functional normally stands for the Kohn–Sham implementation of the theory. Although the initial approaches to the theory can be traced back as far as to the statistical method, independently proposed by Thomas [86] and Fermi [87] (in which the electron density of polyelectronic atoms is treated *locally* as a Fermi gas in which the free-electron relations apply), the Kohn–Sham implementation has gained ground recently mainly due to its similarity with the self-consistent-field Hartree–Fock method.

Compared to high-level ab initio molecular orbital procedures, DFT is substantially simpler and requires less computational resources to give similar results. DFT, therefore, has arisen as the theory of choice in an increasing number of gas phase ion chemistry studies [88].

In essence, the Kohn–Sham formulation of density functional theory relies on the fact that the electron density of the ground state of a system, can be computed as the density of a system of independent particles, moving in an effective one-particle potential, whose precise formal construction forms part of the method. Once this effective potential has been determined, the Kohn–Sham method solves self consistently the nonlinear Kohn–Sham equations which contain an unknown *exchange-correlation* functional [89–91]. The *exchange-correlation* functional contains the description of the electron–electron interactions within the system. This is the difficult part of the theory and still remains far from being well understood. Nevertheless, some authors claim that the reason of the highly accurate DFT estimates of many molecular properties [92–97] stem from the well-balanced account that DFT makes of dynamical and non-dynamical electron correlation [98].

This point is supported further by comparing the Kohn–Sham potentials constructed (i) by taking the functional derivative of the multireference configuration interaction exchange and correlation energy with respect to the electron density [99], with (ii) those regularly used in density functional theory. Namely, it is seen that the dynamical correlation is carried by the correlation functional and the non-dynamical correlation by the exchange functional [100,101].

This is a fundamental point. Recall that most chemical processes involve changes of the electronic configurations of the species involved. Thus, keeping the balance of dynamical and non-dynamical electron correlations in the *exchange-correlation* functional is crucial to obtain reliable predictions [102].

However, in spite of the claims made, there is still considerable semantic confusion and difference of opinion about the relationship between the *exchange-correlation* functional(s) and the *electron correlation* in many electron systems.

In the ab initio molecular orbital theory, Lowdin's definition of electron correlation [103] has been adopted as the standard definition. That is, "*the electron correlation is the difference between the exact eigenvalue of the Hamiltonian and its expectation value in the Hartree–Fock approximation*". To use this definition to find the electron correlation energy contained in a particular calculation it is necessary to be able to compare the results to those of a corresponding calculation at the Hartree–Fock limit. When the calculation *does not* involve conventional ab initio methods, such a comparison may, however, have limited value.

The theoretical foundation for the Kohn–Sham method is the Hohenberg–Kohn theorem [104], which demonstrates that the nondegenerate ground state energy and potential of the exact Hamiltonian can be expressed in terms of unique, universal functionals of the electron density. No reference is made in the proof to the Hartree–Fock level of approximation. That is, the approximations made in DFT enter at the level of the Hamiltonian, when an approximate form for the functional is chosen. This confers different meanings to a number of "concepts" that are used by both molecular orbital and density functional theories under the same name.

One example is the orbital energies in the two approaches. The Hartree–Fock orbital energies represent unrelaxed ionization energies; i.e., the energy required to remove an electron from that orbital to infinity when the other orbitals are kept frozen. In DFT, on the other hand, the orbital energies are derivatives of the total energy with respect to the occupation number of the orbital. They are differential rather that finite-difference quantities. This has raised some interesting discussions about the legitimacy of Kohn–Sham orbitals as to interpret molecular electronic configurations [105,106].

Another example is the *self interaction correction* (SIC), which arises from the incomplete cancellation of the electron–electron self interaction energy carried by the Coulomb electron–electron repulsion energy term. Molecular orbital theory is SIC free by construction because the exchange operator cancels out exactly the self-interaction energy of the Coulomb electron–electron repulsion operator (see Eq. (16)). However, in DFT, since approximate *exchange-correlation* functionals are used, the cancellation of the electronic self-energy is not guaranteed. This can be one of the most serious problems of density functional theory [107] and, although some corrections have been proposed [108] and implemented [109] in current electronic structure packages, many uncertainties remain.

Another serious problem that current density functional methods face are the difficulties found in the proper description of van der Waals interactions. The problem, originally reported by Zaremba and Kohn [110] has received considerable attention since then [111–119]. The interest arises from the fact the current approximate *exchange-correlation* functionals do not reproduce long range forces which extend over regions of space with vanishingly small electron density. Savin and coworkers [120], Gill and coworkers [121] and Hirao and coworkers [119] have recently suggested a procedure to estimate the short- and long-range exchange interaction energies independently. In this scheme, the error function is used to separate the short and long range parts of the $1/r_{ij}$ electron–electron interaction operator and then, the short range is calculated as a functional of the density, while the long range is calculated by the Hartree–Fock exchange integral. The use of the Hartree–Fock exchange integral for the estimation of the long range interactions stems from the fact in the vanishing electron density regions the electrons should mainly be affected by the exchange effects, since dynamical correlation effects decay fast as the electrons separate. Indeed, it is well known that both the Moller–Plesset second order perturbation theory and the coupled cluster singles and doubles methods can be transformed to make the electron correlation effects decay as $\mathcal{O}(r_{ij}^{-6})$ when $r_{ij} \to \infty$, while the Hartree–Fock exchange energy integrals decay only as $\mathcal{O}(r_{ij}^{-1})$ [122,123].

The Kohn–Sham equations were originally formulated for closed-shell systems for which a fictitious noninteracting system is set up, such that the electron densities of both systems is the same Therefore, once the Kohn–Sham equations of the latter system are solved for the orbitals, then the electron density is calculated as the sum of the squares of the occupied orbitals, the same way as we obtain the density of single determinant formed with these orbitals. However, in many cases even the fictitious noninteracting system cannot be represented by a single determinant. The paradigm for this case is the stretched hydrogen molecule, where two determinants are required for a proper description of the system (see Eq. (21)). Many other situations, like for instance, the potential energy curves far from equilibrium, the characterization of structures with biradicaloid character or near-degenerate configurations, are also well-known to require a multiconfigurational reference.

This has motivated several attempts to combine multiconfigurational wave functions with density functional theory. The strategy followed has been to equate the nondynamical electron correlation with the exchange correlation and to assume that it is carried in full by the reference multiconfigurational wave function. Then, the calculation is complemented with a *correlation* functional for the description of the remaining dynamical electron correlation. However, the main difficulty found to proceed is to handle properly the problem of double counting of the dynamical correlation energy already accounted for by the reference multiconfigurational wave function [124]. This has been found to be a difficult task

since the non-dynamical and the dynamical components of the electron correlation in most cases are not easily separable [125].

Despite the many developments made since the seminal work of Lie and Clementi [126,127], which can be traced back from the recent account of McDouall [124], this is still an area of intense research which awaits a successful end.

In the Kohn–Sham DFT method, there are two different kinetic energies that should not be mixed up. On the one hand we have the kinetic energy of the real system and, on the other hand, we have the kinetic energy of the fictitious noninteracting system which is a toy system employed to calculate the electron density of the real system. This electron density enters in the functional expressions that give the total energy of the system of interest. However, we do not know the kinetic energy functional neither for the real system nor for the fictitious system. The practical implementation of the Kohn–Sham DFT method relies on the assumption that one can approximate reasonably well the kinetic energy of the real system by the kinetic energy of the fictitious system calculated in terms of its Kohn–Sham orbitals. The difference is subsumed into the *exchange-correlation* functional, which therefore, contains additionally, a correction term for the kinetic energy.

From a practitioners point of view, density functional theory is nowadays crowded with a number of acronyms with little physical meaning. Indeed, since there is not a clearly established hierarchy for the systematic improvement of the exchange-correlation functionals available in modern electronic structures packages, the field is becoming increasingly messy.

The recent tendency towards the parameterization of the exchange-correlation functionals does not help shedding light on the problem. For instance, it has been found that increasing the parameterization [128,129] of the exchange-correlation functionals, improves the description of the electronic properties because of the additional *flexibility* gained. However, it is our feeling that this overi-parameterization induces considerable additional confusion among regular practitioners aiming to use the calculations to support or rationalize their experimental results.

3.1. The Hohenberg–Kohn theorem

That the electron density is a singular quantity in electronic structure theory is a well-known fact. Thus, if we know the electron density we can already obtain some relevant information about the system, as demonstrated by Bader [130], through his many developments made on the topological analysis of $\rho(\mathbf{r})$. It is nowadays well established that the analysis of the electron density, $\rho(\mathbf{r})$, and its associated gradient $\vec{\nabla}\rho(\mathbf{r})$, and Laplacian $\nabla^2\rho(\mathbf{r})$, tells us much about the chemical bonding within the molecule [88].

In particular, the peaks of $\rho(\mathbf{r})$ reveal the position of the nuclei, RA, and, from Kato's nucleus–electron cusp condition [131–134]:

$$-\frac{1}{2}\left(\frac{\partial \log\rho(\mathbf{r})}{\partial \mathbf{r}}\right)_{\mathbf{r}\to\mathbf{R}_A} = Z_A, \quad \forall A \tag{78}$$

we can readily obtain the charge, Z_A, of the nucleus at RA. Therefore, the molecular identity and geometry are derived from the electron density. Clearly, this fixes the electron–nuclei attraction potential and, since the integration of the electron density over space determines the number of electrons, the Hamiltonian operator of the system, Eq. (7), is also determined.

Consequently, given an electron density ρ, we can built its associated Hamiltonian operator and, from its solution, we obtain its associated wave function. Namely, there exist a functional relation between the electron density and the wave function, and therefore with all observable properties of the system. Whether this relationship is unique is not obvious.

The Hohenberg–Kohn theorem [104] represents one crucial step in this direction. Actually, they demonstrated that all the observable properties of a time-independent, interacting system of many identical particles are uniquely determined by the ground-state electron density.

Suppose that we have a system whose nuclei of charge $\{Z_A\}_{A=1}^M$, are located at $\{\mathbf{R}_A\}_{A=1}^M$. With this information we can univocally write down the interaction of the N electrons with the M nuclei as:

$$\begin{aligned}\hat{V} &= \sum_{i=1}^{N}\sum_{A=1}^{M}\frac{-Z_A}{|\mathbf{r}_i-\mathbf{R}_A|}\\ &= \int d\mathbf{r}\sum_{i=1}\delta(\mathbf{r}-\mathbf{r}_i)\left[\sum_{A=1}^{M}\frac{-Z_A}{|\mathbf{r}_i-\mathbf{R}_A|}\right]\\ &= \int d\mathbf{r}\hat{\rho}(\mathbf{r})\upsilon(\mathbf{r})\end{aligned} \tag{79}$$

where $\hat{\rho}(r)=\sum_{i=1}^{N}\delta(\mathbf{r}-\mathbf{r}_i)$ is the electron density operator and, $\upsilon(\mathbf{r})$ is the so-called *external potential* of an electron. This operator V determines *uniquely* the electronic Hamiltonian of Eq. (9), because the remaining operators, the kinetic energy operator T and, the electron–electron repulsion operator U, depend exclusively on the coordinates of the electrons and their forms are the same for all systems, depending only on the number of electrons. Thus, the total electronic energy of the system depends only on the number of electrons, N, and the external potential $\upsilon(\mathbf{r})$.

Suppose, now, that we have solved the Schrödinger equation for H. Let Ψ be the ground state wave function. Then the electron density can be determined as:

$$\rho(\mathbf{r}) = \langle\Psi|\hat{\rho}|\Psi\rangle \tag{80}$$

The important message here is that given the external potential the electron density is *uniquely* determined. The converse is not obvious and its proof constitutes the seminal contribution made by Hohenberg and Kohn.

3.1.1. The proof of the theorem

The original proof of the theorem is, however, simple and beautiful. Assume that there are two *different* external potentials $\upsilon(\mathbf{r})$ and $\upsilon'(\mathbf{r})$ that yield the *same* electron density $\rho(\mathbf{r})$. These two different external potential generate, through Eq. (79), different operators $\hat{V}$ and $\hat{V}'$, which yield two different Hamiltonians $\hat{H}$ and $\hat{H}'$. The ground states of $\hat{H}$ and $\hat{H}'$ are also different, Ψ and Ψ', with energies E and E'.

Now, if the ground states of H and H' are nondegenerate

$$E' = \langle\Psi'|\hat{H}'|\Psi'\rangle < \langle\Psi|\hat{H}'|\Psi\rangle = \langle\Psi|\hat{H} + \hat{V}' - \hat{V}|\Psi\rangle$$
$$= E + \int \mathrm{d}\mathbf{r}[\upsilon'(\mathbf{r}) - \upsilon(\mathbf{r})]\rho(\mathbf{r}) \tag{81}$$

Alternatively

$$E' = \langle\Psi|\hat{H}|\Psi\rangle < \langle\Psi'|\hat{H}|\Psi'\rangle = \langle\Psi'|\hat{H}' + \hat{V} - \hat{V}'|\Psi'\rangle$$
$$= E' + \int \mathrm{d}\mathbf{r}[\upsilon(\mathbf{r}) - \upsilon'(\mathbf{r})]\rho(\mathbf{r}) \tag{82}$$

where in the last line we have used the assumption that

$$\langle\Psi'|\rho'|\Psi'\rangle = \rho(\mathbf{r}) = \langle\Psi|\hat{\rho}|\Psi\rangle \tag{83}$$

Adding the two inequalities we obtain

$$E' + E < E + E' \tag{84}$$

This result is inconsistent and proves that one assumption is *false*. Thus, the ground state electron density $\rho(\mathbf{r})$ associated with $\upsilon(\mathbf{r})$ cannot be reproduced by the ground state for a different potential $\upsilon'(\mathbf{r})$, and there is a one-to-one connection between the ground state electron densities and the corresponding external potentials.

The Hohenberg–Kohn theorem shows that the electron density uniquely determines the external potential. But the external potential uniquely determines the wave function, through the Schrödinger equation. Thus, the electron density uniquely determines the wave function, Ψ can be seen as a functional of ρ. This in turn implies that the expectation value of any observable is also a functional of the electron density:

$$O[\rho] = \langle\Psi[\rho]|\hat{O}|\Psi[\rho]\rangle \tag{85}$$

As formulated here, the Hohenberg–Kohn theorem establishes the one-to-one correspondence between electron densities ρ that are obtained from the reduction of an N-electron wave function by Eq. (80), and those external potentials whose Hamiltonians possess ground states. Finally, there are two extensions of the Hohenberg–Kohn theorem that need to be mentioned. Mermin [135] has generalized the original Hohenberg–Kohn theorem to finite temperatures and, Rajagopal and Callaway [136] have formulated the relativistic extension of the theorem. We refer to the interested reader to the respective original references.

3.1.2. The Levy formulation

The proof of the Hohenberg–Kohn theorem as presented above applies only to υ-representable densities, that is, only to those electron densities associated with the antisymmetric ground state wave function obtained from a Hamiltonian containing the external potential $\upsilon(\mathbf{r})$. However, not all densities, ρ, come from a single particle external potential $\upsilon(\mathbf{r})$, i.e., not all densities are υ-representable.

However, Levy [137,138] presented a formulation of DFT that eliminates the constraint of υ-representability for the electron density imposed in the proof of the Hohenberg–Kohn theorem. Levy proposed a constrained search approach based upon the bounding properties of the Schrödinger equation. The prescription has the additional advantage that it eliminates the requirement that only nondegenerate ground states can be considered.

3.1.3. The energy variational principle

Define

$$F[\rho] = \langle\Psi[\rho]|[\hat{T} + \hat{U}]|\Psi[\rho]\rangle = T[\rho] + U[\rho] \tag{86}$$

As shown above, the energy can be expressed as:

$$E[\rho] = F[\rho] + \int \mathrm{d}\mathbf{r}\rho(\mathbf{r})\upsilon(\mathbf{r}) \tag{87}$$

Now consider another electron-density $\rho'(\mathbf{r}) \neq \rho(\mathbf{r})$, associated through the above demonstrated one-to-one relationship with another external potential υ'. Then

$$E[\rho'] = F[\rho'] + \int \mathrm{d}\mathbf{r}\rho'(\mathbf{r})\upsilon(\mathbf{r})$$
$$= \langle\Psi'[\rho']|[\hat{T} + \hat{U} + \hat{V}]|\Psi'[\rho']$$
$$> \langle\Psi[\rho]|[\hat{T} + \hat{U} + \hat{V}]|\Psi[\rho]\rangle = E[\rho] \tag{88}$$

This shows that the functional $E_\upsilon[\rho]$ achieves its minimum value for the true ground state electron density associated with the external potential υ.

Consequently the following variational equation:

$$\frac{\delta E[\rho]}{\delta\rho(\mathbf{r})} - \mu = 0 \tag{89}$$

where the Lagrange multiplier μ ensures that the electron density is N normalized, that is

$$\int \mathrm{d}\mathbf{r}\rho(\mathbf{r}) = N \tag{90}$$

determines the energy functional of the electron density.

The quantity μ of Eq. (89) is the *chemical potential* and measures the escaping tendency of the electronic cloud when the system is equilibrium. It is a constant for all points in space and, it equals the slope of the energy at varying electron density for the ground state of the system. The analogy with the ordinary chemical potential of macroscopic systems is clear as recognized by Parr [139]. Indeed, since the energy of

the system depends on the external potential and the number of electrons, we have that:

$$dE = \left(\frac{\partial E}{\partial N}\right)_{\upsilon} dN + \int \left(\frac{\delta E}{\delta \upsilon(\mathbf{r})}\right)_{\rho} \delta\upsilon(\mathbf{r})\, d\mathbf{r} \tag{91}$$

and since differentiating Eq. (90):

$$\int d\mathbf{r}\delta\rho(r) = dN \tag{92}$$

Eq. (91) can be cast as:

$$dE = \int \left(\frac{\delta E}{\delta \rho(\mathbf{r})}\right)_{\upsilon} \delta\rho(\mathbf{r})\, d\mathbf{r} + \int \left(\frac{\delta E}{\delta \upsilon(\mathbf{r})}\right)_{\rho} \delta\upsilon(\mathbf{r})\, d\mathbf{r} \tag{93}$$

Using Eq. (89) and remembering that μ is constant through all space, we obtain

$$dE = \mu\, dN + \int \left(\frac{\delta E}{\delta \upsilon(\mathbf{r})}\right)_{\rho} \delta\upsilon(\mathbf{r})\, d\mathbf{r} \tag{94}$$

Comparison with Eq. (91) leads to the new definition for the chemical potential as the derivative of the energy with respect to the number of electrons at constant external potential:

$$\mu = \left(\frac{\partial E}{\partial N}\right)_{\upsilon} \tag{95}$$

Similarly, from Eq. (87) we obtain that

$$\left(\frac{\delta E}{\delta \upsilon(\mathbf{r})}\right)_{\rho} = \rho(\mathbf{r}) \tag{96}$$

which under substitution into Eq. (94) leads to the fundamental equation for the chemical reactivity

$$dE = \mu\, dN + \int \rho(\mathbf{r})\delta\upsilon(\mathbf{r})\, d\mathbf{r} \tag{97}$$

This equation provides the framework for the precise formulation of concepts relating to chemical reactivity.

For example, electronegativity has been identified [140] with the negative of the chemical potential:

$$\chi = -\mu \tag{98}$$

Differentiation with respect to the number of particles renders global properties, whereas differentiation with respect to the external potential yields properties of a local nature. Hence, from Eq. (95) we can see that the chemical potential is global. In addition, being that μ is a function of N and a functional of $\upsilon(r)$, we obtain upon full differentiation that

$$d\mu = \eta\, dN + \int f(\mathbf{r})\, d\upsilon(\mathbf{r})\, d\mathbf{r} \tag{99}$$

where

$$\eta = \left(\frac{\partial \mu}{\partial N}\right)_{\upsilon(\mathbf{r})} = \left(\frac{\partial^2 E}{\partial N^2}\right)_{\upsilon(\mathbf{r})} \tag{100}$$

is the global hardness of the system [141], and

$$f(\mathbf{r}) = \left[\frac{\delta \mu}{\delta \upsilon(\mathbf{r})}\right]_N = \left(\frac{\partial \rho(r)}{\partial N}\right)_{\upsilon(\mathbf{r})} \tag{101}$$

is the Fukui function [142]. The global hardness can be viewed as a resistance of the system towards charge transfer, and is together with the chemical potential and the global softness (the inverse of the global hardness: $S = 1/\eta$) among the most important properties aimed at describing chemical reactivity. The global softness has been related to dipole polarizabity [143] as well as other chemical concepts like molecular valence [144]. Approximate connections of μ and η to measurable or more readily accessible quantities such ionization potentials, I, electron affinities, A, and the HOMO and LUMO energies, ϵ_{HOMO} and ϵ_{LUMO}, have also been proposed [145,146] and extensively applied:

$$\mu = -\frac{1}{2}(I + A) \approx \frac{1}{2}(\epsilon_{\mathrm{HOMO}} + \epsilon_{\mathrm{LOMO}}) \tag{102}$$

and

$$\eta = \frac{1}{2}(I - A) \approx \frac{1}{2}(\epsilon_{\mathrm{LOMO}} - \epsilon_{\mathrm{HOMO}}) \tag{103}$$

During a chemical reaction, the ground state electron density is redistributed, which may be rationalized in terms of the response of the system as the number of particles N and/or the external potential $\upsilon(\mathbf{r})$ changes. As seen above, the response to variations in N for a fixed potential is measured by the global properties, whereas the local properties such as the Fukui functions describe the response in the case of constant number of particles but varying $\upsilon(\mathbf{r})$. That is to say, the sensitivity of the chemical potential towards external perturbations at a certain point. Being that it is a local property, the Fukui functions provide information related to the reactivity at different sites (atoms, fragments) within a molecule. The concept as such relates back to the frontier orbital theory introduced by Fukui, as a factor governing the regioselectivity of chemical reactions [147].

Analyzing the chemical potential and its derivatives a bit closer we note the important property that μ is discontinuous for integer N. Hence, numerical derivation from the left or from the right allows us to introduce three new definitions of the Fukui functions:

$$\begin{aligned}
f(\mathbf{r})^{+} &= \left(\frac{\partial \rho(\mathbf{r})}{\partial N)}\right)^{+}_{\upsilon(\mathbf{r})}, && \text{governing nucleophilic attack}\\
f(\mathbf{r})^{-} &= \left(\frac{\partial \rho(\mathbf{r})}{\partial N)}\right)^{-}_{\upsilon(\mathbf{r})}, && \text{governing electrophilic attack}\\
f(\mathbf{r})^{0} &= \left(\frac{\partial \rho(\mathbf{r})}{\partial N)}\right)^{0}_{\upsilon(\mathbf{r})}, && \text{governing radical attack}
\end{aligned} \tag{104}$$

Eq. (104) expresses the reactivity index in case of reaction without charge exchange, and can be approximated by use of the average potential $\mu^0 = (\mu^+ + \mu^-)/2$. The function $f^{+}(\mathbf{r})$ is associated with LUMO of the system, and hence measures the

reactivity towards a donor agent, whereas $f^{-}(\mathbf{r})$ is associated with the HOMO and hence the reactivity towards an electron acceptor.

Many additional and very important developments of these basic equations exist, and it is beyond the scope of the present review to cover all of them. We refer to e.g., references [90,148] for more details. We end the section on the connection between the density and its derivatives to thermodynamic quantities and chemical reactivity indexes by mentioning a couple of additional aspects.

In case we are interested in processes or reactions involving, e.g. spin-pairing energies in transition metals, singlet–triplet transitions, and similar, a spin-polarized form of the above reactivity descriptors is required. Much work in this direction has been done by Ghanti and Gosh, and by Galvan and coworkers [149].

A chemical reaction in general involves changes in the nuclear configurations and it may thus also be useful to determine how the density varies with changes in nuclear coordinates. This leads us to the so-called nuclear Fukui function [150,151]

$$\underset{\sim}{\phi}_A = \left(\frac{\partial \underset{\sim}{F}_A}{\partial N}\right)_{\upsilon(\mathbf{r})} \tag{105}$$

where $\underset{\sim}{F}_A$ is the force acting on nucleus A, and the nuclear Fukui function measures its change when the number of electrons is varied; i.e. the magnitude of the onset of the perturbation. Through a Maxwell-type of relation, the nuclear Fukui function can also be shown to represent the change in electronic chemical potential upon nuclear displacement [152]

$$\begin{aligned}\underset{\sim}{\phi}_A &= \left(\frac{\partial E_A}{\partial N}\right)_{\upsilon(\mathbf{r})} = \left(\frac{\partial^2 E}{\partial \mathbf{R}_A \partial N}\right)_{\upsilon(\mathbf{r})} \\ &= \left(\frac{\partial}{\partial \mathbf{R}_A}\left(\frac{\partial E}{\partial N}\right)_{\upsilon(\mathbf{r})}\right)_N = \left(\frac{\partial \mu}{\partial \mathbf{R}_A}\right)_N\end{aligned} \tag{106}$$

3.2. The Kohn–Sham formulation

The Euler equation (Eq. (89)), which determines the energy functional, does not provide any practical means for computational purposes. The task of finding good approximations to the energy functional was greatly simplified by Kohn and Sham [89], just one year after the publication of the DFT foundational paper by Hohenberg and Kohn [104].

Indeed, having in mind Eqs. (86) and (87) the Euler equation can be cast as:

$$\upsilon(\mathbf{r}) + \frac{\delta T[\rho]}{\delta \rho[\mathbf{r}]} + \frac{\delta U[\rho]}{\delta \rho[\mathbf{r}]} = \mu \tag{107}$$

Clearly, its solution requires an explicit functional form for the kinetic and the electron–electron repulsion energy functionals.

Kohn and Sham devised an approximation to the kinetic energy functional that triggers a *familiar* and tractable decomposition scheme for the electron–electron interaction functional. The idea is based on introducing orbitals into the problem. Indeed, if we know the exact wave function, then both the electron density and the kinetic energy can be written down exactly in terms of the *natural orbitals* $\{\phi_i\}_{i=1}^{\infty}$ and their corresponding occupation numbers $\{\eta_i\}_{i=1}^{\infty}$ as:

$$\rho(\mathbf{r}) = \sum_{i=1}^{\infty} \eta_i \phi_i^*(\mathbf{r})\phi_i(\mathbf{r}) \tag{108}$$

$$T = \sum_{i=1}^{\infty} \eta_i \left\langle \phi_i \left| -\frac{1}{2}\nabla^2 \right| \phi_i \right\rangle \tag{109}$$

But the number of terms of these summations are *in principle* infinite, because the *natural orbitals* come from the diagonalization of the exact infinite-expansion first-order reduced density matrix [34].

However, since Gilbert [153] demonstrated that any N-representable density can be obtained from the sum of the squares of a set of N *orbitals* $\{\psi_i\}_{i=1}^{N}$ (unknown for the time being) as:

$$\rho(\mathbf{r}) = \sum_{i=1}^{N} \psi_i^*(\mathbf{r})\psi_i(\mathbf{r}) \tag{110}$$

We can always use these unknown orbitals to estimate a *kinetic energy*

$$T_s = \sum_{i=1}^{N} \left\langle \psi_i \left| -\frac{1}{2}\nabla^2 \right| \psi_i \right\rangle \tag{111}$$

Beware that T_s is not the kinetic energy T, of the system as given in Eq. (109). It is the kinetic energy of *a fictitious system of noninteracting N particles*, whose exact solution is the determinant built with the orbitals $\{\psi_i\}_{i=1}^{N}$, because it is only for this case that the kinetic energy can be expressed as the finite sum of Eq. (111).

Consequently, the total energy functional can be partitioned as:

$$\begin{aligned}E[\rho] = T_s[\rho] + \int \rho(\mathbf{r})\upsilon(\mathbf{r})\,\mathrm{d}\mathbf{r} + \frac{1}{2}\int \mathrm{d}(\mathbf{r})\,\mathrm{d}(\mathbf{r}')\frac{\rho(\mathbf{r})\rho(\mathbf{r}')}{|\mathbf{r}-\mathbf{r}'|} \\ + E_{xc}[\rho]\end{aligned} \tag{112}$$

The third term of the right hand side, which shall be denoted as $J[\rho]$, represents the classical Coulomb repulsion of the electron cloud, plus its *self interaction* energy. The fourth term is called the *exchange-correlation* energy functional and accounts for the self interaction and all other non classical effects of the quantum electron–electron interaction, including the difference $T[\rho] - T_s[\rho]$. Eq. (112) yields the Euler equation rearranged in the following form:

$$\upsilon_{eff}(\mathbf{r}) + \frac{\delta T_s[\rho]}{\delta \rho(\mathbf{r})} = \mu \tag{113}$$

where we have introduced the Kohn–Sham one electron *effective potential*

$$\upsilon_{\text{eff}}(\mathbf{r}) = \upsilon(\mathbf{r}) + \frac{\delta J[\rho]}{\delta\rho(\mathbf{r})} + \frac{\delta E_{\text{xc}}[\rho]}{\delta\rho(\mathbf{r})} \tag{114}$$

which determines the Hamiltonian of the *fictitious non-interacting system*

$$\hat{H}_{\text{s}} = \sum_{i=1}^{N}\left[-\frac{1}{2}\nabla_i^2 + \upsilon_{\text{eff}}(\mathbf{r})\right] \tag{115}$$

The solution of $\hat{H}_{\text{s}}$:

$$\left[-\frac{1}{2}\nabla_i^2 + \upsilon_{\text{eff}}(\mathbf{r})\right]\psi_i = \epsilon_i\psi_i \tag{116}$$

constitutes the set of the *orbitals* whose associated electron density is equal to the electron density of the real system.

In summary, we have to find the electron density ρ that minimizes the energy under the constraint of keeping the number of electrons constant. This optimum energy functional is such that it satisfies the Euler equation. Consider therefore, the variation $\delta E[\rho]$ due to the variations of the electron density $\delta\rho$, such that keep the number of electrons is kept constant, i.e.

$$\int \rho(\mathbf{r})\,\mathrm{d}\mathbf{r} = \int [\rho(\mathbf{r}) + \delta\rho(\mathbf{r})]\,\mathrm{d}\mathbf{r} \Rightarrow \int \delta\rho(\mathbf{r})\,\mathrm{d}\mathbf{r} = 0 \tag{117}$$

From Eq. (112), we obtain:

$$\delta E[\rho] = \delta T_{\text{s}}[\rho] + \int \delta\rho(\mathbf{r})\upsilon(\mathbf{r})\,\mathrm{d}\mathbf{r} + \int \mathrm{d}\mathbf{r}\,\mathrm{d}\mathbf{r}'\frac{\delta\rho(\mathbf{r})\rho(\mathbf{r}')}{|\mathbf{r}-\mathbf{r}|} + \delta E_{\text{xc}}[\rho] \tag{118}$$

Solving for $\delta T_{\text{s}}[\rho]$ from Eq. (113), under the constraint of Eq. (117), and substituting in Eq. (118) we arrive at:

$$\upsilon_{\text{eff}}(\mathbf{r}) = \upsilon(\mathbf{r}) + \int \frac{\rho(\mathbf{r}')\,\mathrm{d}\mathbf{r}'}{|\mathbf{r}-\mathbf{r}'|} + \upsilon_{\text{xc}}(\mathbf{r}) \tag{119}$$

where the *exchange-correlation* potential υ_{xc} is defined by:

$$\delta E_{\text{xc}}[\rho] = \int\left[\frac{\delta E_{\text{xc}}}{\delta\rho(\mathbf{r})}\right]_N \delta\rho(\mathbf{r})\,\mathrm{d}\mathbf{r} = \int \upsilon_{\text{xc}}(\mathbf{r})\delta\rho(\mathbf{r})\,\mathrm{d}\mathbf{r} \tag{120}$$

Consequently, once we know the exchange-correlation functional (this is the weak link of the theory) we can always construct the exchange-correlation potential as indicated in Eq. (120) and, thus determine the Kohn–Sham effective potential through Eq. (119).

In conclusion, the Kohn–Sham operational procedure is as follows:

1. Devise an explicit expression for the exchange correlation energy functional and derive the expression for the exchange correlation potential, Eq. (120).
2. Make a guess for the orbitals ψ_i.
3. Build the expression for the one electron effective potential, Eq. (119).
4. Solve for the orbitals ψ_i, Eq. (116), until consistency.
5. Calculate the total energy form Eq. (112).

We note in passing that the Kohn–Sham theory, described above, is very reminiscent of the Hartree–Fock theory of ab initio molecular orbital theory. However, the similarity is rather fortuitous, since the Kohn–Sham theory is a one-electron model intimately related to the *exact solution* of the problem.

This solution leads to the energy and the electron density of the ground state and to all quantities derivable from them. At variance with the Hartree–Fock exchange potential, i.e., the term associated with the permutator $\hat{\mathcal{P}}_{12}$ in Eq. (13)

$$\upsilon_{\text{x}}^{\text{HF}}(\mathbf{r})\underbrace{\psi_i(\mathbf{r})}_{\uparrow} = -\sum_{j}^{N}\int \mathrm{d}\mathbf{r}'\psi_j^*(\mathbf{r}')\frac{1}{|\mathbf{r}-\mathbf{r}'|}\psi_j(\mathbf{r})\underbrace{\psi_i(\mathbf{r}')}_{\uparrow}$$

which is *non local*, since for evaluate it at a point $\mathbf{r}$, it requires knowledge of the function ψ_i at points $\mathbf{r}'$, the effective potential $\upsilon_{\text{eff}}(\mathbf{r})$ is *local* as it only necessitates *local* knowledge of ψ_i at point $\mathbf{r}$. Thus, with a *local density approximation* to the exchange-correlation functional, the equations present no more difficulties than the solution of the Hartree equations.

3.3. Fractional occupation numbers

The formulation given above has been generalized by Rajagopal [154] and Perdew and Zunger [108], based on an idea originally putted forward by Janak [155], to allow for fractional occupation of the orbitals. Indeed, following Janak, we can construct the following energy:

$$\tilde{E}[\rho] = \sum_{i=1}^{M}\eta_i\left\langle\psi_i\left|-\frac{1}{2}\nabla^2\right|\psi_i\right\rangle + \int\rho(\mathbf{r})\upsilon(\mathbf{r})\,\mathrm{d}\mathbf{r} + \frac{1}{2}\int\mathrm{d}\mathbf{r}\,\mathrm{d}\mathbf{r}'\frac{\rho(\mathbf{r})\rho(\mathbf{r}')}{|\mathbf{r}-\mathbf{r}'|} + E_{\text{xc}}[\rho] \tag{121}$$

where the number M of the occupation numbers of the orbitals, $\{\eta_i|0 \le \eta_i \le 1\}_{i=1}^{M}$, is not less that the number of electrons N, and

$$N = \sum_{i=1}^{M}\eta_i, \qquad \rho(\mathbf{r}) = \sum_{i=1}^{M}\eta_i|\psi_i(\mathbf{r})|^2 \tag{122}$$

Recall, that while $\tilde{E}[\rho]$ is a well defined mathematical object, it is not equal to the total energy $E[\rho]$, because the kinetic entering in $\tilde{E}[\rho]$ differs, in general, from $T_{\text{s}}[\rho]$ for an arbitrary set of occupation numbers $\{\eta_i|0 \le \eta_i \le 1\}_{i=1}^{M}$. However, it is worth pointing out that by construction, $\tilde{E}[\rho]$ acquires the same value as $E[\rho]$, whenever the occupation numbers $\{\eta_i|0 \le \eta_i \le 1\}_{i=1}^{M}$, take the form of the Fermi-Dirac distribution.

Let us differentiate the energy of Eq. (121) with respect to the occupation number η_i of the orbital ψ_i, namely:

$$\frac{\partial \tilde{E}}{\partial \eta_i} = \left\langle \psi_i \left| -\frac{1}{2}\nabla^2 \right| \psi_i \right\rangle + \int \frac{\delta}{\delta\rho(\mathbf{r})}\left[J[\rho] + E_{\mathrm{xc}}[\rho] + \int \rho(\mathbf{r})\upsilon(\mathbf{r})\,\mathrm{d}\mathbf{r}\right]\frac{\partial\rho(\mathbf{r})}{\partial\eta_i}\,\mathrm{d}\mathbf{r} \tag{123}$$

which considering Eqs. (114) and (122) is easily transformed to

$$\frac{\partial \tilde{E}}{\partial \eta_i} = \left\langle \psi_i \left| -\frac{1}{2}\nabla^2 \right| \psi_i \right\rangle + \langle \psi_i | \upsilon_{\mathrm{eff}} | \psi_i \rangle \tag{124}$$

Finally, considering Eq. (116) we obtain the so-called Janak theorem:

$$\frac{\partial \tilde{E}}{\partial \eta_i} = \epsilon_i \tag{125}$$

This justifies our word of caution stated at the beginning of Section 3, about the distinct nature of the Kohn–Sham orbitals relative to the more familiar Hartree–Fock orbitals.

Nevertheless, $\tilde{E}[\rho]$ can also be used to make a continuous connection between the ground state energies of the N and $(N+1)$ electron system. Namely, by integration of the Janak formula, we obtain precise prescriptions to calculate *exactly* two difficult quantities: the electron affinity:

$$\mathrm{EA} = -(E_{N+1} - E_N) = \int_0^1 \epsilon_{\mathrm{LUMO}}(\eta)\,\mathrm{d}\eta \tag{126}$$

and the ionization energy:

$$I = -(E_N - E_{N-1}) = \int_0^1 \epsilon_{\mathrm{HOMO}}(\eta)\,\mathrm{d}\eta \tag{127}$$

Additionally, Harris and Ballone [156] has used Janak theorem to formulate a convenient approach for the estimation of the electron removal energies. Clearly from Eq. (125) we can obtain

$$\Delta E_i = E_i(N-1) - E(N) = \int_0^1 \left(\frac{\partial E}{\partial \eta_i}\right)\mathrm{d}\eta_i = -\int_0^1 \epsilon_i(\eta_i)\,\mathrm{d}\eta_i \tag{128}$$

where it has been assumed that along the entire adiabatic electron removal process, the system satisfies the premises of the density functional theory. This condition will certainly be violated in many cases. Therefore, although the ΔE_i cannot be formally regarded as the removal energy of an electron form the ith Kohn–Sham orbital, we can always evaluate the right hand side of Eq. (128) and see how far we can go as to *estimate* vertical electron removal energies. This, if succeeded, will certainly be useful for the prediction of the photoelectron spectra signals.

Harris and Ballone approach relies on the Taylor expansion for dependence of the orbital energies ϵ_i of the occupation number η_i, namely:

$$\epsilon_i(\eta_i) = \epsilon_i(\eta_i^0) + (\eta_i + \eta_i^0)\frac{\partial\epsilon_i}{\partial\eta_i} + \mathcal{O}(\eta_i - \eta_i^0)^2 \tag{129}$$

The evaluation of the first-order derivative of Eq. (129) can be carried out by virtue of the Hellmann–Feynman theorem as:

$$\frac{\partial\epsilon_i}{\partial\eta_i} = \left\langle \psi_i \left| \frac{\partial \hat{H}_{\mathrm{s}}}{\partial\eta_i} \right| \psi_i \right\rangle \tag{130}$$

which having in mind Eq. (115) for $\hat{H}_{\mathrm{s}}$ and using the *local density approximation* for the exchange-correlation potential is readily cast into:

$$\frac{\partial\epsilon_i}{\partial\eta_i} = \left\langle \psi_i \left| \int \frac{|\psi_i(\mathbf{r}')|^2\,\mathrm{d}\mathbf{r}'}{|\mathbf{r}-\mathbf{r}'|} + |\psi_i(\mathbf{r})|^2\frac{\partial\vartheta_{\mathrm{xc}}[\rho]}{\partial\rho} + \sum_{j\neq 1}\eta_i\left[\int \frac{\partial|\psi_i(\mathbf{r}')|^2}{\partial\eta_i}\frac{\mathrm{d}\mathbf{r}'}{|\mathbf{r}-\mathbf{r}'|} + \frac{\partial|\psi_i(\mathbf{r}')|^2}{\partial\eta_i}\frac{\partial\vartheta_{\mathrm{xc}}[\rho]}{\partial\rho}\right]\right| \psi_i \right\rangle \tag{131}$$

where the exchange-correlation potential, $\upsilon_{\mathrm{xc}}(\mathbf{r}) = \vartheta_{\mathrm{xc}}[\rho]\,\rho(\mathbf{r})$, has been written in its *local density approximation* form, as indicated above. Harris and Ballone made one more approximation at this point. Namely, they neglected the third term of the right hand side, which accounts for the relaxation of the remaining Kohn–Sham orbitals as the electron is removed for the ith orbital. This leads to their final expression for the correction the orbital energy ϵ_i to transform it into the binding energy of this orbital:

$$\Delta E_i = -\epsilon_i + \frac{1}{2}\left[\int \frac{|\psi_i(\mathbf{r}')|^2|\psi_i(\mathbf{r})|^2}{|\mathbf{r}-\mathbf{r}'|}\,\mathrm{d}\mathbf{r}\,\mathrm{d}\mathbf{r}' + \int |\psi_i(\mathbf{r})|^4\frac{\partial\vartheta_{\mathrm{xc}}[\rho]}{\partial\rho}\,\mathrm{d}\mathbf{r}\right] \tag{132}$$

The accuracy of this simple approximation is limited by the relaxation effects neglected in Eq. (131) and by the use of the *local density approximation* for the exchange-correlation potential. The averaged error incurred by such a model, has been estimated, by computation [156,157], to be of the order of 10% of the total electron removal energy.

In spite of the surprisingly reasonable performance of the Harris–Ballone approximation, it should be emphasized that for all electrons other than the most external one, there is no proof that $\tilde{E}_i(N-1) = E_i(N-1)$, where $E_i(N-1)$ is the true energy of the system in which an electron has been stripped off from the ith Kohn–Sham orbital. Therefore, for these electrons the ΔE_i of Eq. (132) cannot be viewed rigorously as the binding of the ith electron.

Jellinek and Acioli [158–162] have devised an elegant strategy to circumvent the neglecting of electron relaxation and, by the same token, they have proposed a new scheme for converting the Kohn–Sham orbital energies into electron

removal energies, independent of the particular choice of the exchange-correlation functional.

The basic idea behind there strategy is that the removal energy of an arbitrary Mth electron of an N electron system, can be calculated within any version of DFT rigorously when this electron is the most external one. Namely, if the Mth electron is the most external one, i.e., the HOMO, it removal energy can be obtained as:

$$\Delta E_M = E(M-1) - E(M) \tag{133}$$

where $E(M)$ is the ground state DFT energy of the system with M electrons and, $E(M-1)$ is the corresponding energy of the system with the most external Mth electron removed. This provides an accurate estimate of the correction term $\Delta_M(M)$ required to convert the negative of the Kohn–Sham orbital energy of the Mth electron into its removal or binding energy. Namely:

$$\Delta_M(M) = \Delta E_M - (-\epsilon_M(M)) \tag{134}$$

However, the correction term $\Delta_M(N)$ required to convert the negative of the Kohn–Sham orbital energy of an arbitrary Mth electron ($1 \le M \le N$) into its binding energy must take into account the shift in the value of the Mth Kohn–Sham orbital energy from $\epsilon_M(M)$ to $\epsilon_M(N)$ as the total number of electrons of the system increases from M to N.

The proposal made by Jellinek and Acioli was formulated as:

$$\Delta_M(N) = \Delta_M(N-1) + [\Delta_{M+1}(N) - \Delta_M(N-1)]\alpha_M(N) \tag{135}$$

with

$$\alpha_M(N) = \frac{\epsilon_M(N) - \epsilon_M(N-1)}{\epsilon_{M+1}(N) - \epsilon_M(N-1)} \tag{136}$$

Eq. (135) represents a recursive procedure to obtain $\Delta_M(N)$, since the corrections $\Delta_{M+1}(N)$ and $\Delta_M(N-1)$ of its right hand side are themselves obtained through recursive application of Eqs. (135) and (136), until they are reduced to $\Delta_K(K)$, $K \in \{M, M+1, \ldots N\}$, which is calculated as prescribed in Eq. (134).

This correction scheme can be carried at any well-defined level of approximation within DFT and, uses only ground state energies and Kohn–Sham orbital energies. It furnishes highly accurate electron binding energies as recently illustrated in applications to atoms, molecules [161] and clusters [160,162].

3.4. The exchange-correlation functional

The advantages of the Kohn–Sham methodology are many and obvious. Thus, efficient algorithms for solving Hartree like equations have long ago been tested and are ideally suited for the Kohn–Sham procedure. Additionally, these algorithms can easily be extended to large systems. For practical uses of the theory, however, one has to find sufficiently simple and yet accurate enough approximations for the exchange-correlation energy functional $E_{xc}[\rho]$. To place such approximations into proper perspective we shall examine now $E_{xc}[\rho]$ in detail.

The Schrödinger equation can also be expressed in terms of the one- and two-electron density functions as:

$$\begin{aligned} E &= T + E_{eN} + E_{ee} \\ &= -\int d\mathbf{r} \frac{\nabla_{\mathbf{r}}^2}{2} \gamma(\mathbf{r}, \mathbf{r}')\Big|_{\mathbf{r}'=\mathbf{r}} + \int d\mathbf{r} \rho(\mathbf{r}) \upsilon(\mathbf{r}) \\ &\quad + \int d\mathbf{r}\, d\mathbf{r}' \frac{\Gamma_2(\mathbf{r}, \mathbf{r}')}{|\mathbf{r} - \mathbf{r}'|} \end{aligned} \tag{137}$$

where

$$\Gamma_2(\mathbf{r}_1, \mathbf{r}_2) = \frac{N(N-1)}{2} \int |\Phi(\mathbf{r}_1, \mathbf{r}_2, \ldots, \mathbf{r}_N)|^2 d\mathbf{r}_3 \ldots d\mathbf{r}_N$$

is the spin-less electron pair density and, the first-order reduced density matrix is given by:

$$\gamma(\mathbf{r}, \mathbf{r}') = N \int \Phi(\mathbf{r}, \mathbf{r}_2, \ldots, \mathbf{r}_N) \Phi(\mathbf{r}', \mathbf{r}_2, \ldots, \mathbf{r}_N)\, d\mathbf{r}_2 \ldots d\mathbf{r}_N \tag{138}$$

which is related with electron density by:

$$\rho(\mathbf{r}) = \gamma(\mathbf{r}, \mathbf{r}) = \sum_{i=1}^{N} \langle \Phi | \delta(\mathbf{r} - \mathbf{r}_i) | \Phi \rangle \tag{139}$$

The electron pair density accounts for the probability $\Gamma_2(\mathbf{r}_1, \mathbf{r}_2)\, d\mathbf{r}_1\, d\mathbf{r}_2$ of one electron being in the volume $d\mathbf{r}_1$ around $\mathbf{r}_1$ when other electron is known to be in the volume $d\mathbf{r}_2$ around $\mathbf{r}_2$. If the electrons were independent [163], clearly: $\Gamma_2(\mathbf{r}_1,\mathbf{r}_2) = \rho(\mathbf{r}_1)\rho(\mathbf{r}_2)$. Therefore, it is then intuitive that for correlated electrons, an *exchange-correlation* contribution which takes into account all kinds of correlations between the electrons must be added to the uncorrelated case. Thus

$$\Gamma_2(\mathbf{r}_1, \mathbf{r}_2) = \frac{1}{2} \rho(\mathbf{r}_1)[\rho(\mathbf{r}_2) + \rho_{xc}(\mathbf{r}_1, \mathbf{r}_2)] \tag{140}$$

Substituting Eq. (140) into the last term of the right hand side of Eq. (137) we obtain that the electron–electron repulsion energy can be expressed as:

$$\begin{aligned} E_{ee} &= \frac{1}{2} \int d\mathbf{r}\, d\mathbf{r}' \frac{\rho(\mathbf{r})\rho(\mathbf{r}')}{|\mathbf{r} - \mathbf{r}'|} + \frac{1}{2} \int d\mathbf{r}\, d\mathbf{r}' \frac{\rho(\mathbf{r})\rho_{xc}(\mathbf{r}, \mathbf{r}')}{|\mathbf{r} - \mathbf{r}'|} \\ &= J[\rho] + [E_{xc}[\rho] - (T[\rho] - T_s[\rho])] \end{aligned} \tag{141}$$

where the definition of $E_{xc}[\rho]$ comes from Eq. (112), which includes the excess kinetic energy term. Nonetheless, density functional theory has devised an elegant way to incorporate this excess kinetic energy term in an *exchange-correlation*

hole description, through the *adiabatic connection* technique [164–167].

The crucial point here is that the relationship between the interacting system and the fictitious non-interacting system, can be realized by considering the electron–electron interaction as $\lambda|\mathbf{r}-\mathbf{r}'|^{-1}=\lambda\hat{U}$, and varying λ from 0 (non-interacting system) to 1 (interacting system). This should be carried out in the presence of an external potential $\hat{V}^{\lambda}$, such that the ground state of the Hamiltonian

$$\hat{H}^{\lambda}=\hat{T}+\hat{V}^{\lambda}+\lambda\hat{U} \tag{142}$$

gives the same ground state electron density ρ as the coupling parameter λ is varied. This $\hat{H}^{\lambda}$ provides a smooth pathway between the non-interacting system and the interacting system, with $\hat{V}^{\lambda}$ chosen in such a way as to preserve the electron density unchanged all along the pathway. Observe that for $\lambda=1$, $|\psi^{\lambda}\rangle$ is the interacting ground state wave function which gives the electron density ρ and, the external potential is that of the real system. Concomitantly, $\lambda=0$, $|\psi^{\lambda}\rangle$ corresponds to the single determinant wave function built with the Kohn–Sham orbitals and, the external potential is the Kohn–Sham effective potential, namely:

$$\upsilon^{\lambda=0}(\mathbf{r})=\upsilon_{\mathrm{eff}}(\mathbf{r}) \tag{143}$$

Let $|\psi^{\lambda}\rangle[\rho]$ be the wave function of $\hat{H}^{\lambda}$, consequently Eq. (141) can now be rewritten as:

$$\begin{aligned}E_{\mathrm{xc}}[\rho]&=\langle\Psi^{\lambda}[\rho]|\hat{T}+\lambda\hat{U}|\Psi^{\lambda}[\rho]\rangle|_{\lambda=1}-\langle\Psi^{\lambda}[\rho]|\hat{T}\\&\quad+\lambda\hat{U}|\Psi^{\lambda}[\rho]\rangle|_{\lambda=0}-J[\rho]\\&=\int_0^1\mathrm{d}\lambda\frac{\mathrm{d}}{\mathrm{d}\lambda}\langle\Psi^{\lambda}[\rho]|\hat{U}|\Psi^{\lambda}[\rho]\rangle-J[\rho]\\&=\int_0^1\mathrm{d}\lambda\langle\Psi^{\lambda}[\rho]|\hat{U}|\Psi^{\lambda}[\rho]\rangle-J[\rho]\end{aligned} \tag{144}$$

where in the last step we have invoked the Hellman–Feynman theorem. Hence, the *adiabatic connection* has adsorbed the excess kinetic energy term into an *exchange-correlation hole description* of the form:

$$E_{\mathrm{xc}}[\rho]=\frac{1}{2}\int\mathrm{d}\mathbf{r}\,\mathrm{d}\mathbf{r}'\frac{\rho(\mathbf{r})\bar{\rho}_{\mathrm{xc}}(\mathbf{r},\mathbf{r}')}{|\mathbf{r}-\mathbf{r}'|} \tag{145}$$

with the adiabatic coupling constant averaged exchange-correlation given by:

$$\bar{\rho}_{\mathrm{xc}}(\mathbf{r},\mathbf{r}')=\int_0^1\rho_{\mathrm{xc}}^{\lambda}(\mathbf{r},\mathbf{r}')\,\mathrm{d}\lambda \tag{146}$$

Recall at this point that Hohenberg and Kohn demonstrated in their *Density Theory Functional* (DFT) foundational paper [104], that all properties of interacting electron systems are completely determined by its ground state electron density, $\rho(\mathbf{r})$. Therefore, ρ_{xc} itself must also be a functional of the ground state electron density in accordance with Eq. (137), although its exact form has been proved difficult to find out [168]. The good news, however, is that the exchange-correlation energy depends only weakly on the details of the exchange-correlation hole functional $\rho_{\mathrm{xc}}[\rho]$. Namely, in order to estimate the exchange-correlation energy $E_{\mathrm{xc}}[\rho]$ we need only an approximation for the spherical average of the exchange-correlation hole $\bar{\rho}_{\mathrm{xc}}$, as defined by:

$$\tilde{\rho}_{\mathrm{xc}}(\mathbf{r},u)=\int\frac{\mathrm{d}\Omega_{\mathbf{u}}}{4\pi}\bar{\rho}_{\mathrm{xc}}(\mathbf{r},\mathbf{r}+\mathbf{u}) \tag{147}$$

Then

$$E_{\mathrm{xc}}[\rho]=\int\mathrm{d}\mathbf{r}\rho(\mathbf{r})\int_0^{\infty}2\pi u\tilde{\rho}_{\mathrm{xc}}(\mathbf{r},u)\,\mathrm{d}u \tag{148}$$

This observation, made first by Gunnarsoon and Lundqvist [169], has facilitated greatly the design of suitable models for the exchange-correlation functional [170].

3.4.1. The experimental route to the exchange-correlation hole

Quasi elastic scattering processes of high-energy X-rays and electrons provide experimental access [171] to both the electron density, $\rho(\mathbf{r})$, and the electron-pair density, $\Gamma(\mathbf{r},\mathbf{r}')$. In particular, it is well-known that the spherically averaged scattering double differential cross section, for the transfer of momentum μ and energy E is given by [172]:

$$\begin{aligned}\frac{\partial^2\sigma}{\partial\Omega\partial E}&=\mathcal{I}_{\mathrm{cl}}\frac{E_1}{E_0}\int\frac{\mathrm{d}\Omega}{4\pi}\left\{\sum_n\left|\left\langle\Phi_n\left|\sum_i\mathrm{e}^{\mathrm{i}\mu\mathbf{r}_i}\right|\Phi_0\right\rangle\right|\right.\\&\quad\left.\times\,\delta(E-E_{n0})\right\}\end{aligned} \tag{149}$$

where $\mathcal{I}_{\mathrm{cl}}$ is the Thomson scattering cross section, E_0 and E_1 the energies of the incident and scattered either photons or electrons, $|\Phi_0\rangle$ and $|\Phi_n\rangle$ the wave functions of the initial and final states of the sample and $\mathbf{r}_i$ the coordinate of its ith electron and E_{n0} is the energy difference between the final and the initial states. Since, the proyectile particles are high energy particles, the energy lose during the scattering process is normally a tiny fraction of their total energy, so that: $E_1/E_0\approx1$. On the other hand if we take advantage of the closure relation for the states of the sample, namely:

$$1=\sum_n|\Phi_n\rangle\langle\Phi_n| \tag{150}$$

Eq. (149) can be integrated over the transferred energy to yield the differential cross-section of the total high-energy X-ray (electron) scattering as:

$$\begin{aligned}\frac{\partial\sigma_{\mathrm{T}}}{\partial\Omega}&=\int\frac{\partial^2\sigma}{\partial\Omega\partial E}\,\mathrm{d}E\\&=\mathcal{I}_{\mathrm{cl}}\left\{N+\int\frac{\mathrm{d}\Omega}{4\pi}\left\langle\Phi_0\left|\sum_{i\neq j}\mathrm{e}^{\mathrm{i}\mu(\mathbf{r}_i-\mathbf{r}_j)}\right|\Phi_0\right\rangle\right\}\end{aligned} \tag{151}$$

Now, if we complete the integration of the right hand side of Eq. (151) over the radial component of the transferred

momentum μ and, recall the Fourier transform integrals of the Dirac's delta function, i.e.

$$\delta(\mathbf{z}) = \frac{1}{(2\pi)^3}\int \mathrm{d}\zeta \mathrm{e}^{\mathrm{i}\zeta\cdot\mathbf{z}} \tag{152}$$

a relation between the integrated total X-ray scattering intensity and the electron-pair density can be stabilized as:

$$\mathcal{I}_{\mathrm{T}} = N + \frac{1}{\mathcal{I}_{\mathrm{cl}}}\int_0^\infty \mu^2\,\mathrm{d}\mu \int \frac{\mathrm{d}\Omega}{4\pi}\frac{\partial\sigma_{\mathrm{T}}}{\partial\Omega}$$
$$= N + 4\pi^2\int \Gamma_2(\mathbf{r}_1,\mathbf{r}_2)\delta(\mathbf{r}_1-\mathbf{r}_2)\,\mathrm{d}\mathbf{r}_1\,\mathrm{d}\mathbf{r}_2 \tag{153}$$

This equation establishes the link between high-energy X-ray and electron scattering experiments and the electron-pair density.

Furthermore, the integral of right hand side of Eq. (153) is just the normalization of the so-called on-top pair density [173,174]:

$$P(\mathbf{r},\mathbf{r}) = 2\Gamma_2(\mathbf{r},\mathbf{r}) \tag{154}$$

Its normalization:

$$\frac{1}{2}\int P(\mathbf{r},\mathbf{r})\,\mathrm{d}\mathbf{r} = \langle\Phi|\hat{\delta}(\mathbf{u}-\mathbf{r}_1+\mathbf{r}_2|\Phi\rangle_{\mathbf{u}\to 0} = I(0) \tag{155}$$

renders the electron–electron coalescence density [175–178], $I(0)$. Consequently:

$$\mathcal{I}_{\mathrm{T}} = N + 4\pi^2 I(0) \tag{156}$$

The elastic scattering contribution to the total scattering intensity, i.e. the term $n=0$ in Eq. (149), can be transformed likewise into:

$$\mathcal{I}_{\mathrm{el}} = \frac{1}{\mathcal{I}_{\mathrm{cl}}}\int_0^\infty \mu^2\,\mathrm{d}\mu \int \frac{\mathrm{d}\Omega}{4\pi}\frac{\partial\sigma_{\mathrm{el}}}{\partial\Omega}$$
$$= 2\pi^2\int \rho(\mathbf{r}_1)\rho(\mathbf{r}_2)\delta(\mathbf{r}_1-\mathbf{r}_2)\,\mathrm{d}\mathbf{r}_1\,\mathrm{d}\mathbf{r}_2 = 2\pi^2\int \rho^2(\mathbf{r})\,\mathrm{d}\mathbf{r} \tag{157}$$

Finally, the inelastic scattering cross section, which is also-called incoherent scattering factor or static structure factor, is obtained by subtracting the elastic scattering contribution from the total scattering intensity.

The total integrated elastic and inelastic intensities can be related to the charge concentration and the system-averaged on-top exchange-correlation hole density [179]. To show this, substitute Eq. (140) into Eq. (153) to obtain the integrated total X-ray scattering intensity as:

$$\mathcal{I}_{\mathrm{T}} = N + 2\pi^2\left\{\int \rho^2(\mathbf{r})\,\mathrm{d}\mathbf{r} + \int \rho(\mathbf{r})\rho_{\mathrm{xc}}(\mathbf{r},\mathbf{r})\,\mathrm{d}\mathbf{r}\right\} \tag{158}$$

Consequently, the integrated total inelastic X-ray scattering intensity is given by:

$$\mathcal{I}_{\mathrm{in}} = N + 2\pi^2\int \rho(\mathbf{r})\rho_{\mathrm{xc}}(\mathbf{r},\mathbf{r})\,\mathrm{d}\mathbf{r} \tag{159}$$

Recall that our Eq. (157) generalizes a previous result by Hyman et al. [180] for a sample of N identical non-overlapping atoms of finite size. The above integrated formulae corroborate the theoretical interpretation attributed to these components: the elastic component is related to the electron distribution and inelastic component is mostly concerned with the details of electron–electron interactions.

Eqs. (158) and (159) constitute one strong bridge between experiment and theory. On one hand, experimental work can provide values for the scattering intensities $\partial\sigma_{\mathrm{T}}/\partial\Omega$ and $\partial\sigma_{\mathrm{el}}/\partial\Omega$ for a sufficiently large number of transferred radial momentum values, μ, and on the other hand theoreticians can obtain accurate system average electron densities $\langle\rho\rangle$, and design reliable exchange-correlation hole density functions, $\rho_{\mathrm{xc}}(\mathbf{r},\mathbf{r}')$. These two independent developments must fulfill the requirements imposed by Eqs. (158) and (159). The comparison with experimental data is, nonetheless, tied to the availability of data for a wide range of incident angles (related to μ) in the experimental measurement of X-ray scattering intensities [181].

Nevertheless, it would be highly desirable that approximate density functionals should reproduce the experimentally obtained integrated intensities of Eqs. (158) and (159), in view of the importance of $\rho_{\mathrm{xc}}(\mathbf{r},\mathbf{r}')$ in modeling the correct electron pair distribution [182].

3.4.2. The local (spin) density approximation

The original approach of Kohn and Sham for the exchange-correlation energy was a gradient expansion like:

$$E_{\mathrm{xc}}[\rho]\int \rho(\mathbf{r})\varepsilon_{\mathrm{xc}}[\rho(\mathbf{r})]\,\mathrm{d}\mathbf{r} + \mathcal{O}(|\nabla\rho(\mathbf{r})|^2) \tag{160}$$

Keeping only the leading term of Eq. (160), renders the so-called *local density approximation* (LDA). The functional $\varepsilon_{\mathrm{xc}}[\rho(\mathbf{r})]$ is the exchange-correlation energy density of a *uniform electron gas*, except that the constant electron gas density has been replaced by the local of the inhomogeneous interacting system $\rho(\mathbf{r})$.

One of the simplest implementations of the local density approximation is the *Xα* method proposed by Slater [183]. It is often called the exchange-only version of the local density approximation, since the exchange-correlation energy functional is further divided into the exchange and the correlation contributions and the latter is neglected. The former term, the exchange-only energy density functional is:

$$\varepsilon_{\mathrm{x}}^{\mathrm{LDA}}[\rho(\mathbf{r})] = -\frac{9}{4}\alpha\left(\frac{3}{4\pi}\right)^{1/3}\rho(\mathbf{r})^{1/3} \tag{161}$$

the value of $\alpha = 2/3$ renders the exact exchange-only functional of the uniform electron gas.

For the case of spin polarized systems, the α and β spin densities are used instead in Eq. (161), and this yields the

exchange-only *local spin density approximation* (LSD):

$$\varepsilon_{\mathrm{x}}^{\mathrm{LSD}}[\rho(\mathbf{r})] = -\frac{9}{4}\alpha\left(\frac{3}{4\pi}\right)^{1/3}[\rho_\alpha(\mathbf{r})^{1/3} + \rho_\beta(\mathbf{r})^{1/3}] \qquad (162)$$

The correlation contribution to the exchange-correlation energy density functional has been built into a tractable formula by Vosko et al. [184]. This completes the expression for the exchange-correlation energy functional:

$$E_{\mathrm{xc}}^{\mathrm{LSD}}[\rho] = \int \rho(\mathbf{r})[\varepsilon_{\mathrm{x}}^{\mathrm{LSD}}[\rho(\mathbf{r})] + \varepsilon_{\mathrm{c}}^{\mathrm{LSD}}[\rho(\mathbf{r})]]\,\mathrm{d}\mathbf{r} \qquad (163)$$

and permits starting the iterative process mentioned above to obtain the solution of our many-electron system just solving one-electron equations.

In spite of its simplicity the local density approximation has been extremely successful, even addressing systems with highly inhomogeneous electron density [185] like atoms and molecules. One of the reasons of the accuracy of LDA certainly relies on the fact that the details of the exchange-correlation hole are not critical for the purposes of energy determination (see Eq. (148)), as long as its system and spherically average, the $\int \rho(\mathbf{r})\tilde{\rho}(\mathbf{r}, u)\,\mathrm{d}\mathbf{r}$ piece of Eq. (148), is reasonable. Also, because the exchange-correlation hole of LDA has been derived from a *real* physical system, the uniform electron gas, it satisfies a number of exact conditions common to all electronic systems. Consequently, it should lead to moderately reliable modeling for all kind of systems.

3.4.3. The failures of the local density approximation

For systems with larger density and smoother density, the local density approximation works increasingly better. However, for systems with substantial electron density gradients, its simple form is often not accurate enough. More importantly, the local density approximation violates some exact conditions. For instance, the correlation energy functional, $\varepsilon_{\mathrm{c}}[\rho]$, does not scale properly at the high-density limit [186] and it does not display the derivative discontinuity at integer values of the occupation numbers [187]. Also the decay of the LDA effective potential is not proportional to r^{-1} at $r \to \infty$.

Perhaps the most embarrassing failure of the local density approximation occurs for the simplest case of one electron. One electron does not interact with itself so $E_{\mathrm{xc}}[\rho] \equiv E_{\mathrm{x}}[\rho]$ must cancel exactly the self-interaction energy present in the classical Coulomb repulsion term $J[\rho]$, that is:

$$J[\rho] + E_{\mathrm{x}}[\rho] = 0 \qquad (164)$$

and similarly for the potentials

$$\int \frac{\rho(\mathbf{r}')}{|\mathbf{r} - \mathbf{r}'|}\,\mathrm{d}\mathbf{r} = \frac{\delta E_{\mathrm{x}}[\rho]}{\delta\rho} \qquad (165)$$

The local density approximation does not satisfy these conditions and gives unreliable results for all one-electron systems [188], like the hydrogen atom or H_2^+.

3.4.4. The gradient expansions

Eq. (160) already suggests a natural way to improve LSD for inhomogeneous systems. Indeed, LSD can be view as the zeroth-order term in a Taylor expansion for the exchange-correlation functional about the uniform density and then higher-order terms are to be included. This is the gradient expansion approximation (GEA). The leading term of this expansion, namely, the lowest-order gradient correction to LSD is uniquely determined by dimensional analysis, and is given by:

$$E_{\mathrm{xc}}^{\mathrm{GEA}}[\rho] = E_{\mathrm{xc}}^{\mathrm{LSD}}[\rho] + \sum_{\sigma,\sigma'} C_{\sigma,\sigma'} \int \frac{\vec{\nabla}\rho_\sigma(\mathbf{r})}{\rho_\sigma^{2/3}(\mathbf{r})} \frac{\vec{\nabla}\rho_{\sigma'}(\mathbf{r})}{\rho_{\sigma'}^{2/3}(\mathbf{r})}\,\mathrm{d}\mathbf{r} \qquad (166)$$

The coefficients $C_{\sigma,\sigma'}$ vary slowly with the density [189,190]. This expression constitutes the next systematic correction to the LSD functional in the limit of slowly varying electron density. For the exchange part of the functional a simplified form of Eq. (166) containing only the two diagonal terms of $C_{\sigma,\sigma'}|_{\sigma=\sigma'} = -\beta$, namely:

$$E_{\mathrm{x}}^{\mathrm{GEA}}[\rho] = E_{\mathrm{x}}^{\mathrm{LSD}}[\rho] - \beta \sum_\sigma \int \frac{|\vec{\nabla}\rho_\sigma(\mathbf{r})|^2}{\rho_\sigma^{4/3}(\mathbf{r})}\,\mathrm{d}\mathbf{r} \qquad (167)$$

was introduced empirically by Herman et al. [191] and latter discussed by Sham [192] in the context of formal density functional theory. However, it was Becke who in a seminal paper [193] found a model exchange-correlation hole density that yields the functional of Eq. (167) and provided an estimate for the constant β that agreed well with previous numerically estimated values of its optimal value [194,195].

In contrast with the considerations made above, this lowest-order gradient correction degrades the results for both the correlation energy and the total exchange-correlation energy with respect to LSD, except for systems with slowly varying density [196–198]. Indeed, this approximation is well-known to suffer from severe deficiencies. For example, its corresponding exchange-correlation potential diverges asymptotically in atoms and molecules. This failure is due to the fact that unlike the LSD exchange-correlation hole, the exchange-correlation hole associated with Eq. (166), which is a truncated expansion, does not correspond with the hole of any physical system and hence many of the exact conditions satisfied by the LSD hole are now violated [197]. In general, both the exchange and the correlation holes associated with Eq. (166) are more accurate at short interelectronic separations, relative to the LSD holes, but are worse at large interelectronic separations, causing the divergence of the exchange-correlation potential.

3.4.5. Generalarized gradient approximations

The failure of the gradient expansion for the exchange-correlation energy has motivated the advent of the so-called generalarized gradient approximations (GGA), a term coined

by Perdew and Yang [198], and that refers to exchange-correlation functionals which incorporate information about not only the electron density itself but also their local gradients:

$$E_{\mathrm{xc}}^{\mathrm{GGA}}[\rho] = \int \mathrm{d}\mathbf{r}\, f^{\mathrm{GGA}}(\rho_\sigma, \vec{\nabla}\rho_\sigma), \quad \sigma = \alpha, \beta \tag{168}$$

Two remarkably successful strategies to design suitable approximations for the function f^{GGA} have flourished during that last 15 years. On one hand, Becke has led a pragmatic *empirical* approach, while Perdew has championed a non-empirical approach.

Thus, Becke introduced in 1986 the following *semiempirical* exchange density functional [199]:

$$E_{\mathrm{x}}^{\mathrm{B86}}[\rho] = E_{\mathrm{x}}^{\mathrm{LSD}}[\rho] - \beta \sum_\sigma \int \rho_\sigma^{4/3}(\mathbf{r}) \frac{x^2}{1+\gamma x_\sigma^2}\, \mathrm{d}\mathbf{r} \tag{169}$$

where x_σ is the dimensionless ratio

$$x_\sigma = \frac{\vec{\nabla}\rho_\sigma(\mathbf{r})}{\rho_\sigma^{4/3}(\mathbf{r})} \tag{170}$$

The parameters β and γ were fitted to a set of selected atomic data. The explicit form of the functional was chosen in order to satisfy (i) dimensional consistency, (ii) that the GEA of Eq. (167) is recovered in the limit of small density gradients, and (iii) that the exchange *potential* is well behaved in the tail of the atomic and molecular distributions, i.e., in the limit of large x_σ.

In a subsequent paper [200], Becke improved upon his initial proposal. Thus, considering in addition to the conditions mentioned above, the exact behavior of the exchange-energy density:

$$\lim_{r\to\infty} \varepsilon_{\mathrm{x},\sigma} = -\frac{1}{r} \tag{171}$$

and of the spin electron density [201]:

$$\lim_{r\to\infty} \rho_\sigma(\mathbf{r}) = \mathrm{e}^{-a_\sigma r} \tag{172}$$

with a_σ being a constant related to the ionization energy, he proposed the following exchange energy functional:

$$E_{\mathrm{x}}^{\mathrm{B88}}[\rho] = E_{\mathrm{x}}^{\mathrm{LSD}}[\rho] - \beta \sum_\sigma \int \rho_\sigma^{4/3}(\mathbf{r}) \frac{x_\sigma^2}{1+(6\beta x_\sigma/\sinh x_\sigma)}\, \mathrm{d}\mathbf{r} \tag{173}$$

which reproduces exactly the conditions of Eqs. (171) and (172). The parameter β of Eq. (173) was chosen on the basis of a least-squares fit to the exact Hartree–Fock exchange energy of the noble gases as calculated from the Clementi–Roetti exponential-type orbitals [202].

This functional for the exchange appears normally associated with the correlation functional of Lee et al. [203], which is a density gradient expansion based on the orbital functional for the correlation energy of Colle and Salvetti [204]. In their model, Colle and Salvetti accounted for the electron correlation by approximating the electron-pair density as the non-interacting pair density times a correlation factor, which includes the electron density, the electron–electron coalescence density and the Laplacian of the pair density, together with four constants which were fitted to the Hartree–Fock orbital of helium. Later, Lee et al., expressed the non-interacting pair density in terms of the density and first-order density matrix. It results that the correlation energy can be cast into a close form involving only the electron density and the kinetic energy of the non-interacting system. A density gradient expansion of the latter [205,206] renders the correlation energy as a functional of the electron density and its gradient.

The resulting exchange-correlation density functional is known under the BLYP acronym and is very popular in quantum chemistry.

The PW91 is also a widely used exchange-correlation density functional in modern quantum chemistry. This functional has its roots in an earlier proposal of Perdew and Yang [198], known under the acronym PW86. In this functional the exchange hole and the exchange energy functional are those of GEA (Eq. (166)), but with sharp cut offs chosen so that the resulting exchange hole density satisfies the upper boundary condition:

$$\rho_{\mathrm{x}}(\mathbf{r}, \mathbf{r}') \le 0, \quad \forall(\mathbf{r}, \mathbf{r}') \tag{174}$$

and the normalization condition, namely:

$$\int \rho_{\mathrm{x}}(\mathbf{r}, \mathbf{r}')\, \mathrm{d}\mathbf{r}' = -1, \quad \forall\mathbf{r} \tag{175}$$

For the correlation functional the PW86 involves the wave vector space cut off of Langreth and Mehl [207]. Namely, the correlation energy functional $E_{\mathrm{c}}^{\mathrm{PW86}}$ is written in terms of the Fourier transform of $1/u$ as:

$$E_{\mathrm{c}}^{\mathrm{PW86}}[\rho] = \frac{N}{2}\frac{1}{2\pi^3}\int_{k_{\mathrm{c}}}^{\infty} \mathrm{d}k\, 4\pi k^2 \langle\tilde{\rho}_{\mathrm{c}}(k)\rangle \frac{4\pi}{k^2} \tag{176}$$

where

$$\langle\tilde{\rho}(k)\rangle = \int_0^\infty 4\pi u^2 \langle\tilde{\rho}_{\mathrm{c}}(u)\rangle \frac{\sin(uk)}{uk} \tag{177}$$

is the Fourier transform of the system averaged spherically averaged correlation hole density. The lower limit of the integral in Eq. (176):

$$k_{\mathrm{c}} = 0.15 \times \frac{|\vec{\nabla}\rho|}{\rho} \tag{178}$$

remedies the spurious behavior at small k. In subsequent works Perdew and coworkers [208–210] introduced another cut off radius in order to force the correlation hole density to satisfy the exact sum rule:

$$\int \rho_{\mathrm{c}}(\mathbf{r}, \mathbf{r}')\, \mathrm{d}\mathbf{r}' = 0, \quad \forall\mathbf{r} \tag{179}$$

which in turn assures the Lieb and Oxford bound [211]

$$E_{xc}^{PW91}[\rho] \geq 2.273 E_x^{LDA}[\rho] \tag{180}$$

to be satisfied as well. With all these exact conditions satisfied, the PW91 exchange-correlation functional results in a rather well balanced approximate functional which behaves satisfactorily for most purposes, including extended systems such as surfaces and solids [212].

3.4.6. Meta generalized gradient approximations

These functional constitute a step beyond the generalarized gradient approximation. Indeed, these functionals take the more general form

$$E_{xc}^{mGGA}[\rho] = \int \mathrm{d}\mathbf{r}\, f^{mGGA}(\rho_\sigma \vec{\nabla}\rho_\sigma, \nabla^2\rho_\sigma, \tau_\alpha),$$
$$\sigma = \alpha, \beta \tag{181}$$

where

$$\tau_\sigma(\mathbf{r}) \sum_{i=1} |\vec{\nabla}\psi_i(\mathbf{r})|^2, \quad \sigma = \alpha, \beta \tag{182}$$

is the Kohn–Sham orbital kinetic energy density for electron of spin σ. The added ingredients are justified because the short-range behavior of the spherical averaged exchange hole density [193]:

$$\tilde{\rho}_\sigma(\mathbf{r}, u) \approx \tilde{\rho}_\sigma(\mathbf{r}) + \frac{1}{6}\left[\nabla^2\tilde{\rho}_\sigma(\mathbf{r}) - 2\tau_\sigma(\mathbf{r}) + \frac{|\vec{\nabla}\tilde{\rho}_\sigma(\mathbf{r})|^2}{2\tilde{\rho}_\sigma(\mathbf{r})}\right]u^2$$

involves these added terms. Meta-GGA's that use the kinetic energy density are explicitly orbital-dependent. Nevertheless, it should be pointed out that because the Kohn–Sham orbitals are functionals of the electron density, the meta-GGA's are still density functionals. However, this introduces one more difficulty for self-consistent Kohn–Sham calculations because it is not obvious how can be obtained the *effective potential* of Eq. (119), when the exchange-correlation functional depends explicitly on the orbitals. The Optimized Potential Method [213–216] removes this problem, but has not yet been implemented in most DFT computer programs that are in use, and may also turn out to be very computationally demanding.

Because of the difficulties mentioned above most meta-GGA's are most often applied as a post GGA treatment, in the sense that the Kohn–Sham orbitals are determined by use of a GGA functional, and the meta-GGA energy is then calculated afterwards using the GGA-orbitals. This makes it more difficult to make geometry optimizations, as the forces within the scheme become unknown.

3.5. Hybrid functionals

At the lower limit ($\lambda = 0$, see Eq. (142)) of the adiabatic coupling parameter, since the electron–electron interaction is suppressed, the exchange-correlation functional must contain only exchange effects. Even more, since as mentioned in Section 3.4, $|\Psi^{\lambda=0}\rangle$ is the single determinant wave function built with Kohn–Sham orbitals, the *exact* expression for the exchange-correlation functional corresponds to the Hartree–Fock exchange (see Eq. (15)) as evaluated with the Kohn–Sham orbitals:

$$E_x[\rho] = -\frac{1}{2}\int \mathrm{d}\mathbf{r}\,\mathrm{d}\mathbf{r}'\,\frac{|\gamma(\mathbf{r}, \mathbf{r}')|^2}{|\mathbf{r} - \mathbf{r}'|} \tag{183}$$

where the one particle density matrix (Eq. (138)) of the non-interacting fictitious system is given exactly as:

$$\gamma(\mathbf{r}, \mathbf{r}') = \sum_{i=1}^{N} \psi_i^*(\mathbf{r})\psi_i(\mathbf{r}') \tag{184}$$

This observation led to Becke [217,218] to conclude that a fraction of the exchange evaluated as in Eq. (183), normaly referred to as *exact*, mixed with GGA exchange and correlation would improve the accuracy of the functional. The simplest such hybrid functional can be cast as:

$$E_{xc}^{hyb}[\rho] = E_x^{exact}[\rho] + (1 - a)(E_x^{GGA}[\rho] - E_x^{exact}[\rho]) + E_c^{GGA}[\rho] \tag{185}$$

This projects the following picture for the modeling of the electron-interaction: the subtleties of the short-range interelectronic interactions are carried by the $E_c^{GGA}[\rho]$ and the nondynamic electron correlation is modelled by $(1 - a)(E_x^{GGA}[\rho] - E_x^{exact}[\rho])$. In particular Becke [218] proposed the following construction:

$$E_{xc}^{hyb}[\rho] = E_{xc}^{LSD}[\rho] + a_0(E_x^{exact}[\rho] - E_x^{LSD}[\rho]) + a_x\Delta E_x^{B88}[\rho] + a_c E_c^{PW91}[\rho] \tag{186}$$

where the Δs indicate the difference of the corresponding functional with respect to the LSD functional. The coefficients a_0, a_x and a_c are empirically optimized for the calculation of atomization energies of a selected set of sample molecules. Ironically, the most popular hybrid functional, namely the B3LYP:

$$E_{xc}^{BLYP}[\rho] = E_{xc}^{LSD}[\rho] + 0.20(E_x^{exact}[\rho] - E_x^{LSD}[\rho]) + 0.72\Delta E_x^{B88}[\rho] + 0.81 E_c^{LYP}[\rho] \tag{187}$$

was published as a remark at the side [219], and then just included for the first time in the commercial program package Gaussian [220]. Today, B3LYP is probably the most used density functional in chemistry, and the reason for the growing popularity of DFT in calculations of molecules. Indeed, B3LYP has been found to give surprisingly accurate results in many cases. Thus, for the G2 set of compounds (a standardized test set of small molecules), its mean error to the atomization energy is around 2.5 kcal/mol, to be compared with 78 kcal/mol for HF theory, and in the range of 1 kcal/mol for the most accurate correlated ab initio methods [21,221].

For most cases in which a moderately sized system (10–50 atoms) is to be investigated, the B3LYP functional is today the method of choice.

Subsequent to these developments, much mostly empirical work has been devoted to improve the "mixture" of various functionals to generate better hybrid approximate functionals. A number of proposals have appeared in the literature and can conveniently be traced from the manuals of popular electronic structure program packages [222–224].

3.6. Time dependent density functional theory

Time-dependent density functional theory [225] provides a formally rigorous extension of Hohenberg–Kohn–Sham density-functional theory, to the situation where a system, initially in its ground stationary state, is subject to a time-dependent perturbation modifying its external potential υ. This allows for the description of various time-dependent phenomena, such as atoms and solids in time-dependent electric or magnetic fields. In addition, TDDFT provides an efficient way to calculate the dynamic polarizability, required to describe the optical properties of matter.

The first step in the development of the theory is to demonstrate the existence of an unique correspondence between the time dependent one-body density $\rho(\mathbf{r}, t)$ and the time-dependent potential $\upsilon(\mathbf{r}, t)$. This mapping is proven in the Runge–Gross theorem [226], which can be considered as the time-dependent generalization of the Hohenberg–Kohn theorem. Then, a corresponding Kohn–Sham construction of the theory can be used that leads to a set of practical equations for the calculations:

$$i\frac{\partial}{\partial t}\psi_i(\mathbf{r}, t) = \left[-\frac{\nabla^2}{2} + \upsilon_{\text{eff}}(\mathbf{r}, t)\right]\psi_i(\mathbf{r}, t) \tag{188}$$

where $\psi_i(\mathbf{r}, t)$ are the time-dependent Kohn–Sham orbitals which constructs the one-body density:

$$\rho(\mathbf{r}, t) = \sum_{i=1}^{N} |\psi_i(\mathbf{r}, t)|^2 \tag{189}$$

As in ordinary Kohn–Sham DFT, here we use an auxiliary system of non-interacting electrons subject to a $\upsilon_{\text{eff}}(\mathbf{r}, t)$ potential which is chosen such that the density built from these Kohn–Sham orbitals is the same as the density of the original interacting system. If the exact time-dependent Kohn–Sham potential is known $\upsilon_{\text{eff}}(\mathbf{r}, t)$, then the equations stated above would lead to the exact one-body density. This $\upsilon_{\text{eff}}(\mathbf{r}, t)$ potential can be divided in different contributions which read as follows:

$$\upsilon_{\text{eff}}(\mathbf{r}, t) = \upsilon_{\text{ext}}(\mathbf{r}, t)\upsilon_{\text{Hartree}}(\mathbf{r}, t) + \upsilon_{\text{xc}}(\mathbf{r}, t) \tag{190}$$

where $\upsilon_{\text{Hartree}}(\mathbf{r}, t)$ accounts for the classical electrostatic interaction between electrons

$$\upsilon_{\text{Hartree}}(\mathbf{r}, t) = \int \mathrm{d}\mathbf{r}' \frac{\rho(\mathbf{r}', t)}{|\mathbf{r} - \mathbf{r}'|} \tag{191}$$

and the external potential $\upsilon_{\text{ext}}(\mathbf{r}, t)$ accounts for the interaction of the electrons with the nuclei (whose positions could change dynamically) and any other external potential that is dependent on time. For example if one wants to study the optical absorption of a molecule subject to the effect of a laser of a given frequency the external potential would be

$$\upsilon_{\text{ext}}(\mathbf{r}, t) = \underbrace{-\sum_{\alpha}\frac{Z_\alpha}{|\mathbf{r} - R_\alpha(t)|}}_{\upsilon_{\text{nuclei}}(\mathbf{r},t)} + \underbrace{Ef(t)\sin(\omega t)\mathbf{r}\alpha}_{\upsilon_{\text{laser}}(\mathbf{r},t)} \tag{192}$$

where $\upsilon_{\text{laser}}(\mathbf{r}, t)$ accounts for the laser field in the dipole approximation and $f(t)$ is a function that controls the laser pulse.

Finally, $\upsilon_{\text{xc}}(\mathbf{r}, t)$ needs to be defined. The time-dependent exchange-correlation potential can be formally defined as the functional derivative of the exchange-correlation part of the quantum mechanical action of the electronic system ($\mathcal{A}_{\text{xc}}$)

$$\upsilon_{\text{xc}}(\mathbf{r}, t) = \frac{\delta\mathcal{A}_{\text{xc}}}{\delta\rho(\mathbf{r}, t)} \tag{193}$$

In contrast to ordinary DFT, approximations to $\upsilon_{\text{xc}}(\mathbf{r}, t)$ are still in their infancy. The majority of the existing functionals make use of the adiabatic approximation [227,228], which allows the use of the existing time-independent exchange-correlation functionals. The approximations is as follows, let us assume that $\tilde{\upsilon}[\rho]$ is an approximation to the ground-state exchange-correlation potential, then the adiabatic time-dependent exchange-correlation potentials is written as:

$$\upsilon_{\text{xc}}^{\text{adiabatic}}(\mathbf{r}, t) = \tilde{\upsilon}[\rho(\mathbf{r})|_{\rho=\rho(t)}] \tag{194}$$

That is, the adiabatic approximation consists of using the same exchange-correlation potential as in the time-independent theory but evaluated with the electron density at time t, $\rho(\mathbf{r}, t)$. The functional is local in time, and this is of course a quite dramatic approximation. In cases where the temporal dependence is large, like interactions with strong lasers pulses with matter, one should go beyond the present approximation. Apart from approximations to the exchange-correlation potential, the scheme described so far is perfectly general and can be applied to essentially any time-dependent situation. Nevertheless, in practice two different regimes are considered. In the case that the time dependent potential is weak, linear-response theory can be applied to solve the problem [229–233]. On the contrary, if the time-dependent potential is strong a full solution of the Kohn–Sham equations is required [228,234]. We next describe these two different approaches.

3.6.1. Time-dependent density-functional response theory

It can be shown that the vertical excitation energies ($w_I = E_I - E_0$) from the molecular electronic ground state to the excited state I ($I \leftarrow 0$) can be obtained from the poles of the

mean dynamic polarizability:

$$\bar{\alpha}(w) = \frac{1}{3}\,\mathrm{tr}\alpha(w) = \sum_I \frac{f_I}{w_I^2 - w^2} \tag{195}$$

The calculation of the dynamical polarizability is difficult. However, for a system of electrons, TDDFT allows us to calculate the response of the density to a time-dependent perturbing potential at frequency w. The response function has poles at *all* the excitation energies of the system. So it has the necessary information to calculate all the excitations of the system.

The linear response approximation [229–233] only takes into account the component that depends linearly on the external potential:

$$\delta\rho(\mathbf{r}, w) = \int \mathrm{d}\mathbf{r}'\chi(\mathbf{r}, \mathbf{r}', w)\delta\upsilon_{\mathrm{ext}}(\mathbf{r}', w) \tag{196}$$

where $\chi(\mathbf{r}, \mathbf{r}', w)$ is the *density–density response function*, that gives the density response of the system to a time dependent perturbation $\delta\upsilon_{\mathrm{ext}}(\mathbf{r}, w)\mathrm{e}^{-\mathrm{i}wt}$.

The exact χ response function which is defined as:

$$\chi^{-1}(\mathbf{r}, \mathbf{r}', w) = \frac{\delta V_{\mathrm{ext}}(\mathbf{r}, w)}{\delta\rho(\mathbf{r}', w)} \tag{197}$$

is hard to calculate. Alternatively, TDDFT allows one to express the exact density response $\delta\rho$ via the response function χ_{s} of the non-interacting KS system.

$$\delta\rho(\mathbf{r}, w) = \int \mathrm{d}\mathbf{r}'\chi_{\mathrm{s}}(\mathbf{r}, \mathbf{r}', w)\delta\upsilon_{\mathrm{eff}}(\mathbf{r}', w) \tag{198}$$

$\delta\upsilon_{\mathrm{eff}}(\mathbf{r}', w)$ is the linearized time-dependent Kohn–Sham potential and is divided in three contributions:

$$\delta\upsilon_{\mathrm{eff}}(\mathbf{r}', w) = \delta\upsilon_{\mathrm{ext}}(\mathbf{r}', w) + \int \mathrm{d}\mathbf{r}''\frac{\delta\rho(\mathbf{r}'', w)}{|\mathbf{r}' - \mathbf{r}''|} \tag{199}$$

$$+ \int \mathrm{d}\mathbf{r}''\, f_{\mathrm{xc}}(\mathbf{r}, \mathbf{r}', w)\delta\rho(\mathbf{r}'', w) \tag{200}$$

In the above equation f_{xc} is the exchange correlation kernel, defined as the functional derivative of the exchange-correlation potential with respect to the density, evaluated at the ground state density, and then, Fourier transformed to the w-space.

$$f_{\mathrm{xc}}(\mathbf{r}, t, \mathbf{r}', t') = \left[\frac{\delta\upsilon_{\mathrm{xc}}[\rho](\mathbf{r}, t)}{\delta\rho(\mathbf{r}', t')}\right]_{\rho_0} \tag{201}$$

The response function of the KS system can be expressed in terms of the stationary KS-orbitals as:

$$\chi_{\mathrm{s}}(\mathbf{r}, \mathbf{r}', w) = \sum_{j,k}(f_k - f_j)\frac{\psi_j(\mathbf{r})\psi_k^*(\mathbf{r})\psi_j^*(\mathbf{r}')\psi_k(\mathbf{r}')}{w - (\epsilon_j - \epsilon_k) + i\eta}$$

with f_k being the Fermi occupation number (0 or 1) of the kth KS-orbital.

Substituting the expressions for $\delta\upsilon_{\mathrm{eff}}$ and χ_{s} into Eq. (198) leads to the following equation:

$$\int \mathrm{d}\mathbf{r}''\left[\delta(\mathbf{r} - \mathbf{r}'' - \int \mathrm{d}\mathbf{r}'\chi_{\mathrm{s}}(\mathbf{r}, \mathbf{r}', w)\left(\frac{1}{|\mathbf{r}' - \mathbf{r}''|} + f_{\mathrm{xc}}(\mathbf{r}', \mathbf{r}'', w)\right)\right]\delta\rho(\mathbf{r}'', w) = \int \mathrm{d}\mathbf{r}'\chi_{\mathrm{s}}(\mathbf{r}, \mathbf{r}', w)\delta\upsilon(\mathbf{r}', w) \tag{202}$$

In this equation, $\delta\rho(\mathbf{r}'', w)$ at the LHS shows poles at the exact excitation energies (Ω), but the RHS part of the equation shows poles at $(\epsilon_j - \epsilon_k)$. It is important to note that the excitation energies will be different to the difference in the Kohn–Sham orbital energies. Therefore, as $w \to \Omega$ the RHS of the equation has a finite value. The only possibility for the equality to hold when $w \to \Omega$ is that the term within brackets vanishes when $w \to \Omega$. This condition, leads to the following equation:

$$\lambda(w)(\mathbf{r}, w) = \int \mathrm{d}\mathbf{r}'\chi_{\mathrm{s}}(\mathbf{r}, \mathbf{r}', w)\int \mathrm{d}\mathbf{r}''\left[\frac{1}{|\mathbf{r}' - \mathbf{r}''|} + f_{\mathrm{xc}}(\mathbf{r}', \mathbf{r}'', w)\right] \times \gamma(\mathbf{r}, w)$$

with $\lambda \to 1$ as $w \to \Omega$. After some algebra [232,233], this equation can be recast into an eigenvalue problem:

$$\sum_{q'}(M_{qq'}(\Omega) + w_q\delta_{qq'})\beta_{q'} = \Omega\beta_q \tag{203}$$

where q denotes a pair of KS-orbitals (j, k), w_q is the difference in orbital energy of the corresponding pair of KS-orbitals $(\epsilon_j - \epsilon_k)$, and $M_{qq'}$ are elements of the so-called *coupling matrix*:

$$M_{qq'} = (f_{k'} - f_{j'})\int \mathrm{d}\mathbf{r}\int \mathrm{d}\mathbf{r}'\psi_k(\mathbf{r})\psi_j^*(\mathbf{r}) \; times \left[\frac{1}{|\mathbf{r} - \mathbf{r}'|} + f_{\mathrm{xc}}(\mathbf{r}, \mathbf{r}', w)\right]\psi_{k'}^*(\mathbf{r}')\psi_{j'}(\mathbf{r}')$$

The solution of Eq. (203) gives the true excitation energies (Ω), as long as we know the exact exchange-correlation kernel f_{xc} and the KS orbitals that builds up the exact stationary one-body density. The quality of the KS orbitals is dictated by the quality of the static exchange-correlation potential used to solve the time-independent Kohn–Sham equations. As seen in the previous section, the exact static υ_{xc} is still not known, but several approximations have been developed that gives reasonable results. To get a functional for f_{xc} is a bit more complicated, since it depends, in principle, on the dynamical υ_{xc} through the relation (201). One can uses the adiabatic approximation (Eq. (194)) and the relation (201) to develop an expression for f_{xc} based on the form of the approximate static υ_{xc}. It has been shown, that even

considering the LDA approximation (*Adiabatic Local Density Approximation* (ALDA)) one can get good results at low frequencies. In other cases, however, it is mandatory to go beyond this simple functional forms to get reliable excitation energies.

Another problem with Eq. (203) is that has to be truncated to become practical, and this gives rise to different levels of approximations. The most drastic truncation would imply to expand Eq. (203) about one particular KS-orbital energy difference and calculate only one term of the coupling matrix:

$$\Omega = (\epsilon_j - \epsilon_k) + M_{qq} \tag{204}$$

where M_{qq} is the element of the coupling matrix that corresponds to the (j, k) excitation ($q \equiv (j, k)$), that is the following integral

$$M_{qq} = \int\int \mathrm{d}\mathbf{r}\,\mathrm{d}\mathbf{r}'\psi_j(\mathbf{r})\psi_k^*(\mathbf{r})\left[\frac{1}{|\mathbf{r}-\mathbf{r}'|} + f_{\mathrm{xc}}(\mathbf{r}, \mathbf{r}', w)\right] \times \psi_j^*(\mathbf{r}')\psi_k(\mathbf{r}') \tag{205}$$

This truncation is denoted as the single-pole approximation (SPA) and already gives a remarkable agreement with the experimental values in many cases. Table 3 shows experimental excitation energies for various atoms compared to the difference in the Kohn–Sham orbital energies ($\Delta\epsilon_{\mathrm{KS}}$) and to the SPA excitation energies. The use of $\Delta\epsilon_{\mathrm{KS}}$ alone to calculate the excitation spectrum is quite poor. However, the SPA correction to $\Delta\epsilon_{\mathrm{KS}}$ does remarkably well compared to the experimental spectrum.

We can also go beyond the single-pole approximation and consider more terms of the Eq. (203). For a review on the different approaches in TDDFRT with respect to both truncations in (203) and exchange-correlation kernels there is an extensive literature.

Among the highest impact of TDDFRT applications, there is the calculation of vertical excitation energies of molecules. A *frozen position* of the nuclei of a molecule is considered and the TD-DFRT equations are solved to yield the corresponding optical absorption of the molecule. In Section 5, we describe some examples of the application of this theory to the determination of optical spectra in molecules.

Table 3
Experimental excitation energies, in eV, for the $^1\mathrm{S} \rightarrow {}^1\mathrm{P}$ transition compared to the differences in the corresponding KS-orbital energies and theoretical excitation energies from single-pole approximation (SPA)

Atom	Experimental	$\Delta\epsilon_{\mathrm{KS}}$	$\Delta\epsilon_{\mathrm{KS}} + M$ (SPA)
Be	0.388	0.259	0.391
Mg	0.319	0.234	0.327
Ca	0.216	0.157	0.234
Zn	0.426	0.315	0.423
Sr	0.198	0.141	0.210
Cd	0.398	0.269	0.391

Data taken from [231].

3.6.2. Full solution of TDDFT Kohn–Sham equations

There are circumstances in which the application of TD-DFRT is non-adequate. These are for example the study of non-linear optical properties, or if one is interested in following a photochemical reaction process [234]. In that case, one should solve the TDDFT Kohn–Sham equations:

$$i\frac{\partial}{\partial t}\psi_i(\mathbf{r}, t) = \left[-\frac{\nabla^2}{2} + \upsilon_{\mathrm{KS}}(\mathbf{r}, t)\right]\psi_i(\mathbf{r}, t) \tag{206}$$

That means that starting from an initial state $\rho(\mathbf{r}, t_0)$ (in most cases, the ground state of the system) generated from the KS-orbitals $\psi_i(\mathbf{r}, t_0)$, we propagate this state according to changes in the KS-orbitals following Eq. (206) until some final time t_{f}. It is more convenient to rewrite Eq. (206) in its integral form:

$$\psi_i(\mathbf{r}, t_{\mathrm{f}}) = \hat{U}(t_{\mathrm{f}}, t_0)\psi_i(\mathbf{r}, t_0) \tag{207}$$

where the time-evolution operator $\hat{U}$ is defined by:

$$\hat{U}(t', t) = \hat{T}\exp\left[-\mathrm{i}\int_t^{t'}\mathrm{d}\tau\,\hat{H}_{\mathrm{KS}}(\tau)\right] \tag{208}$$

Note that $\hat{H}_{\mathrm{KS}}$ is explicitly time-dependent due to the Hartree and exchange-correlation potentials. The exponential in the expression is clearly too complex to be applied directly and needs to be approximated in some suitable manner. One possibility is to approximate the exponential in the time-evolution operator in a power series of Δt using schemes specially designed to enforce time-reversal symmetry, or approximate the integral in the exponent by a trapezoidal rule. To reduce errors in the propagation from t_0 to t_{f}, this large interval is usually split into smaller sub-intervals of length Δt. The wave-functions are then propagated from $t_0 \rightarrow t_0 + \Delta t$, then from $t_0 + \Delta t \rightarrow t_0 + 2\Delta t$ and so on. Typical values for the time step are of the order of 0.001 fs. The total simulation time is determined by the accuracy required in the energy. For a required 0.1 eV accuracy, one has to go to simulation times of the order of 15 fs.

In addition, one can couple the electronic degrees of freedom with the nuclear ones, by propagating the nuclei position in time according to the Newton's equations of motion, using the Verlet algorithm:

$$\mathbf{R}_A(t + \Delta t) = 2\mathbf{R}_A(t) - \mathbf{R}_A(t - \Delta t) + \mathbf{a}(t)\Delta t^2 \tag{209}$$

To calculate the accelerations on the nuclei, the Hellman–Feynmann theorem is used to account for the forces that the electrons exert on the nuclei.

$$F_A(\mathbf{R}, t) = -\left\langle \Psi(t)\left|\frac{\partial}{\partial \mathbf{R}_A}\hat{H}\right|\Psi(t)\right\rangle \tag{210}$$

Solving the coupled Eqs. (206) and (209) leads to a combined electron–nuclei dynamics, which can be used to study

the dynamics of many interesting phenomena [225], like photochemical isomerization reactions, laser-induced dissociations, etc.

4. Surface-hopping and two-state reactivity

Spin-forbidden chemistry has been studied for a long time, but mainly related to problems in photochemistry. Many studies have focussed for example on the singlet–triplet intersystem crossing of different chemical systems including various organic reactions [235,236]. However, there is recently a growing interest on spin-forbidden processes for thermal reactions, that are important not only for organic chemistry but also in different fields such as atmospheric chemistry, astrochemistry, combustion processes or energetic materials. A number of interesting reviews, such as those by Yarkony [237] and Minaev and Agren [238], have addressed some of these topics. Spin-forbidden processes can also be quite relevant in transition metal chemistry. Minaev and Agren [238] refer in their review to spin-catalysis, to account for those chemical reactions whose velocity is enhanced by substances aiding in provoking spin changes and therefore leading to the observation of spin-forbidden processes. The role of spin flip in organometallic chemistry has also been stressed by Schröder et al. [239] and recently reviewed by the latter author [240]. These authors have introduced the paradigm of *Two-State Reactivity* in organometallic chemistry, according to the following definition: *A thermal reaction which involves spin crossover along the reaction coordinate from reactants to products needs to be described in terms of two-state reactivity, if product formation arises from an interplay of spin inversion and the respective barrier heights on both spin surfaces*. Therefore, combining spin inversion with a more favourable transition state on a potential surface of different spin multiplicity than the starting one, a low-energy path can be obtained allowing the progress of a chemical process that could be rather difficult to take place on the initial reactants surface. Some examples in the gas-phase where two-state reactivity may occur have been found for different chemical reactions involving elements such as scandium [241], vanadium [242,243] or iron [244–246]. It should be stressed at this point that spin-forbidden chemistry is not only restricted to reactions where reactants and products correspond to different spin multiplicity. There are some cases where a formally spin-allowed reaction cannot progress under thermal conditions unless one takes into account steps involving spin-crossing. This is the case for the reaction of FeO^+ with H_2 [247,248], where a double spin crossing between the low-spin and high-spin surfaces is found along the reaction coordinate. In other cases the kinetic features of some formally spin-allowed reactions can only be explained invoking spin crossover, and in fact the spin-forbidden step might become the rate-determining step of the whole process [249]. Spin-forbidden processes, where total electron spin is not conserved, are undoubtedly closely related to spin–orbit coupling, and therefore it is of utmost importance to have a basic knowledge of spin–orbit coupling theory in the framework of molecular structure.

4.1. Spin–orbit coupling

Spin–orbit coupling results from the magnetic interaction between spin and orbital angular momenta. An almost classical reference for the spin–orbit coupling in molecules is the book by Richards et al. [250], and a more recent complement is the review by Hess et al. [251]. We will introduce the spin–orbit coupling in the framework of the Breit-Pauli Hamiltonian [252,253], which essentially modifies the non-relativistic Born-Oppenheimer Hamiltonian including different additive terms to account for several spin and relativistic corrections. The additive contribution corresponding to the microscopic spin–orbit Hamiltonian is given by:

$$\hat{H}_{\mathrm{SOC}} = \frac{\mathrm{e}^2\overline{h}}{4m^2c^2}\left[\sum_{\alpha}\sum_{i} Z_\alpha \frac{\boldsymbol{r}_{i\alpha}\times\mathbf{p}_i}{r_{iA}^3}\cdot\mathbf{s}_i - \sum_{i\neq j}\frac{\mathbf{r}_{ij}\times\mathbf{p}_i}{r_{ij}^3}(\mathbf{s}_i+2\mathbf{s}_j)\right] \tag{211}$$

where α denotes the different nuclei of the molecule, whereas i and j run over the electrons. Position vectors are denoted by $\mathbf{r}$, $\mathbf{p}$ represents a linear momentum vector, and spin angular momentum is denoted by $\mathbf{s}$. The first term in Eq. (211) is a one-electron term representing the spin-same-orbit interaction. On the other hand, the second term corresponds to a two-electron contribution resulting from the coupling caused by the motions of the electrons, and represents the *spin-other-orbit* term.

A few comments about the spin–orbit Hamiltonian are appropriate. Since the average distance of an electron from the nucleus scales approximately as $1/Z$, it is readily seen from Eq. (211) that the spin–orbit term scales as Z^4, and therefore its importance increases for heavier elements, for example transition metals. It turns out that spin–orbit interactions might be of comparable magnitude to the electron repulsion interactions for transition metals, and therefore they should be carefully treated. Nevertheless, we should point that for molecules containing heavy elements of course relativistic (kinematic) effects are also crucial and they must be taken into account.

It is also interesting to note that in fact the Breit-Pauli approximation breaks down for large Z [254]. Consequently different approaches [255,256] have been devised in order to account for the main effects omitted in the simplified Breit-Pauli treatment.

In molecules it is quite often assumed that the spin–orbit Hamiltonian can be approximated by an effective one-electron one-center operator [257]. A usual procedure is to employ effective charges for each atom to empirically account for two-electron effects [258], which substantially simplifies the computation of spin–orbit couplings.

After inspection of equation Eq. (211) one would be tempted to conclude that in those cases where the orbital angular momentum for a molecule becomes zero, a situation which is quite usually fulfilled in polyatomic molecules, the spin–orbit coupling would also be zero. However, this is not necessarily true, since even though the orbital angular momentum operator is usually zero, its matrix elements between wavefunctions of states corresponding to different symmetry can have non-zero values [238]. This is the case when both states differ for example by rotation of an atomic orbital on a center of the molecule. The one-center orbital rotation in the course of the transition induces a torque for the spin change [259].

Once the spin–orbit Hamiltonian is formulated one should compute the corresponding matrix elements between the states of interest. Usually, the wavefunctions for both states are expressed in terms of a basis of configuration state functions (CSF), which turn out to be linear combinations of Slater determinants. One of the most usual approaches is employing the C ASSCF method (complete-active-space self-consistent-field) [260]. In the CASSCF approach the molecular orbitals are divided first into inactive and active. Then the wavefunction is expanded in all CSFs that can be formed by occupying doubly all the inactive orbitals and distributing the remaining electrons among the active orbitals in all possible ways consistent with a given spin and space symmetry. Essentially the wavefunction for each state is expressed as a linear combination:

$$\Psi = \sum_i c_i \phi_i \tag{212}$$

and the matrix elements that must be computed are expressed as:

$$\langle \Psi_j | H_{SO} | \Psi_k \rangle \tag{213}$$

We will not go further in the different procedures for the evaluation of these matrix elements, and we will just mention an important aspect concerning the molecular orbitals employed. In principle one could employ different sets of molecular orbitals to describe each state, since in that way the description of both states could be much better [261]. However, this procedure is highly demanding, because one should evaluate matrix elements between non-orthogonal molecular orbitals. It is then preferred to employ the same set of molecular orbitals in order to describe both states, and to compensate a somewhat poorer description to include a larger number of CSFs in the expansion [262].

4.2. Transition probabilities

Once the basic tools for evaluating the spin–orbit coupling are available, we now turn to the question of how to estimate the propensity of a system to undergo a spin-forbidden process. The first problem is to identify the nuclear coordinate region where it is more likely that such process could take place. This is not a trivial question, since there is no rule, such as in spin-forbidden radiative processes, to characterize such region. In radiative processes the Franck-Condon principle generally provides some clues about the favourable nuclear region. In the case of non-radiative spin-forbidden processes other approaches should be employed. A first requisite for a spin-forbidden process to take place is that the two surfaces must actually cross. Within the adiabatic representation two surfaces of different multiplicity can intersect each other in a space of dimension $F-1$, where F is the number of internal degrees of freedom [263]. This space is usually called the it crossing hypersurface, and its characterization is computationally very complicated. Nevertheless there is a simplification which consists in determining only the minimum (or minima) of that hypersurface, defined as the *minimum energy crossing point* (MECP), which does not require the complete characterization of the crossing hypersurface. It has been pointed out [264] that the MECP can be considered to play the role of the transition state in reactions taking place on a single surface. In other words, the MECP acts as the transition state for the spin-forbidden process.

It is possible to obtain the location of the MECP without prior determination of the crossing surface employing procedures similar to those used in geometry optimization algorithms [265]. The procedures to obtain a MECP are in principle not too complicated, since obtaining a MECP is in fact a constrained optimization: one must minimize the energy on one of the surfaces imposing the condition that both spin states (surfaces) have the same energy. Some of the most usual are gradient-based techniques [266–270] where the energy gradient is analytically computed. The choice of the level of calculation heavily depends on the nature of the system under study, and it is also common to include an estimation of the zero-point vibrational energy at the MECP through the curvature of the seam.

If the location of the true MECP is not possible or computationally expensive sometimes a possible alternative is to employ a partial optimization procedure. That is, one performs partial optimizations at fixed values of an appropriate geometrical parameter or reaction coordinate for both surfaces and locates the point at which the crossing occurs. For example in the π attack of an atom or molecular fragment to acetylene, an obvious choice would be the distance between the atom or fragment and the C–C middle point. If the σ attack is being studied one could follow the process in terms of the distance between the atom or fragment and a carbon atom. In any case optimizations at fixed distances can be carried out for both states, and the corresponding curves analyzed to detect the crossing between them. This point can be taken as an approximation to the true MECP.

Once the MECP is located the spin–orbit coupling matrix elements between the two states of different multiplicity can be computed at that geometry. These data, together with the electronic structure data, can be employed to treat the dynamics of the spin-crossing. A first step is to evaluate

the probability of surface hopping taking place. There are different models to compute that probability in an approximate way that could provide some clues about the propensity of a system to undergo spin-flip. Some of the most simple are the Landau-Zener and Rosen-Zener one-parameter models [271,272]. Within the Landau-Zener approximation the probability for surface hopping is estimated according to

$$P_{\mathrm{LZ}} = \mathrm{e}^{-\pi\xi/4} \tag{214}$$

is a parameter which can be computed as:

$$\xi = 8\frac{|\langle\Psi_1|\hat{H}_{\mathrm{SO}}|\Psi_2\rangle|^2}{h\sum_\alpha g_A \cdot \mathbf{v}_A} \tag{215}$$

where g is the energy difference gradient (evaluated at the crossing point) between both surfaces, 1 and 2, and $\mathbf{v}$ is an appropriate nuclear velocity vector. Therefore, it is fairly clear that the probability of surface hopping does not depend exclusively of the magnitude of the spin–orbit coupling between both surfaces at the crossing point, $(\Psi_1|H_{\mathrm{SO}}|\Psi_2)$, but also the way in which both surfaces intersect is also crucial through the energy difference gradient.

The probability for intersystem crossing on a single pass through the crossing point is $1 - P_{\mathrm{LZ}}$. Taking into account the probability of hopping in the reverse direction, $P_{\mathrm{LZ}}(1 - P_{\mathrm{LZ}})$, one finally reaches the probability for surface hopping $P = (1 + P_{\mathrm{LZ}})(1 - P_{\mathrm{LZ}})$. It is usually assumed that in the case of small spin–orbit coupling the following approximate expression can be employed:

$$P \approx 4\pi\frac{|\langle\Psi_1|\hat{H}_{\mathrm{SO}}|\Psi_2\rangle|^2}{h\sum_\alpha g_A \cdot \mathbf{v}_A} \tag{216}$$

Another approximation leads to the monodimensional Delos formula [273,274]:

$$P = 4\pi^2|\langle\Psi_1|\hat{H}_{\mathrm{SO}}|\Psi_2\rangle|^2\left(\frac{2\mu}{\hbar^2 g\Delta g}\right)^{2/3} \times \mathrm{Ai}^2\left[E\left(\frac{2\mu\Delta g^2}{\hbar^2 g^4}\right)^{1/3}\right] \tag{217}$$

where μ is the reduced mass along the direction orthogonal to the seam, Δg and g are, respectively, the norm of the difference of the gradients and their geometric mean, μ, is the reduced mass along the direction orthogonal to the seam, and Ai is the Airy function. The advantage of the Delos-Thorson treatment over the Landau-Zener approximation is that in general is more appropriate for weak-coupling surfaces, and is also active below the crossing point.

4.3. Transition metal compounds

It is well-known that there are some inherent difficulties in the theoretical treatment of transition metal compounds. Describing correlation effects in a balanced way is not easy for transition metals, and also one must take into account kinematic relativistic corrections. Generally most of the treatments employ effective core or model potentials. We will not go any further on this issue now, since we have previously addressed this point, and we will focus on some aspects concerning spin-forbidden chemistry in the context of transition metal compounds.

Transition metal compounds are certainly peculiar in the context of spin-forbidden chemistry. This is obviously related to the fact that usually there is a possibility for several low-lying electronic states emerging from the proximity of d^n, $d^{n-1}s^1$, and $d^{n-2}s^2$ configurations from the transition metal. In addition there are different ways in which d electrons can be distributed, giving rise to a large number of ways in which angular momenta can be coupled. Furthermore, even for first-row transition elements, spin–orbit interactions can be of considerable magnitude, and this enhances the possibility of spin-forbidden processes. In fact it has been argued [275] that in fact spin-forbidness is a concept of relative value for transition metal compounds, due to the large spin–orbit coupling usually exhibited by these compounds. Perhaps more properly it could be said that there is a certain degree of spin-forbidness for a certain process, depending on the precise magnitude of the spin–orbit coupling [276].

Paradoxically it has even been reported that there is a possibility for a spin-forbidden reaction to proceed faster than a spin-conserving process, and this has been termed by Poli [277] as *spin acceleration*. This spin acceleration was first reported for the ligand exchange process on the complex $[CpMoCl_2(PR_3)_2]$ [278]. The reason for this observation is that this 17-electron complex has a doublet ($S = 1/2$) ground state, whereas the resulting dissociation products (15-electron complex $[CpMoCl_2(PR_3)] + PH_3$) have a quartet ground state ($S = 3/2$) lying about 2–6 kcal/mol lower in energy than the corresponding doublet [279]. A computational study [280] allowed a characterization of the MECP for the spin crossing between both surfaces, showing that the MECP lies about 5 kcal/mol below the doublet dissociation products, therefore proving that spin-crossover is kinetically favored over the spin-conserving process. The overall reaction is therefore faster because a spin flip is possible, due to the combined circumstances that spin–orbit coupling is high and a crossing point between both surfaces is energetically favourable.

Many examples involve only a single cross between two surfaces of different spin-multiplicity, and therefore the overall process is spin-forbidden. This situation is qualitatively depicted in Fig. 1. In this schematic representation we have chosen the high-spin reactants to lie below the low-spin ones, whereas for the corresponding products the situation is reversed. If spin–orbit coupling is high enough to produce a relatively high surface hopping probability, the reaction should proceed preferentially through the low-spin surface towards the most stable products. Nevertheless, there are other examples that imply a double spin crossing. This is the case for a process already mentioned previously, the reaction of iron

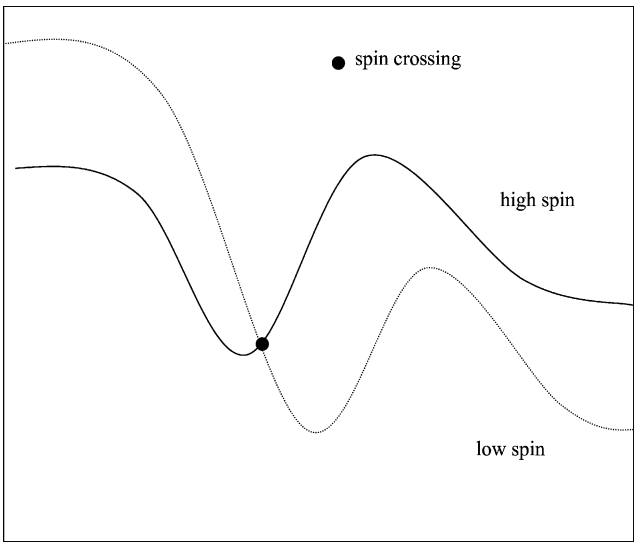

Fig. 1. Qualitative diagram showing a typical spin-forbidden reaction involving a single spin crossing.

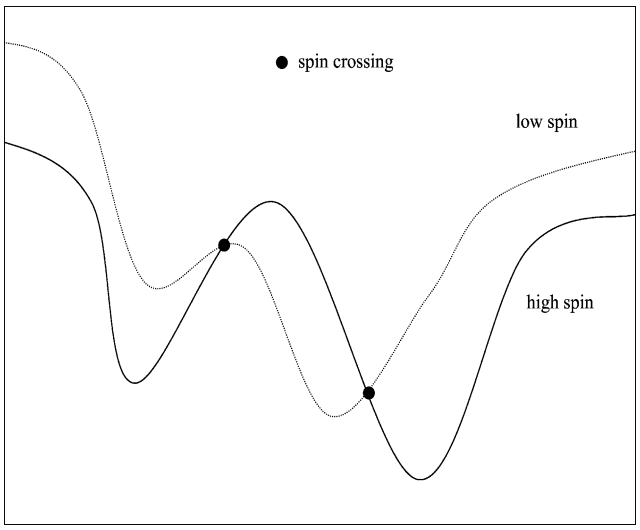

Fig. 2. Qualitative diagram showing a typical case where the overall process is spin-allowed, but involves spin-forbidden reaction steps.

oxide cation with hydrogen molecule:

$$FeO^+ \left({}^6\sum{}^+\right) + H_2 \left({}^1\sum_g^+\right) \rightarrow Fe^+({}^6D) + H_2O({}^1A_1) \quad (218)$$

Apparently, since both iron oxide cation and Fe^+ have a sextet ground state, the reaction is spin-allowed and could take place on the sextet surface. Nevertheless, a computational study [247] shows that on the sextet surface there is a significant activation barrier (about 8.4 kcal/mol) for the insertion of FeO^+ into the H–H bond. This barrier is very difficult to overcome, since the molecules hardly would get the required energy under low-density and normal temperature conditions. However, even though the reaction is reported to be rather slow for an ion–molecule reaction [281], actually the reaction proceeds toward the products. In order to explain the characteristics of this reaction Filatov and Shaik [247] invoke two-state reactivity. According to the theoretical study there is a low-lying transition state on the quartet $[FeOH_2]^+$ surface (lying about just 0.6 kcal/mol above the reactants), and therefore a possible explanation for the behaviour of this reaction should be a spin crossing to the quartet surface, which allows to overcome more easily the barrier. Once the insertion product is formed, a second spin change to the sextet surface should finally lead to the ground state products.

Another globally spin-allowed process involving two consecutive spin-forbidden steps is the rearrangement of the iron ethyl cation, $FeC_2H_5^+$, to $(C_2H_4)FeH^+$ [246]. In this case, both species have quintet ground states, but a more favourable conversion can take place on the triplet surface, since the corresponding transition state lies about 8 kcal/mol lower than the TS on the high-spin surface. This stabilization of transition states is normally associated to favourable interactions of the empty metal orbitals, which are not possible in the high-spin state. Fiedler et al. [246] clearly illustrated the stabilization of the triplet state in $FeC_2H_5^+$, where an agostic interaction between σ_{C-H} molecular orbitals and the empty d_{Fe} orbital is only possible for the triplet and not for the quintet state. A qualitative general picture of an overall spin-allowed reaction involving two spin crossings is depicted in Fig. 2. We have shown the high-spin reactants and products below the low-spin ones, as in the cases of the two examples discussed above, but obviously in principle the opposite situation could also occur. Most reactions whose mechanisms can be interpreted within two-state reactivity correspond to any of the two general models shown above, and the concept of two-state reactivity has been applied to several processes corresponding to different types of reactions. To mention just a few of them, one of the most interesting areas involving transition metal chemistry is the activation of the C–H bond in alkanes. For example the reactions of FeO^+ with methane [282], benzene [283], and norbornane [245] have been shown to involve spin-crossings. In many reactions of hydrocarbons with bare metals or cations two-state reactivity must be invoked. This is the case for example for the reaction of Sc^+ with methane [284] where, despite the triplet ground state of the metal cation, the products of the reaction ($ScH_2^+ + H_2$) appear in their singlet states. In fact, due to the peculiarity of transition metals where there is a wealth of spin states for both their neutral atoms and their cations, it is expected that in many processes a spin-crossing could be eventually involved. Recent studies on several metallocenes have also extended the scope of two-state reactivity to this area. For example for tungsten [285], molybdenum [286], and iridium [287] compounds different theoretical studies revealed that C–H oxidation processes involving them take place through spin crossing. It should be pointed out that only in some of these studies the true MECPs are actually characterized, whereas in others only approximate locations of the crossing points between the two in-

volved surfaces are in fact made. Although, as established previously, locating a MECP should not be a too complicated mathematical problem, a profound knowledge of both surfaces is required from the chemical point of view. In fact qualitative previous explorations of both surfaces, for example carrying out partial optimizations following the reaction coordinate, help substantially. This qualitative approach is sometimes enough to make also approximate estimations of the probability for surface hopping, but for a rigorous analysis of the possibility of two-state reactivity, as well as for making quantitative predictions concerning the reactivity of a system, characterization of the MECP would be desirable. Moreover, theoretical methods of enough quality should be applied in order to obtain the MECP, since otherwise the results could be misleading because large errors in the determination of the point where the crossing takes actually place would lead to large uncertainties in the probabilities for spin crossover. Therefore, theoretical methods should be previously checked in order to confirm that they are able to predict correctly the essential properties of the system (high-spin versus low-spin relative energies in particular).

4.4. Kinetic calculations

Once a general picture of the global process, including a good knowledge of both surfaces and a determination of spin crossings (preferably through the connecting MECPs), is available, a determination of the rate constant can be tackled. The application of the statistical kinetic theories [288] can provide very interesting information on the different factors affecting the rate coefficient, and therefore a more fruitful comparison with the experimental results might be possible. Although usually these applications have been restricted to systems of small size, recently the study of bimolecular reactions in the framework of these theories has proved to be very useful for understanding relatively complex systems [289–296].

Of course the first step in order to compute thermal rate coefficients for a certain reaction is to devise a mechanistic model where adiabatic and non-adiabatic (spin crossing) processes should be included. Unimolecular processes can be taken into account through RRKM theory [297,298] employing standard formulas. The information required (apart form the energetics) concerns basically the vibrational frequencies and moments of inertia of the minima and transition states involved in the different processes. In the case of unimolecular spin-forbidden reactions a non-adiabatic version of the RRKM theory [299–301] should be employed:

$$k_i^{\mathrm{n.a.}}(E, J) = \frac{1}{h\rho_i(E, J)} \int \mathrm{d}E_h P(E_h, J)\rho^{\mathrm{MECP}}(E - E_h, J) \tag{219}$$

where E_h is the fraction of the non-fixed energy reversed in the coordinate orthogonal to the seam and $P(E_h, J)$ is the surface hopping probability, which can be calculated according to one of the models mentioned above. $\rho_i(E, J)$ is the density of states of the starting dissociating intermediate, whereas $\rho^{\mathrm{MECP}}(E - E_h, J)$ plays the role of the density of states for the transition state in an adiabatic process.

The initial capture process for ion–molecule reactions usually does not involve any energy barrier. Therefore, in those cases the capture and other barrierless dissociations that might take place along the reaction should be treated in terms of the variational transition state theory (VTST). The usual procedure implies following the reaction coordinate, making partial optimizations at selected values of the reaction coordinate. Then at each step the hessian should be computed and corrected projecting out the centre of mass translation and external rotations, as well as the reaction coordinate in order to obtain the modes orthogonal to the path. The sum of states is minimized for every E and J value obtaining the location of the loose transition state.

The overall process of obtaining the rate constant for a reaction involving spin crossing is therefore quite demanding, since it must combine several steps from the quantum chemistry calculations on both surfaces to the statistical kinetic treatment, passing through the evaluation of the probability for surface hopping. Nevertheless, it should be stressed that once this treatment is carried out, a wealth of information is provided for the interpretation of experiments as well as for predictive purposes. For example the application of microcanonical VTST allows to predict the competition between adiabatic and non-adiabatic processes and how this competition is affected by the reaction conditions. It is then hoped that as techniques for obtaining MECPs become available to the interested scientific community, more kinetic studies on reactions involving two-state reactivity will be performed.

5. Illustrative examples

5.1. Getting chemical insight from the analysis of the Kohn–Sham orbitals: the aromaticity of B_{13}^+

As mentioned in Section 2, the best orbitals for a single determinant wave function are the Hartree–Fock orbitals. The Kohn–Sham orbitals are obtained from the solution of Eq. (116) and, can be viewed as just another set of one-electron orbital functions, as many of the earlier proposed sets (Bruekner orbitals, Dyson amplitudes, etc.). However, the Kohn–Sham orbitals and their associated orbital energies have been recommended [105,106] as tools for traditional molecular orbital qualitative reasoning [302]. This proposal has been reinforced by recent comparative studies of the Kohn–Sham molecular with the Bruekner [303] and the Hartree–Fock [304] molecular orbitals.

Here, we will illustrate how the analysis of the molecular Kohn–Sham orbitals of B_{13}^+ can provide clues that explain its remarkable stability.

The B_{13}^+ has been regarded as an intriguing cluster after Hanley et al. [305] in 1988 found that together with B_5^+, it is especially stable as it yields a very intense peak

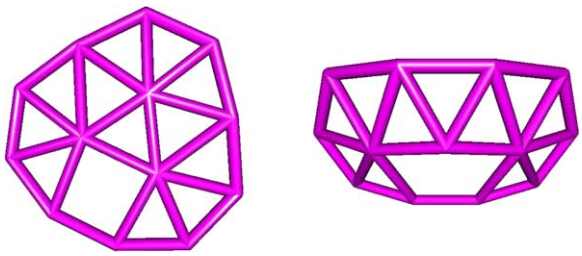

Fig. 3. B_{13}^+ most stable complexes. Ricca structure, at the left hand side is around 27 kcal/mol more stable than Boustani structure (right hand side).

in their mass spectra studies of boron clusters. Later experiments [306–309], putted forward the *anomalous* low reactivity of B_{13}^+. These two reasons together, provided a favorite playground for theoreticians, the results of Anderson's group inspired several theoretical studies of small boron clusters and especially the B_{13}^+ cation [310–317]. Especially interesting have been the discussion of π delocalization in quasi-planar, tubular, layered, and the hypothetical boron quasicrystal [315,318–321]. This triggered structural determination studies [313,314] for the various isomer of B_{13}^+. In Fig. 3 are shown the geometries two most stable isomers. We complemented these studies with a detailed investigation of various charge states of the B_{13} cluster and provided a more complete understanding of its electronic structure [322]. Experiments tell us that the B_{13}^+ cation is especially stable. Theory indicates that the structure, which is especially stable for the cation becomes relatively unstable as electrons are added. The examination of the molecular Kohn–Sham orbitals of our two lowest-lying isomers (shown in Fig. 3) will allow us to understand why.

Fig. 4 compares the benzene Kohn–Sham π-orbitals (b) and the corresponding molecular orbitals of B_{13}^+ Ricca (r) and Boustani's (B) structures. The orbital nodes are marked, and observe that orbitals with 0 and 1 nodes are binding orbitals while the two-node orbitals are antibonding. The occupation of these orbitals accounts for the high stability of B_{13}^+.

The Ricca isomer is planar, thus the pairs of orbitals with an equal number of nodes remain almost degenerate, Boustani's structure, however, is a non-planar oval shape, and its orbitals are split. Both cationic clusters have six π electrons, meaning that the orbitals with 0 and 1 nodes are filled with

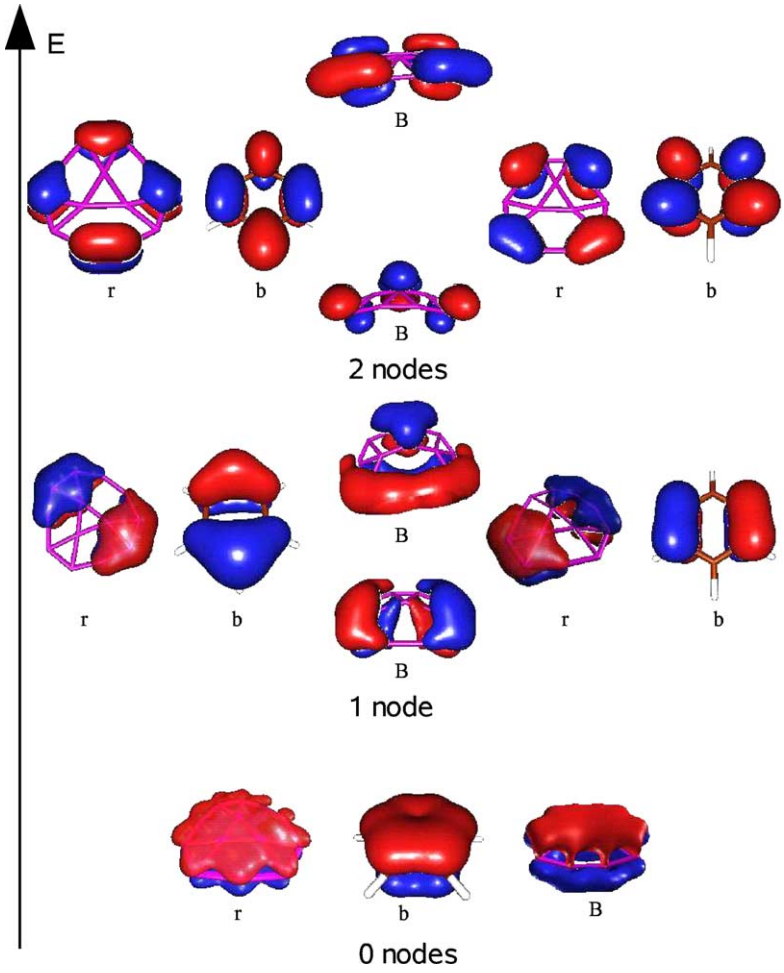

Fig. 4. Ricca (r) and Boustani (B) B_{13}^+ π-orbitals compared with benzene (b) ones.

two electrons each. The cationic Boustani structure adopts a C_s non-planar structure which reduces the favorable interactions between the π-orbitals. The Ricca structure, on the contrary, favors highly the π delocalization. Thus, its planar structure helps in understanding why is the most stable of the cations. As we add electrons, the two-node Kohn–Sham π orbitals are filled. Again, while Ricca two-node orbitals are near degenerate, Boustani's are not. Thus, the Ricca cluster has open a pair of quasi-degenerate orbitals, both of which lie higher in energy than that available to the Boustani isomer. The addition of one electron to the cationic clusters reduces the energetic difference between the two. This effect is repeated when a second electron is added making the Boustani anion more stable than the Ricca anion.

This analysis of the Kohn–Sham orbitals agrees with the prediction of a singlet ground state for the Boustani anion, a triplet ground state for the Ricca anion, and the difference in relative energies among the various charge states. It is also in support of the argument that the B_{13}^+ cationic cluster is especially stable because it is aromatic. Our hypothesis was later corroborated by Aihara [323].

5.2. Weak intermolecular interactions

Intermolecular interactions are normally much weaker than the normal intramolecular covalent bonds. Typically, the energies involved are 2.0–20.0 eV for valence covalent bonds, 0.03–0.3 eV for hydrogen bonds and charge-transfer interactions and 0.01–0.001 eV for van der Waals complexes.

The controlled making and breaking of covalent bonds constitutes the basis of molecular chemistry and lies at the core of the chemical sciences, which have acquired an enormous sophistication during the years. Besides, recently, attention has been given to the intermolecular interactions with aim of making highly complex chemical suprastuctures from molecules interacting through non-covalent intermolecular forces. Thus, the educated manipulation of intermolecular interactions has yield an entire new field beyond molecular chemistry called, *supramolecular chemistry* [324].

The precise understanding of the forces governing these weak intermolecular interactions is of paramount importance, therefore. However, since they amount for only tenths of a millionth of the total energy of the systems, calculations must be carried our with extreme care.

These weak interactions are dominated by electron correlation and consequently, they cannot be adequately described by the Hartree–Fock model, which normally yields almost zero intermolecular interaction energies and unreasonably large intermolecular equilibrium distances, or purely repulsive potential energy curves [325]. Consequently, post Hartree–Fock methods are mandatory. Among them, MP2 has been widely used as it represents an affordable compromise between cost and accuracy [326]. For instance, the basis set limit of the interaction energy of the hydrogen-bonded water dimer has been estimated [327] to be 0.212 eV at the MP2 level, whereas the highly costly (though accurate) CCSD(T) predicts an interaction energy of 0.215 eV. Both values compare well with the experimental estimate [328] of 0.234 ± 0.003 eV and suggests that correlation effects beyond MP2 are small in this case. However, even for systems of medium size, often MP2 calculation become impracticable. At this point density functional theory offers an alternative. One example is our recent B3LYP/6-311++G(d,p) study of the hydrogen bonding interactions between formic acid and pyridine [329]. The carboxylic acid–pyridine complexes have been studied extensively by Langner and Zundel [330] using infrared spectroscopy. Therefore, a wealth of experimental data is available for the purposes of comparison with the theoretical results.

In particular, we have been able to characterized a number of stable structures for this complex, which are shown in Fig. 5. The calculated harmonic vibrational frequencies scaled down by 0.9613, as recommended by Wong [331], are collected in Table 4, which contains data directly comparable with the experimental information available. Inspection of Table 4 reveals that the agreement between experiment and theory is remarkably good, which is very supportive of the reliability of the calculated structures and their relative stability order. Even more, the DFT calculations also helped in the identification of unassigned spectral features, like the small peak found in the far-IR spectrum of monochloroacetic acid–pyridine complex by Langner and Zundel as shown in their Fig. 7 of reference [330]. Our calculations demonstrated that the vibrational mode associated with the hydrogen bond vibration, with librational character, of the C–H···O hydrogen bonding interaction of 1, lies at 77.6 cm^{-1} and has a small IR intensity of 4 km/mol. This band nicely fits with the finding of Langner and Zundel and confirms further our structural predictions.

Table 4
Frequency shifts upon complexation of the fully symmetrical stretching vibration of pyridine, $\Delta\nu_1$, and of the stretching mode of the formic acid's H–O bond, $\Delta\nu_2$, in cm^{-1}

Structure	ν_1	ν_2	ν_{hbl}	ν_{hbs}	ν_3	ν_4
Present work Py···HCOOH						
1	14.8	776	120	192	78	1699
2	13.2	526	107	162	–	1758
Experimental values for Py···CH_3COOH						
	13.5	714–857	124	172	75	1700

Frequencies of the hydrogen bond vibrational modes, ν_{hbl} with more librational character and, ν_{hbs} with more stretching character, in cm^{-1}. Frequencies of the stretching modes of CH···O hydrogen bond, ν_3, and of the C=O of the formic acid, ν_4, in cm^{-1}.

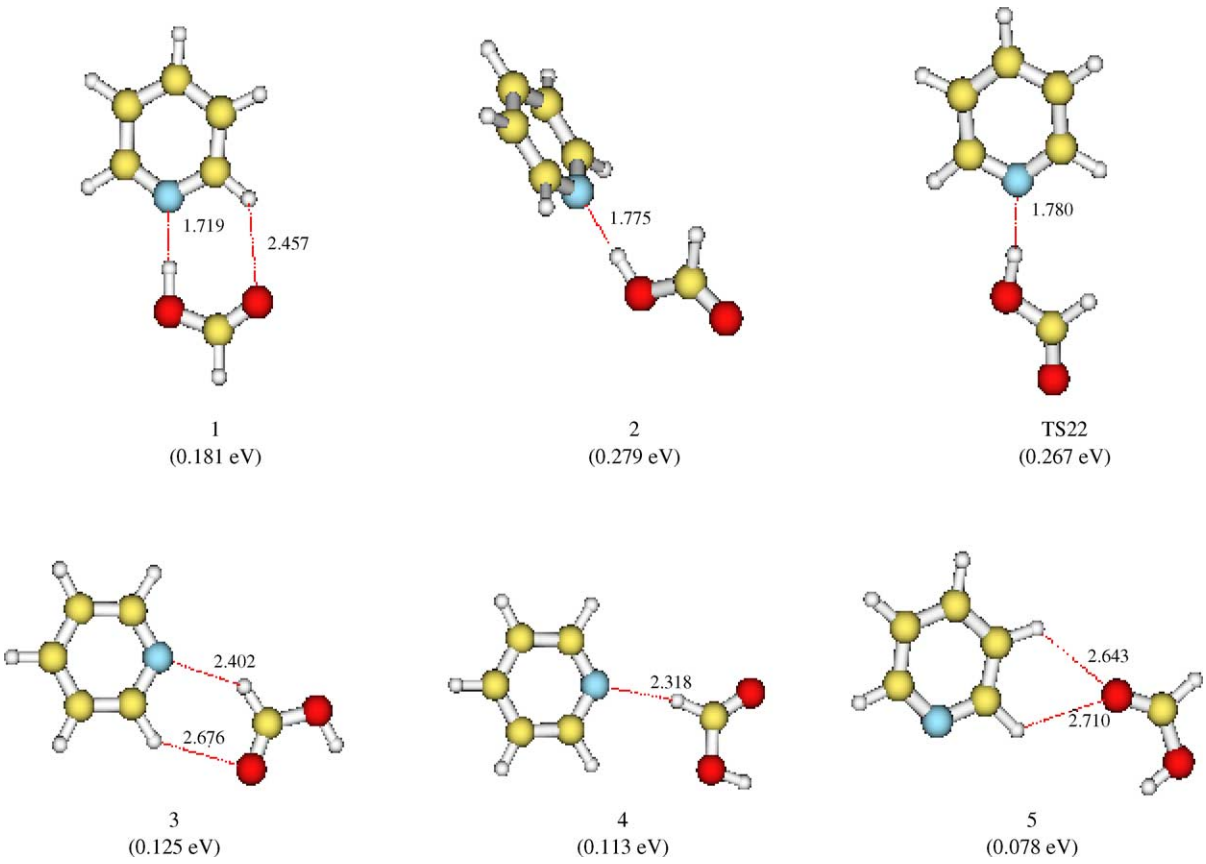

Fig. 5. Geometries of the pyridine–formic acid binary complexes optimized at the B3LYP/6-311++G(d,p) level of theory. Distances shown are in Å and, binding energies, in eV, in parenthesis.

The B3LYP approximate hybrid functional has also been helpful for the recent characterization of the intramolecular *blue-shifted* C–H···O hydrogen bond of the TG(T|G′) conformer of 1-methoxy-2-(dimethylamino)ethane (MDAE) [332], shown in Fig. 6. Indeed, Matsuura et al. characterized 14 isomers of MDAE, but found than only the two most stables ones were present when the molecule was prepared at low temperatures (12 K). Upon annealing at 41 K they observed that some of the experimentally recorded IR spectrum bands of the sample decreased their intensity, while several other band remain intact. By comparison with the B3LYP/6-311G+(d,p) vibrational frequencies, they rationalize that the bands which decreased their intensity belong to the second most stable isomer, the TT(T|G), which isomerizes to the most stable conformer TG(T|G′) during the annealing cycles. Interestingly, the intramolecular C–H···O hydrogen bond was found at 3016.5 cm^{-1}, a bit higher than the wavenumbers of C–H stretching vibrations of this type. Comparison with the corresponding C–H vibrational frequency of the TT(G|T) isomer, which has no intramolecular hydrogen bond, revealed that it was blue-shifted by at least 35 cm^{-1} due to the C–H···O hydrogen bond. This is the first experimental observation of intramolecular blue-shifting hydrogen bonding.

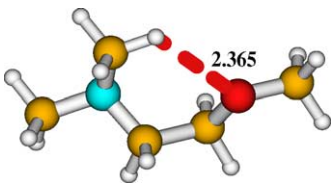

Fig. 6. The structure of the TG(T|G′) conformer of 1-methoxy-2-(dimethylamino)ethane optimized at the B3LYP/6-311++G(d,p) level of theory. Distances shown are in Å.

Nevertheless, it is worth mentioning that B3LYP is not an *all purpose* functional. For instance, Dunbar and coworkers [333] have recently studied the most favorable complexation site of aniline towards Cr^+. B3LYP predicts the side-chain site to be 0.075 eV more favorable that the ring site. However, the MPW1PW91 approximate hybrid functional of Adamo and Barone [334,335] favors the ring-bound structure by 0.072 eV. However, the experimental infrared spectrum agrees remarkably with theoretical spectrum calculated (both B3LYP and MPW1PW91 are very similar) for the ring-bound complex and does not have the intense peak near 1070 cm^{-1} corresponding to the frustrated inversion of the NH2 of the side-chain-bound complex. This supports the prediction for ring coordination of Cr to aniline, and suggests that the N-bound structure is at least ∼0.050 eV less stable. The

Table 5
The intermolecular distance, in Å, of the $H_3N\cdots F_2$ charge transfer complex at various levels of theory with the 6-311++G(2df,2p) basis set

MP2[a]	B3LYP	MPW1PW91	BH&HLYP	Experimental
2.572.70	2.085 (2.093)	2.036 (2.331)	2.710 (2.739)	2.706

Counterpoise corrected values in parenthesis.
[a] From [338].

MPW1PW91 approximate hybrid functional accounts for these facts. The superiority of MPW1PW91 over B3LYP has also been recently documented for transition metal–phenol complexes [336] and for the transition metal complexes with the curved π surfaces of corannulene and coronene [337].

However, the MPW1PW91 approximate hybrid functional presents as well, severe limitations for the investigation of some charge transfer complexes. Thus, the $H_3N\cdots F_2$ $n{\cdot}a\sigma$ charge transfer complex is poorly described by this functional, as revealed by inspection of Table 5.

Observe that inclusion of the counterpoise correction during the optimization process does not help much neither to the MPW1PW91 and to the B3LYP hybrid functionals.

On the other hand, the BH&HLYP hybrid functional does a nice job and provides a fairly good agreement with experimental data. Indeed, this functional has been found [339–341] to be very good for the whole series of ammonia–dihalogen complexes $H_3N\cdots XY$, with X, Y = F, Cl, Br. Observe from Table 6 that it consistently predicts the experimental intermolecular distance and force constant. Notice that due to the strong anharmonicity of the intermolecular stretching potential, the force constant has been obtained from the numerical solution of the Schrödinger equation with the potential $V(R)$ evaluated at selected intermolecular distance, which yields the energies, $E_{v=0,1,2,\ldots}$, of the vibrational states associated with the intermolecular stretching. Then, the intermolecular stretching force constant is estimated as:

$$k_\sigma = \nu^2\mu \tag{220}$$

where μ is the reduced mass of the reduced mass of the intermolecular stretching mode and ν is:

$$\nu = \frac{1}{h}(E_{v=1} - E_{v=0}) \tag{221}$$

the frequency of the $1 \leftarrow 0$ vibrational transition. Notice that R_e represents the minimum energy intermolecular distance, while R_o stands for the expectation value of the intermolecular distance in the vibrational intermolecular stretching ground state. This is the quantity that is measured in the experiments and for which the BH&HLYP/6-311++G(2df,2p) is rather accurate for these charge transfer complexes as shown in Table 6.

As mentioned above, van der Waals complexes have interaction energies as small as a few meVs. For such small interaction energies, it does not come as a surprise that the BSSE will represent a problem, most of the cases. Therefore, the computational strategy has to consider using basis sets as large as possible, in order to minimize the basis set superposition error. For instance, the basis set superposition error of the neon dimer at the experimental [342] equilibrium separation of 3.09 Å is 0.0054 eV at the MP2/cc-pVTZ level of theory. The corresponding van der Waals interaction energy is 0.0022 eV, less than half of the error due to the superposition of the basis sets. This demonstrates that for an accurate calculation of dispersion (van der Waals) interaction energies it is essential to account for the BSSE. Even more, there is a mounting evidence that BSSE influences the structure optimization process. Hence, explicit consideration of BSSE must be applied during the optimization of the complex structure, even when large basis sets have been used. This point has been illustrated recently by Lundell and coworkers [343] for the van der Waals complex between formic acid and argon. They used the algorithm of Simon et al. [344] to include BSSE effects during the geometry optimizations and found that both the intramolecular stretching modes decreased and intermolecular stretching increased, compared to calculations without the BSSE correction.

All these considerations pinpoint the necessity of using very computationally demanding molecular orbital theory methods to handle properly this kind of weakly bound systems. Hence, only the very small ones are amenable to MO theory investigation. For larger ones, density functional theory appears as the most reliable alternative [345,346]. Within this context, recent efforts by Zhao and Truhlar [347] have crystallized in two promising new hybrid meta functionals that give reasonable results for thermochemistry, thermochemical kinetics, hydrogen bonding and van der Waals in-

Table 6
BH&HLYP/6-311++G(2df,2p) minimum energy intermolecular distance R_e, in Å, equilibrium intermolecular distance R_o, in Å, and intermolecular stretching force constant, in N/m, along with their experimental counterparts

XY	R_e	R_o	Experimental	k_σ	Experimental
F_2	2.710	2.722	2.706	4.75	4.70
Cl_2	2.697	2.730	2.730	13.54	12.71
Br_2	2.660	2.686	2.720	18.30	18.50
ClF	2.350	2.367	2.370	32.90	34.40
BrCl	2.587	2.630	2.628	25.29	26.70

teractions.

As indicated in above, all current DFT functionals are based on the local electron density, its gradient, and the local kinetic energy density, $\sum_i^N \vec{\nabla}\psi(\mathbf{r})^* \cdot \vec{\nabla}\psi(\mathbf{r})$. Consequently, since the van der Waals interactions contribute at regions where the electron overlap is negligible, these approximate functionals are not properly designed to reproduce the leading R^{-6} van der Waals dispersion interaction term correctly [348]. Nevertheless, it is worth noting that for some particular cases, currents DFT calculations yield satisfactory results [349–351]. This apparent success, though, is now well established that results from fortuitous favorable cancellation of errors [352,353].

To overcome this deficiency, two approaches have been pursued. On the one hand, new density functionals are developed that allow for the correct description of the van der Waals interaction. Within this context, the work of Kohn et al. [116] is remarkable for it provides an exact description of the dispersion interactions at all intermolecular distances. However, their procedure is computationally extremely demanding.

On the other hand, a more practical empirical procedure was suggested by the earlier work of Thakkar and coworkers [354]. The procedure consists of adding a damped correction term to the regular DFT total energy:

$$E_{\text{tot}} = E_{\text{DFT}} + E_{\text{disp}} \tag{222}$$

The general form of the correction term agreed in the literature is:

$$E_{\text{disp}} = \sum_n \sum_{\alpha<\beta} f_{d,n}(R_{\alpha\beta}) \frac{C_{n,\alpha\beta}}{R^n_{\alpha\beta}} \tag{223}$$

where α and β are the centers of the interacting atom pairs, $R_{\alpha\beta}$ is the distance between them and $f_{d,n}$ and $C_{n,\alpha\beta}$ are the related damping polynomial function of order n and the interaction coefficients, which are calculated either from averaged atomic or molecular polarizabilities [355].

This approach has been recently tested by Parrinello and coworkers [356] for the water–benzene van der Waals complex. They found that of all the approximate functionals checked B3LYP in combination with the damping function of Wu and Yang [357]:

$$f_d = \frac{1}{1 + \mathrm{e}^{-23(R_{\alpha\beta}/R_m - 1)}} \tag{224}$$

R_m being the sum of the atomic van der Waals radii of atoms α and β obtained from Bondi [358], and the Slater–Kirkwood combination rule for the interaction coefficients, namely:

$$\mathcal{C}_{6,\alpha\beta} = \frac{2(\mathcal{C}^2_{6,\alpha\alpha}\mathcal{C}^2_{6,\beta\beta}N_\alpha N_\beta)^{1/3}}{(N^2_\beta \mathcal{C}_{6,\alpha\alpha})^{1/3} + (N^2_\alpha \mathcal{C}_{6,\beta\beta})^{1/3}} \tag{225}$$

where N_α stand for the effective number of electrons of atom α and is estimated by the empirical formula of Halgren [359], yields the most consistent description of the interaction energies. Nevertheless, it is cautiously warned that careful validation of the procedure is needed for every new class of systems.

5.3. Dissociation energies of ferrocene ion–molecule complexes

Since its fortuitous discovery [360], ferrocene $(C_5H_5)_2Fe$, is an ubiquitous molecule for many branches of chemistry. However, the theoretical description of many of its properties has been found challenging. In the present example, we will discuss on various properties of ferrocene, like the metal-to-ring distance (Table 7), the heterolytic dissociation energy, as dictated by:

$$FeCp_2 \rightarrow Fe^{2+}(1I) + 2Cp^- \tag{226}$$

and the energies and structures of its ion–molecule complexes with H^+ and Li^+.

Although most theoretical procedures predict in agreement with the available experimental results, that the eclipsed configuration of ferrocene is slightly more stable than staggered, the prediction of the metal-to-ring equilibrium distance in ferrocene has been reported as notoriously difficult [363,365,367].

It has been pointed out that the metal–ligand distance is a problem in ferrocene because of the dynamic correlation [365,367]. Hence, both a size-extensive treatment of correlation effects and, a large enough basis set as to balance properly the electron relaxation effects are needed to reproduce

Table 7
Iron-cyclopentadienyl vertical distance, in Å, in the ferrocene molecule

Method	Distance
B3LYP/DZVP [361]	1.672
B3LYP/TZVP+G(3df,2p) [361]	1.689
Experiment [362]	1.66
HF [363]	1.88
HF [364]	1.872
MP2/[16s12p8d6f] (58)[364]	1.489
MP2-R12/[16s12p8d6f] (58) [364]	1.481
MP2/[16s12p8d6f] (66) [364]	1.474
MP2-R12/[16s12p8d6f] (66) [364]	1.468
MCPF/ [4s4p3d 1f] (66) [365]	1.684
MP2[a] [365]	1.65–1.67
MCPF[b] [365]	1.727
MCPF[c] [365]	1.865
CASSCF(10,10)/[6s5p4d2f] [366]	1.716
CASPT2(10,10)/[6s5p4d2f] (58) [366]	1.617
CASPT2(10,10)/[6s5p4d2f] + BSSE (58) [366]	1.643
CCSD/DZP (66) [66,367]	1.675
CCSD/DZP (96) [96,367]	1.672
CCSD/TZV2P+f (66) [367]	1.672
CCSD/TZV2P+f (96) [367]	1.664
CCSD(T)/DZP (66) [367]	1.665
CCSD(T)/TZV2P+f (66) [367]	1.660

In parenthesis the number of correlated electrons.
[a] Values calculated replacing the iron atom by a +2 point charge.
[b] Single excitations excluded.
[c] Single excitations included.

Table 8
Zero-point vibrational energy corrections ZPVE, basis set superposition error corrections (BSSE), and dissociation energies (D_0) in kcal/mol, for the heterolytic reaction [226]

Method	ZPVE	BSSE	D_0
B3LYP/DZVP [361]	−8.008	10.350	676
B3LYP/TZVP+G(3df,2p) [361]	−7.913	1.962	656
SCF [366]		9	570
SCF [367]		6	572
MP2 (58) [366]		28	706
MP2 (58) [367]		15	699
MP2 (66) [366]		45	732
MP2 (66) [367]		20	724
CCSD (66) [367]			706
CCSD(T) (66) [367]			728
CASSCF [366]			650
CASPT2 [366]			745
Theoretical estimate (CASPT2) [364]	−7		657
Theoretical estimate (CCSD(T)) [364]	−7		653
LDA [369]	−7	7	733
BPW91 [369]	−7	6	663

In parenthesis the number of correlated electrons.

the correct equilibrium structure of ferrocene within 0.01 Å.

In Table 7, we collect the calculated metal-to-ring distances of ferrocene found in the literature. We have separated the DFT and MO results. Naturally, the best accord with experiment is obtained with the extremely expensive CCSD(T)/TZV2P+f level of theory. However, critical inspection of the data given in Table 7 highlights the reliability of the remarkably less costly B3LYP hybrid functional.

The same conclusion is reached by the analysis of the dissociation energy of ferrocene as calculated in accordance with Eq. (226). Observe from Table 8 that the best DFT result [361] of 656 kcal/mol for the dissociation energy leads to a value of 648 kcal/mol for the dissociation enthalpy at 298 K, which overestimates slightly the experimental value [368] of 635 ± 6 kcal/mol.

Even more, the proton affinity of ferrocene at temperature T, calculated as:

$$PA(T) = \Delta E_e + \Delta E_v + \Delta E_r + \frac{5}{2}RT \quad (227)$$

where ΔE_e, ΔE_v and ΔE_r are, respectively, the electronic, vibrational, and rotational energy differences of the following reaction:

$$FeCp_2 + H^+ \rightarrow FeCp_2 \cdots H^+ \quad (228)$$

has also been extensively studied. Notice that ΔE_v can be taken approximately as the zero-point vibrational energy difference of reaction [228], Table 9 shows some of the values for $T = 298$ K which can be found in the open chemical literature. These data confirms that the B3LYP hybrid approximate functional constitutes a convenient low-cost computational procedure for the theoretical investigation of the ferrocene ion–molecule complexes.

Consequently, we studied the Ferrocene···Li^+ ion–molecule complex at the B3LYP/TZVP+G(3df,2p) level of theory (see Fig. 7). Two different minimum energy structures were found, ring-bonded and metal-bonded. These structures are both stable for the case of the lithium cation, opposite to the protonated ferrocene for which only one stable structure was found. Calculations at the B3LYP/TZVP+G(3df,2p) level of theory predicted that the metal-bonded isomer of $Cp_2Fe\cdots Li^+$ lies 8.52 kcal/mol higher in energy than the ring-bonded isomer.

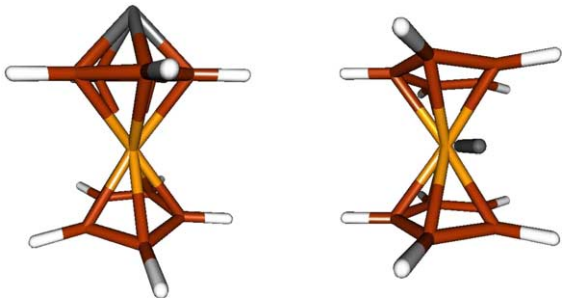

Fig. 7. Ferrocene···Li^+ stable structures. Ring-bonded complex on the left and metal-bonded on the right.

However, the metal-bonded structure is unique for it constitutes a pure *planetary system* with the lithium cation *orbiting* around the ferrocene on a *planar* orbit, since the transition state connecting any two adjacent equivalent forms are separated by a barrier of only 2.6 kcal/mol [361]. To our knowledge this was the first *planetary system* found up to date having one and only one *planar* orbit.

Remarkably, Scheibitz et al. [372] have recently provided experimental evidence for the existence of this metal-bonded structure.

5.4. Electron detachment energies

The electron detachment energy (EDE) is an experimentally accessible quantity and consequently has been the target of intense theoretical efforts. Some of them have yielded inaccurate procedures (Koopmans' theorem based procedures [26]) and some have yielded substantially more accurate ones, but very demanding from the computational viewpoint (the outer valence green functions (OVGF) [373] method, for instance).

However, in Section 3.3 we have described the strategy of Jellinek and Acioli [158–162] to convert the Kohn–Sham orbital energies into electron detachment energies. This strategy provides a fast, and cheap (by means of computational cost) way to calculate EDEs not only of the external electrons, but also the internal ones.

Table 9
Proton affinity of ferrocene, in kcal/mol, for $T = 298$ K

Method	PA(T)
B3LYP/DZVP [361]	207.6
B3LYP/TZVP+G(3df,2p) [361]	207.2
Experimental [370]	207 ± 1
CCSD/DZVP [371]	217.7

Table 10
Experimental and theoretical EDEs, in eV, for the pyramidal $LiAl_4^-$

MO	EDE (experimental)	EDE (OVGF)	EDE (Jellinek)
$3a_1$	2.15 ± 0.06	2.09	1.94
$1b_1$	2.20 ± 0.06	2.17	2.03
$2a_1$	2.82 ± 0.08	2.69	2.64
$1b_2$	3.09 ± 0.04	2.97	3.22

We have chosen the recently detected [374] all-metal aromatic molecule $LiAl_4$, in order to illustrate the Jellinek approach to calculate the EDEs of various electrons of the molecule. Li et al. detected this species with a laser vaporization source and a negative ion photoelectron spectroscopy. They were able to measure the EDEs, and by comparing these experimentally obtained EDEs with the calculated ones, they proposed that the $LiAl_4^-$ compound corresponded to a pyramidal structure, where the Al_4 atoms form a perfect square with the lithium atom above it, forming a pyramid. In Table 10 we collect the experimental and theoretical EDE values they reported for this molecule. We also collect the values calculated using the Jellinek approach and describe in detail the steps for calculating them.

According to the Jellinek procedure, the EDE of both HOMO electrons, is given by Eq. (133), which is just the vertical EDE, and in our 56-electron system is written as:

$$\mathrm{BE}(56) = E(55) - E(56) \tag{229}$$

where the $E(56)$ is the energy of our molecule and $E(55)$ the energy of the same molecule but with 55 electrons.

In order to calculate the EDE of electron 54, we must follow Eqs. (134)–(136). These equations turn out to be:

$$\Delta_{54}(56) = \Delta E_{54}(56) - (-\epsilon_{54}(56)) \tag{230}$$

where

$$\Delta_{54}(56) = \Delta_{54}(55) + [\Delta_{55}(56) - \Delta_{54}(55)]\alpha_{54}(56) \tag{231}$$

and

$$\alpha_{54}(56) = \frac{\epsilon_{54}(56) - \epsilon_{54}(55)}{\epsilon_{55}(56) - \epsilon_{54}(55)} \tag{232}$$

$\alpha_{54}(56)$ is easily calculated with the values of Table 11 ($\alpha_{54}(56) = 0.9807$) and applying again Eq. (135) we can calculate $\Delta_{54}(55)$, i.e.

$$\Delta_{54}(55) = \Delta_{54}(54) + [\Delta_{55}(55) - \Delta_{54}(54)]\alpha_{54}(55) \tag{233}$$

with

$$\alpha_{54}(55) = \frac{\epsilon_{54}(55) - \epsilon_{54}(54)}{\epsilon_{55}(55) - \epsilon_{54}(54)} \tag{234}$$

which has a value of $\alpha_{54}(55) = 0.9935$.

$\Delta_{55}(55)$ and $\Delta_{54}(54)$, which are the external electrons, are directly calculated from Eq. (133):

$$\begin{aligned}\mathrm{BE}_{55}(55) &= E(54) - E(55) \\ &= (-977.0367744) - (-977.2651138) \\ &= 0.2283394\,\text{a.u.}\end{aligned} \tag{235}$$

then,

$$\begin{aligned}\Delta_{55}(55) &= \mathrm{BE}_{55}(55) - (-\epsilon_{55}(55)) \\ &= 0.2283394 - 0.17046 = 0.0578794\,\text{a.u.}\end{aligned} \tag{236}$$

and similarly $\Delta_{54}(54) = 0.0664019$. Substituting $\Delta_{54}(54)$, $\Delta_{55}(55)$ and $\alpha_{54}(55)$ in Eq. (233), we get that $\Delta_{54}(55) = 0.05793446$. We still need to know the value for $\Delta_{55}(56)$, which is obtained in the same way:

$$\Delta_{55}(56) = \Delta_{55}(55) + [\Delta_{56}(56) - \Delta_{55}(55)]\alpha_{55}(56) \tag{237}$$

with

$$\alpha_{55}(56) = \frac{\epsilon_{55}(56) - \epsilon_{55}(55)}{\epsilon_{56}(56) - \epsilon_{55}(55)} \tag{238}$$

analyzing $\alpha_{55}(56)$, one easily deduce its value is 1, since $\epsilon_{55}(56)$ and $\epsilon_{56}(56)$ are both the HOMO electrons, and have the same energy. Thus, $\Delta_{55}(56) = \Delta_{56}(56) = 0.0498903$. And we can now solve Eq. (231):

$$\begin{aligned}\Delta_{54}(56) &= 0.057934 + [0.0498903 - 0.0578794]0.980774 \\ &= 0.050098\,\text{a.u.}\end{aligned} \tag{239}$$

and finally:

$$\begin{aligned}\mathrm{BE}_{54}(56) &= \Delta_{54}(56) - \epsilon_{54}(56) = 0.02456 + 0.050098 \\ &= 0.074658\,\text{a.u.} = 2.030\,\text{eV}\end{aligned} \tag{240}$$

Table 11
Orbital energies (a.u.), of the $LiAl_4^-$ and its different charged states used in the Jellinek approach

$LiAl_4^-$		$LiAl_4$		$LiAl_4^+$		$LiAl_4^{2+}$	
Orbital	Energy	Orbital	Energy	Orbital	Energy	Orbital	Energy
$\epsilon_{56}(56)$	−0.02168						
$\epsilon_{55}(56)$	−0.02168	$\epsilon_{55}(55)$	−0.17046				
$\epsilon_{54V}(56)$	−0.02456	$\nu_{54}(55)$	−0.17148	$\epsilon_{54}(54)$	−0.32832		
$\epsilon_{53}(56)$	−0.02456	$\epsilon_{53}(55)$	−0.16758	$\epsilon_{53}(54)$	−0.32832	$\epsilon_{53}(53)$	−0.51700
$\epsilon_{52}(56)$	−0.04656	$\epsilon_{52}(55)$	−0.18975	$\epsilon_{52}(54)$	−0.34386	$\epsilon_{52}(53)$	−0.52288
$\epsilon_{51}(56)$	−0.04656	$\epsilon_{51}(55)$	−0.18737	$\epsilon_{51}(54)$	−0.34386	$\epsilon_{51}(53)$	−0.51394
$\epsilon_{50}(56)$	−0.06399	$\epsilon_{50}(54)$	−0.36640	$\epsilon_{50}(53)$	−0.54424		
E_{B3LYP}	−977.3367	E_{b3LYP}	−977.2651	E_{B3LYP}	−977.0368	E_{B3LYP}	−976.6420

The number in parentheses corresponds to the total electron number, and the subscript is the energy of the numbered electron

$BE_{52}(56)$ is calculated in the same manner and the obtained value is reported in Table 10. Observe that EDEs obtained following the Jellinek procedure are very close to the experimental values, and also agree very well with the OVGF calculated EDEs. But the procedure describe above does not require that much calculation time, only three extra energy calculations in order to calculated EDEs up to the sixth electron.

5.5. Discordant results on the $FeO^+ + H_2$ reaction reconciled by quantum Monte Carlo theory

The reaction of the iron oxide with the hydrogen molecule has been extensively studied both experimentally [375–377] and theoretically [378–381], for it represents an appropriate example [378] in order to develop chemical understanding for the reactivity of the late transition metal oxides toward activation of σ-bonds.

In spite of the intense effort dedicated to this reaction and the *qualitative* agreement achieved between experiment and theory [379,380], theory does not yet concur *quantitatively* with the well established experimental facts. Thus, in the $FeO^+ + H_2 \rightarrow Fe^+ + OH_2$ reaction, experimentalists [375,376] observed a very inefficient barrierless reaction (once in every 600 collisions) and a very efficient reaction with a barrier of ∼0.6 eV. Concomitantly, theoreticians using both, multi-reference CASPT2 [378] and single-reference CCSD(T) [381] methods, have been able to characterized a transition state of sextet spin multiplicity 0.55 eV above the separated $FeO + (^6\Sigma) + H_2$ ground state reactants, which is in concurrence with the efficient reaction with barrier. However, the quartet spin multiplicity transition state associated with the $FeO + (^4\Phi) + H_2$ excited state process, lies higher in energy than $FeO + (^6\Sigma) + H_2$ by 0.33 eV. This means that a barrierless pathway, inefficient due to spin crossing, would not agree with the theoretical predictions. Density functional theory calculations [379,381] predict the quartet transition state at only 0.045 eV above the $FeO + (^6\Sigma) + H_2$ asymptote and hence, could account for the inefficient barrierless reaction. However, DFT does badly at the exit channel, placing the ^4F state of Fe^+ 0.18 eV below the ^6D state, which well-known to be ground state of the iron cation.

In this example, the diffusion quantum Monte Carlo method [382,383] has been used for the calculations. The structures used throughout this work were previously optimized at the B3LYP/TZVP+(3df,2p) level of theory [381]. Confidence on these structures is lend by the remarkable agreement with recent accurate bond length determination of the $^6\Sigma$ ground state of FeO^+. For the DMC single point calculations Slater–Jastrow type guiding wave functions, consisting of the product of a Slater determinant built with the B3LYP/TZVP+(3df,2p) orbitals and a Jastrow correlation factor [384] have been used. The Stuttgart pseudopotentials which include relativistic corrections [385] have been used for Fe and O, motivated by their earlier successful performance in DMC calculations on Fe atom [386]. For the hydrogen atoms the 6-311++G(2df,2p) basis set of Pople and coworkers [387] was chosen. The nonlocal energy was evaluated stochastically within the locality approximation [83,388,389]. The 25-parameter Jastrow factors were optimized using efficient variance minimization techniques [390,391]. All of the DMC calculations were performed using the CASINO code [392]. We emphasize that the DMC energies are not limited by the basis set or the detailed form of the orbitals. The DMC energy is fixed only by the nodal surface of the guiding wave function.

In order to check the reliability of our DMC method, we have compared with the best experimental data available, the calculated lowest electronic excitation energies of the iron oxide and the iron cation and the ionization potentials of iron and oxygen. See Table 12.

It can be observed that the theoretical results agree well with the experimental data, thus validating our level of theory for the investigation of the $FeO^+(^6\Sigma) + H_2 \rightarrow Fe^+(^6D) + H_2O$ and $FeO^+(^4\Phi) + H_2 \rightarrow Fe^+(^4F) + H_2O$ potential energy surfaces (PES), which are shown in Fig. 8.

Observe that the $^6\Sigma$ ground state of FeO^+ is 0.36 eV more stable than its $^4\Phi$ quartet state. This agrees with earlier DFT results [379,381], but it does not come along with the substantially larger splitting energies of the CASPT2 [378], 0.82 eV, and CCSD(T) [381], 0.54 eV, methods.

Both the sextet and quartet potential energy surfaces correspond with a two-step reaction, having two transition states. In both cases the first step determines the reaction kinetics. Following the sextet reaction path it may be observed that the TS1(6) structure lies 0.56 eV above the reactives. This is in concurrence with the experimental efficient reaction path with a barrier of ∼0.6 eV.

Experimentally, when the reactants have been carefully prepared in their ground state [376], another barrierless and inefficient reaction path, is also observed which has challenged the theoretical interpretation.

According to Fig. 8, there is a spin-crossing from the sextet potential energy surface to the quartet potential en-

Table 12
Experimental and DMC electronic excitation energies, ΔE in eV, between lowest lying electronic states of FeO and Fe^+ and, and experimental and DMC ionization potentials, IP in eV, of O and Fe

	ΔE			IP	
	DMC	Experimental		DMC	Experimental
$FeO: {}^5\Delta \rightarrow {}^5\Sigma$	0.54 ± 0.04	0.49	O	13.56 ± 0.02	13.62
$Fe^+: {}^6D \rightarrow {}^4F$	0.32 ± 0.04	0.25	Fe	7.67 ± 0.07	7.87

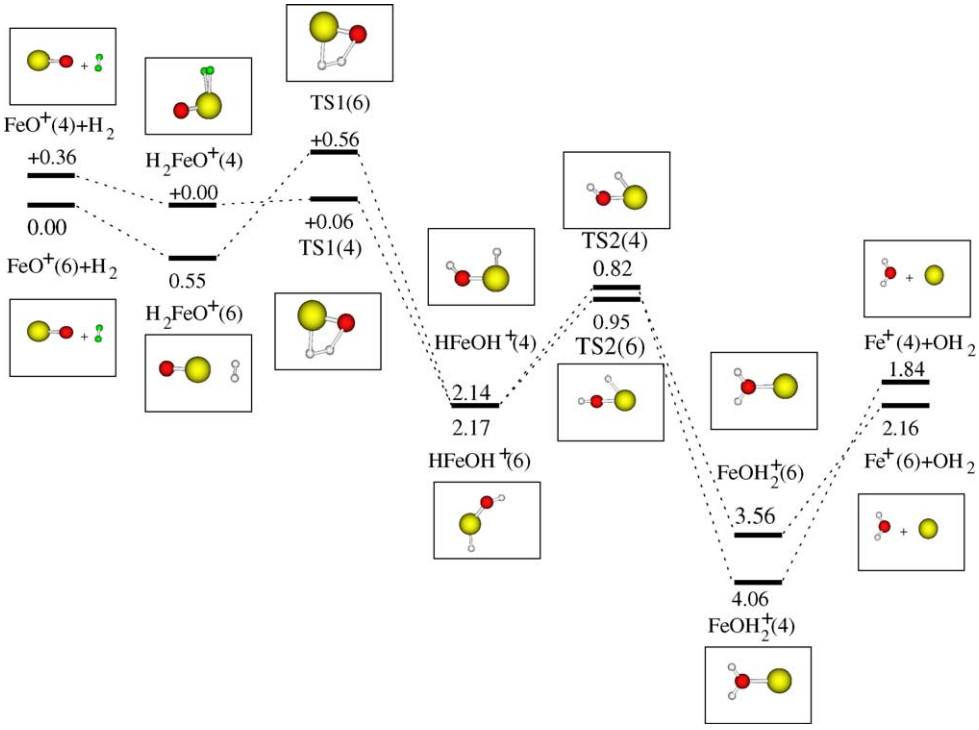

Fig. 8. DMC//B3LYP potential energy surface following the $Fe^+ + OH_2 \rightarrow FeO^+ + H_2$ reaction path. Energies are given in eV and are relative to the ground state reactants, $FeO + (^6\Sigma) + OH_2$.

ergy surface nearby the TS1 region. The barrier on this path is 0.06 eV, an energy which is easily gained at room temperature. This explains that the reaction is barrierless, and the fact that a spin-crossing has to occur accounts for the inefficiency of the reaction. Both reaction paths end up at the $Fe^+(^6D) + H_2O$ asymptote, which lies 2.16 eV below the reactives. The calculated energy difference between the ^6D ground state of Fe^+ and its the lowest lying quartet ^4F state is 0.32 ± 0.03 eV, which agrees well with the experimental estimate of 0.25 eV. Consequently, our calculations account correctly for the experimental facts at both ends of the reaction.

One more controversial point of this reaction concerns with the relative stability between the quartet and sextet electromers of the inserted hydrido iron hydroxide cation $HFeOH^+$. Thus, earlier CASPT2 calculations [378] placed the quartet 0.48 eV below the sextet, which agrees qualitatively with the DFT value [380,381] of 0.13 eV. However, CCSD(T) reversed the stability [381] and the sextet was calculated to be ground state, however the quartet lies only 0.065 eV higher in energy. DMC predicts that both electromers are essentially degenerate in energy, although the sextet is 0.03 eV more stable.

Observe that DMC provides a *consistent* explanation of the experimental evidences all along the reaction path. This should be ascribed to the fact that DMC calculates almost all the correlation energy, which is of paramount importance for the correct description of the electronic structure of the transition metals in general and for iron in particular.

5.6. Stability and aromaticity of B_iN_i rings and fullerenes

Relative energies between different cluster structures of the same size are usually accurately calculated by current approximate DFT methods. Therefore, the most stable structure for each cluster size can be predicted. However, for several cases, the accuracy of the DFT method is not sufficient and, the incorrect structure is predicted to be the most stable, as it occurs for pure carbon clusters near the crossover to fullerene stability [393]. In order to predict correctly the most stable structure, DMC method was used. A similar case occurs for BN clusters, as we show in this example.

In order to characterize the cluster geometries we use the hybrid B3LYP exchange-correlation functional within density functional theory with soft pseudopotentials to model the core electrons [394], which are important for efficient quantum Monte Carlo calculations. These pseudopotentials were combined with an optimize set of uncontracted Gaussian basis functions for the valence electrons, which contains five s-type, five p-type, and one d-type functions for both B and N. However, energy differences obtained within density functional theory may not be as accurate as one would like, and therefore when the energy differences are small we have performed DMC calculations with Slater–Jastrow type guiding wave functions as described above. The Jastrow factors, up to 25 parameters, were optimized using efficient variance minimization techniques. All of the DMC calculations were performed using the CASINO [392] code.

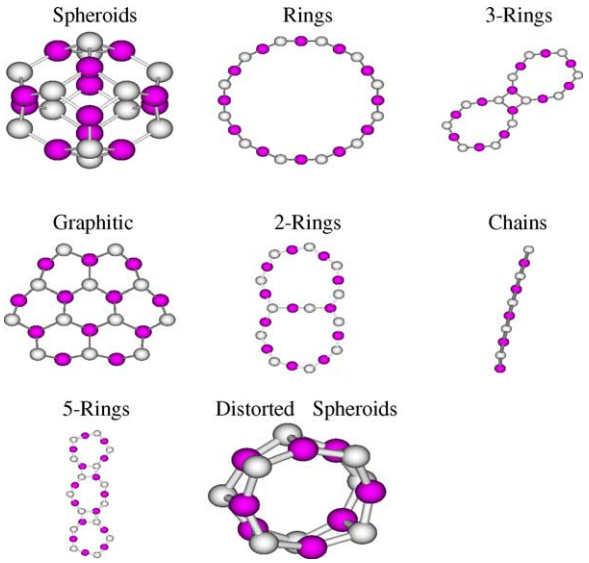

Fig. 9. Model structure for each family.

The characterized structures can be divided into different families, namely, rings (R), chains (C), two-rings (2R), three-rings (3R), five-rings (5R), graphitic-like (G), three-dimensional spheroids (S), and distorted spheroids (D). Spheroids are built from squares and hexagons. The number of squares remains constant and equal to 6, while the number of hexagons increases as the cluster size increases. A representative structure of each family is depicted in Fig. 9. The structures are labeled according to the following system: $B_iN_i^a$, where i denotes the number of BN units, and the superscript a denotes the family of the structure. In Fig. 10, all B3LYP energies of each structural family, relative to the rings, are depicted as a function of the cluster size. We observe that rings are the global minimum structures for $i = 2$–11,13, and spheroids for $i = 12$, 14, 15. In the small cluster size region, $i = 2$–5, rings clearly dominate, except for $i = 2$, where the chain structure lies close in energy. Then, as the cluster size increases, the energy differences of all the families decreases, specially that of spheroids, which become the most stable structures for larger cluster sizes. The three-ring structures also lie close in energy for large cluster sizes. DMC calculations will provide a more accurate picture of the relative energies for regions where different structures lie close in energy. The structures chosen for the DMC calculations are the ring and chain for $i = 2$, and rings, three-rings and spheroids for $i = 8$–13.

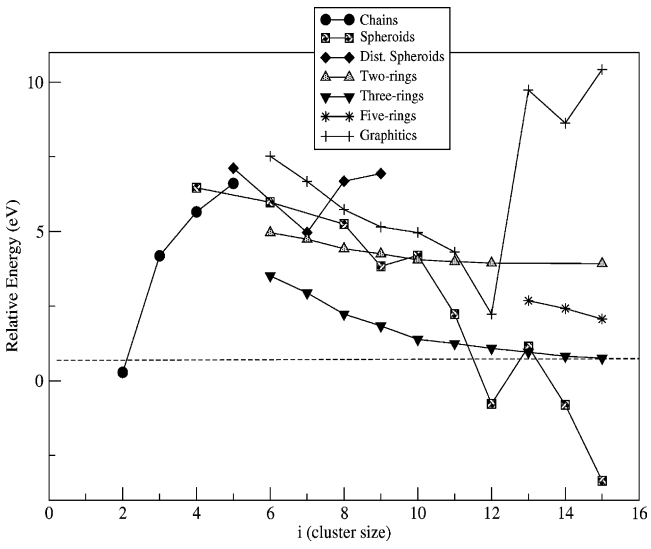

Fig. 10. Energy differences between the ring and the remaining structure in kJ/mol at the R3TVP level of theory.

Before calculating the DMC energies let us analyze the aromaticity of $B_iN_i^R$ and $B_iN_i^{3R}$ structures. In order to do this, we use the NICS method, which is a magnetic criterion that mirrors the ring current. The NICS values are calculated using the gauge-including atomic orbitals (GIAO) method at the B3LYP level of theory. Recall that the aromaticity of a ring structure can be studied by computing the NICS value in the center of the structure, either in the plane of the ring or 1 Å out of the plane, which are generally denoted as NICS(0) and NICS(1), respectively. If the corresponding NICS values are negative, the structure is aromatic [395,396]. Negative values arise when diatropic ring currents dominate, i.e., aromaticity, while positive values arise when paratropic currents dominate, i.e., anti-aromaticity. The NICS(0) value, calculated at the center of the ring, is influenced by the σ-bonds, and therefore calculation of the NICS(1), 1 Å out of the plane, yields a more reliable result, because these values are mainly influenced only by the π system [396]. The obtaine NICS(1) results are given in Table 13. In the case of $B_iN_i^R$ structures, rings with odd values of i are aromatic, and anti-aromatic for i even, except for $i = 2$. As the size of the ring increases the aromaticity decreases, $B_7N_7^R$ being the largest aromatic ring. For $B_7N_7^{3R}$ structures, which are built from two B_iN_i rings linked together by a B_2N_2 ring, only structures containing B_iN_i $i = 3$, 5 rings are aromatic. Comparing these results with isolated ring results, we see that the aromaticity of these rings decreases from isolated rings to rings within $B_iN_i^{3R}$ structures. In this way, isolated $B_2N_2^R$ and $B_7N_7^R$ are aromatic, but are anti-aromatic when fused with other rings within $B_iN_i^{3R}$ structures. Similarly, notice that for all even-i rings the anti-aromaticity increases, compared with their corresponding values for isolated rings.

The relative energies calculated in DMC and B3LYP are compared in Table 14. For the $i = 2$ case, DMC confirms the B3LYP result, where the ring is more stable than the chain. For larger clusters, $i = 8$–13, the results have to be discussed in a deeper way. First of all, recall that $B_iN_i^R$ structures are predicted not to be aromatic for $i \geq 8$, while $B_iN_i^{3R}$, $i = 9$, 10, 11 have aromatic components, which are the B_5N_5 rings. For $i = 8$, 9 DMC and B3LYP results are in agreement, and both predict B_iN_i clusters to be the global minima. The case of $i = 10$ is different. DMC predicts $B_{10}N_{10}^{3R}$ to be the global minimum, which has two aromatic B_5N_5 rings, while B3LYP predicts the anti-aromatic $B_{10}N_{10}^R$ to be most stable. The results of the DMC calculations are therefore in agreement with

Table 13
NICS(1) values, calculated 1 Å out the plane, for $B_iN_i^R$ and $B_iN_i^{3R}$ structures

$B_iN_i^R$		$B_iN_i^{3R}$						
			B_2N_2	B_3N_3	B_4N_4	B_5N_5	B_6N_6	B_7N_7
$B_2N_2^R$	−10.81	$B_6N_6^{3R}$	4.01	−0.88	–	–	–	–
$B_3N_3^R$	−2.80	$B_7N_7^{3R}$	3.25	−1.43	0.45	–	–	–
$B_4N_4^R$	1.89	$B_8N_8^{3R}$	3.34	–	0.89	–	–	–
$B_5N_5^R$	−2.05	$B_9N_9^{3R}$	–	1.16	−1.05	–	–	
$B_6N_6^R$	0.61	$B_{10}N_{10}^{3R}$	5.73	–	–	−0.95	–	–
$B_7N_7^R$	−0.55	$B_{11}N_{11}^{3R}$	5.33	–	–	−0.89	5.33	–
$B_8N_8^R$	0.66	$B_{12}N_{12}^{3R}$	5.16	–	–	–	1.16	–
$B_9N_9^R$	0.30	$B_{13}N_{13}^{3R}$	6.11	–	–	–	1.14	0.89
		$B_{14}N_{14}^{3R}$	6.97	–	–	–	–	0.90

Table 14
Calculated energy differences, ΔE, in eV, at the B3LYP and DMC levels of theory

	B3LYP	DMC
$\Delta E(E_{B_2N_2^R} - E_{B_2N_2^C})$	+0.283	$+1.392 \pm 0.055$
$\Delta E(E_{B_8N_8^R} - E_{B_8N_8^{3R}})$	+2.233	$+1.541 \pm 0.160$
$\Delta E(E_{B_9N_9^R} - E_{B_9N_9^{3R}})$	+1.837	$+2.227 \pm 0.123$
$\Delta E(E_{B_{10}N_{10}^R} - E_{B_{10}N_{10}^{3R}})$	+1.387	-1.685 ± 0.127
$\Delta E(E_{B_{10}N_{10}^R} - E_{B_{10}N_{10}^S})$	+4.200	$+2.081 \pm 0.172$
$\Delta E(E_{B_{11}N_{11}^R} - E_{B_{11}N_{11}^S})$	+2.232	-1.490 ± 0.151
$\Delta E(E_{B_{11}N_{11}^R} - E_{B_{11}N_{11}^{3R}})$	+1.248	$+2.557 \pm 0.223$
$\Delta E(E_{B_{12}N_{12}^R} - E_{B_{12}N_{12}^S})$	−0.770	-7.750 ± 0.169
$\Delta E(E_{B_{13}N_{13}^R} - E_{B_{13}N_{13}^S})$	+1.141	-4.412 ± 0.178

the aromaticity picture. For larger cases, $i > 11$, DMC predict spheroids to be the global minima. Therefore, according to our DMC results, ring structures are the global minima for $i = 2$–9, the three-ring structure for $i = 10$ and spheroids for $i > 11$.

5.7. Electronic metastable bound states of Mn_2^{2+} and Co_2^{2+}

The vast majority of quantum chemical density functional theory calculations use Gaussian-type basis sets. The second most used type of basis sets are made of Slater-type functions. The latter type of basis set functions allow a much better treatment of the point symmetry of linear molecules and, in particular, of homonuclear diatomics. Hence, in some respect, Slater-type basis functions sets seem to be superior for the study of small high symmetry molecules. In this section, we shall compare the ability of Gaussian- versus Slater-type basis function sets to describe the metastable bound states of the Mn_2^{2+} and Co_2^{2+} transition metals dimers, as implemented in the two most widely used computational packages, Gaussian [222] for the Gaussian-type basis sets and ADF [397] for the Slater-type basis functions sets.

A prior study by Liu et al., within the frame work of both the tight binding method and the local density approximation to the density functional theory, concluded that there is no barrier against the dissociation of Ni_2^{2+} into two singly charged nickel ions [398]. In contrast, results based on the generalized gradient approximation to the density functional theory allowed the characterization of nine metastable states for Ni_2^{2+}, all of them presenting four unpaired electrons [399]. These previous investigations have been extended [400] to the Mn_2^{2+} and Co_2^{2+} species.

The total energy curves of Mn_2^{2+} and Co_2^{2+} as a function of the interionic distance have been studied using the density functional theory with both the Amsterdam density functional, ADF2000.02, code [397] (ADF from now on) and the Gaussian98 program [222] (G98 from now on). The generalized gradient approximation to exchange and correlation effects developed by Perdew is used within ADF, combined with a triple-zeta plus polarization basis sets of Slater-type orbitals available as set IV in the package, hereafter referred to as PW91/sto. The frozen core approximation up to the 3p orbital (included) is utilized. On the other hand, the gradient-corrected exchange functional due to Becke and the correlation functional containing both local and gradient-corrected terms developed by Lee, Yang, and Parr are utilized within G98, combined with the all-electron, triple-zeta basis set 6-311+G, hereafter referred to as BLYP/gto. All the metastable states found in this work are characterized by their equilibrium bond lengths, barrier heights, harmonic vibrational frequencies, and total energy at the equilibrium bond length relative to the lowest-energy metastable state of each dimer. The dissociation products are not considered to avoid any possible misinterpretation of our results due to the single determinantal nature of the Kohn–Sham version of the density functional theory.

Table 15 summarizes the results for those metastable states of Mn_2^{2+} and Co_2^{2+} with lower total energies calculated at the equilibrium bond length. In the case of Mn_2^{2+}, according to PW91/sto, the lowest-energy metastable state corresponds to a singlet state in which the two Mn ions are antiferromagnetically coupled, state **1**, a metastable state with 10 unpaired electrons, state **2**, being only 0.13 eV above in energy. BLYP/gto, on the other hand, predicts metastable state **2** to be the lowest-energy one for Mn_2^{2+}, being unable to describe the antiferromagnetic state found with PW91/sto. To our opinion, this shortcoming exhibited by BLYP/gto is mainly due to its inability to describe situations in which a symmetry-breaking

Table 15
Complete valence electronic configuration, equilibrium bond distance in, barrier height in eV, harmonic vibrational frequencies in cm^{-1}, and energies relative to the lowest-energy minimum, in eV, of lowest characterized metastable states of both Mn_2^{2+} and Co_2^{2+}, calculated with PW91/sto and BLYP/gto

	Configuration	$(2S+1)$	PW91/sto				BLYP/gto			
			r_e	BH	w_e	ΔE	r_e	BH	w_e	ΔE
Mn_2^{2+}										
1	$1\sigma^2 2\sigma^2 1\pi^4 1\delta^4$	1	2.94	0.16	130	0.0	–	–	–	0.0
2	$1\sigma^2 2\sigma^1(\uparrow) 3\sigma^{*1}(\uparrow) 1\pi^2(\uparrow) 2\pi^{*2}(\uparrow) 1\delta^2(\uparrow) 2\delta^{*2}(\uparrow)$	11	2.89	0.57	161	0.13	2.89	0.49	157	0.13
3	$1\sigma^2 2\sigma^1(\uparrow) 1\pi^3(\uparrow) 2\pi^{*2}(\uparrow) 1\delta^2(\uparrow) 2\delta^{*2}(\uparrow)$	9	2.91	0.31	127	1.75	2.93	0.17	111	1.41
4	$1\sigma^2 2\sigma^1(\uparrow) 1\pi^2(\uparrow) 2\pi^{*2}(\uparrow) 1\delta^3(\uparrow) 2\delta^{*2}(\uparrow)$	9	3.45	0.05	61	2.15	3.74	0.004	22	1.61
Co_2^{2+}										
1	$1\sigma^2 2\sigma^1(\uparrow) 3\sigma^{*1}(\uparrow) 1\pi^4 2\pi^{*2}(\uparrow) 1\delta^4 2\delta^{'2}(\uparrow)$	7	2.26	0.95	237	0.0	2.22	0.94	243	0.0
2	$1\sigma^2 2\sigma^1(\uparrow) 1\pi^4 2\pi^{*3}(\uparrow) 1\delta^4 2\delta^{*2}(\uparrow)$	5	2.55	0.20	139	0.43	2.52	0.18	143	0.31
3	$1\sigma^2 2\sigma^1(\uparrow) 1\pi^4 2\pi^{4*2}(\uparrow) 1\delta^4 2\delta^{*3}(\uparrow)$	5	2.37	0.37	191	0.60	2.33	0.37	193	0.40

Bold-faced numbers are used to label the states of a simpler manner, $(2S+1)$ is the electronic multiplicity.

treatment is needed, and it bears no relation to the fact that ADF and G98 use different exchange-correlation functionals and basis functions. In spite of the above controversy on the ground state the two codes used in this work agree very well in the prediction of properties given in Table 15. A very important amount of the states investigated for Co_2^{2+} prove to be metastable states. Those with lower total energies calculated at the equilibrium bond length are summarized in Table 15. It can be seen that both methods agree to predict the septet state to be that with the lowest total energy at the equilibrium bond distance. Both PW91/sto and BLYP/gto also point to the fact that several quintet metastable states lie between 0.30 and 0.70 eV higher in energy than the septet state, states **2** and **3** being described by the same electronic configuration in both programs.

For the characterized metastable states with small barrier heights prediction of their lifetimes is mandatory. However, the potential energy curves of these states are expected to be remarkably anharmonic, as can be seen in Fig. 11. Therefore, for the selected low barrier height states we have calculated the full potential energy curve, $V(R)$, being R the internuclear distance and then have solved numerically the corresponding Schrödinger equation for the motion of the nuclei. It has been solved using a Numerov approach to estimate the energies E_v of the vibrational states v supported by the potential energy curve $V(R)$. Then, the lifetimes corresponding to each of the vibrational states are estimated using the semiclassical WKB approximation. Finally, the lifetimes averaged over the vibrational states for a number of selected metastable states of both Mn_2^{2+} and Co_2^{2+} have been calculated at different temperatures according to the canonical average.

Table 16 lists the absorption frequencies calculated for the vibrational transition $v = 0 \rightarrow 1$ (see Eq. (221)) and the vibrationally averaged lifetimes at two different temperatures. Inspection of this table reveals that comparison between the experimental vibrational absorption frequency and the calculated harmonic frequencies might be very poor, for anharmonicity effects are exceedingly larger than 10% for all the states shown. Hence, earlier published scaling factors may be not accurate enough for the highly charged diatomic species studied in the present investigation. In particular, notice that for state **1** of Mn_2^{2+} the anharmonicity lowers the predicted harmonic vibrational absorption frequency by 23%.

About lifetimes, we can observe that even though the PW91/sto barrier height for state **1** of Mn_2^{2+} is larger than for state **4**, the lifetime of the former state is shorter. This is due

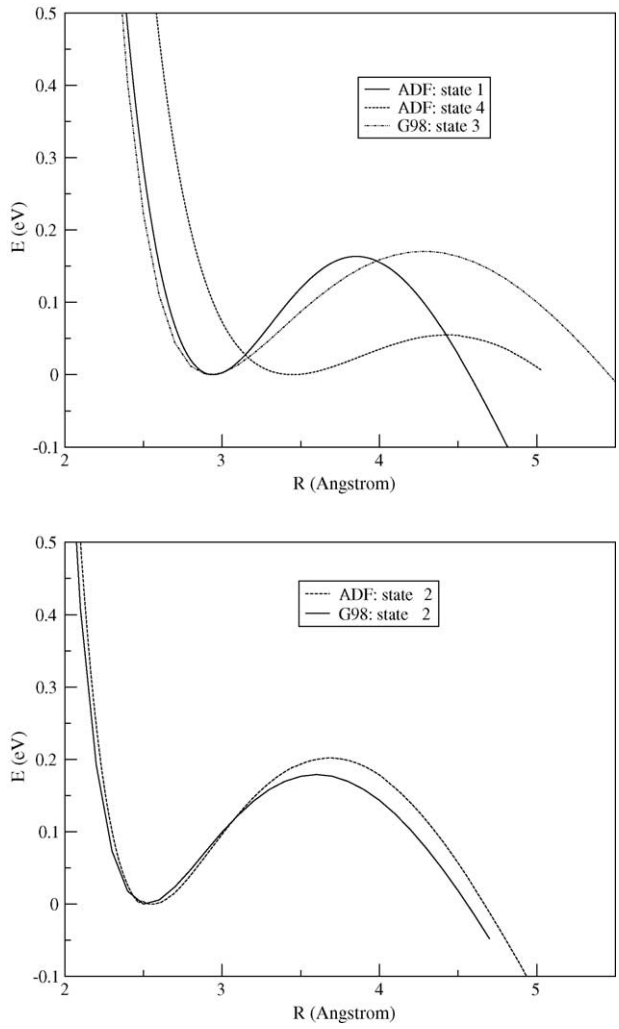

Fig. 11. Potential energy curves of metastable states **1**, **3**, and **4** of Mn_2^{2+}, above, and metastable state **2** of Co_2^{2+}, below.

Table 16
Absorption frequencies, w_e^a, of the $v = 0 \rightarrow 1$ vibrational transitions, in cm^{-1}, and vibrationally averaged lifetimes, τ, in s, for the metastable states shown in Fig. 11

State	PW91/sto						BLYP/gto					
	Mn_2^{2+}			Co_2^{2+}			Mn_2^{2+}			Co_2^{2+}		
	w_e^a	$\langle\tau\rangle$ (300 K)	$\langle\tau\rangle$ (1000 K)	w_e^a	$\langle\tau\rangle$ (300 K)	$\langle\tau\rangle$ (1000 K)	w_e^a	$\langle\tau\rangle$ (300 K)	$\langle\tau\rangle$ (1000 K)	w_e^a	$\langle\tau\rangle$ (300 K)	$\langle\tau\rangle$ (1000 K)
1	103	4.5×10^6	2.8×10^6									
2				119	6.7×10^{52}	3.4×10^{52}				119	4.2×10^{45}	2.1×10^{45}
3							99	2.1×10^{59}	9.3×10^{58}			
4	51	5.9×10^{11}	4.1×10^{11}									

to the fact that the tunneling potential of state **4** is wider than the one of state **1**, as shown in Fig. 11, and hence tunneling becomes less probable. On the other hand, the lifetimes obtained with BLYP/gto and PW91/sto for state **2** of Co_2^{2+} are consistent and their differences reveal the small differences between the BLYP/gto and PW91/sto potential energy curves as shown in Fig. 11. It is worth mentioning that the calculation of the whole tunneling potential energy curve is mandatory for a reliable estimation of the lifetimes since relative heights at the top of the barrier might be misleading.

Finally, the vibrationally averaged lifetimes have been evaluated at two different temperatures. The results shown in Table 15 are very supportive towards the experimental detection of the metastable states investigated, for their lifetimes are found to be long enough even at a temperature of 1000 K.

5.8. Charge induced fragmentation of biomolecules

The effects of radiation leading to electron uptake or removal are of outmost importance in biological systems, as these can cause irreversible damage to DNA, lipid membranes and proteins. Damages to proteins and their constituents can lead to altered chemistry carried out by the system, whereas damages to lipid membranes in general lead to either fragmentation of lipids (rupture of the membrane and cell death) or polymerisation reactions leading to reduced permeability. Damage to DNA can result in reduced capability for transcription and replication, breakage of the DNA strands, or to structural modifications that after faulty repair in the worst case can yield carcinogenic mutations of the nucleobases.

In this subsection, we will outline the chemistry of a biomolecule, serine phosphate (SP), that has been used in order to gain insight into possible mechanisms for radiation induced strand breakage or loss of nucleobases in DNA. Albeit representing a very small model system of DNA, SP contains some of the key elements thereof. We have a phosphate–ester bond, an efficient electron sink (the carboxylic group) and an amine group. When irradiated, SP is known to undergo several different fragmentation reactions depending on whether an electron is removed from the system or if an ejected electron is captured by another molecule (cf. Fig. 12) [401]. Ionization as well as electron gain leads to the formation of a radical system. Albeit these in general are very reactive species, one means of stabilizing them is by low temperature matrix isolation techniques, followed by the recording of and electron paramagnetic resonance (EPR, ESR) or related (ENDOR, field swept ENDOR) magnetic spectrum. This provides information about the distribution of the unpaired electron within the radical, and thus indirect structural data. Such parameters (hyperfine coupling constants and *g*-values) can also be computed to high accuracy, and thus assist in the interpretation of the observed spectra [402,403]. In this context, the DFT based methods have provided a highly successful alternative to the very demanding correlated ab initio methods (MR-CI, CCSD(T)) otherwise needed for accurate EPR calculations [404].

Using matrix isolation techniques, Sanderud and Sagstuen were able to identify three different radical intermediates resulting from irradiation of crystals of SP. Two of these were ascribed to systems resulting from electron gain (radicals I and III in Fig. 12), and one from the ionization of SP (radical II in Fig. 12). Radical I was the dominating species observed, and was interpreted as the deamination product—corresponding to base release in DNA. In Table 17, we show the experimental and computed proton hyperfine couplings, giving a clear support for radical I being the deamination product. The proton is connected to the deaminated

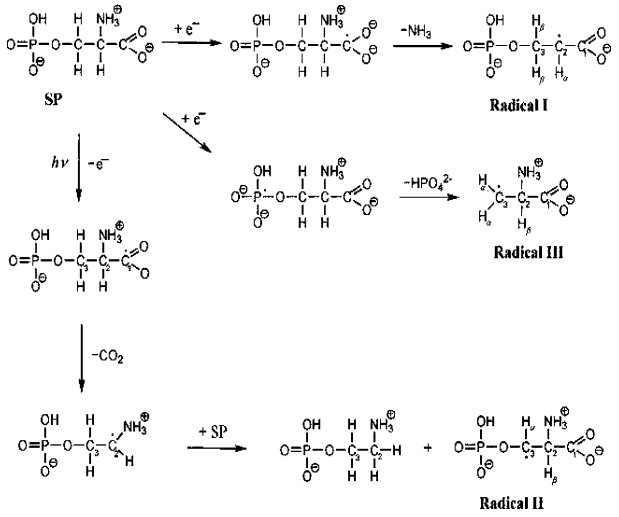

Fig. 12. Proposed reaction mechanisms of serine phosphate in frozen crystals upon radiation induced electron uptake/removal [401].

Table 17
Experimental [401] and B3LYP/6-311G(2df,p)//B3LYP/6-31G(d,p) computed [405] radical HFCCs of deamination product radical I of SP

Atom	A_{iso}	T_{xx}	T_{yy}	T_{zz}
α-H (calculated)	−15.3	10.0	0.4	−10.5
α-H (experimental)	−19.3	11.5	−1.2	−10.3
β-H1 (calculated)	37.6	3.1	−0.9	−2.2
β-H1 (experimental)	37.1	2.6	−0.7	−1.9
β-H2 (calculated)	20.6	3.0	−1.3	−1.7
β-H2 (experimental)	20.4	2.9	−1.4	−1.5

All data in Gauss units.

carbon C2, and the two couplings arise form the hydrogens attached to C3.

When modelling reactions in gas phase, it is in general very difficult to obtain convergence for zwitterionic species (systems carrying both negative and positive charge). Recall also, that zwitterions usually are not stable chemical entities in the gas phase. Solvation is required to stabilize their charge separation. In the calculations, we therefore protonated the carboxylate and phosphate groups, and de-protonated the amine group, as compared to the actual experimental conditions. When the species gained the additional electron, the energy prior to nuclear relaxation was found to be lowered by ca. 27 kcal/mol. Letting the geometry relax led to an irreversible, barrierless deamination, as depicted in Fig. 13. The resulting species lies an additional 45 kcal/mol lower in energy than the initial starting point. Similar analyses (and positive identification) were made for radicals II and III, in terms of geometry optimization and calculation of HFCCs, and their respective reactions were modelled [405]. Like radical I and III is also observed after electron uptake, but this time undergoes a dephosphorylation reaction. Immediately after serine phosphate has accepted the extra electron, but before nuclear rearrangement, the spin is delocalised over the entire molecule. The main component is found on the carboxylic carbon (C1; 0.74), but with a significant fraction (0.50) also on the phosphorous. The components on the other atoms are C2; 0.34, C3; 0.34 and N; 0.31. The large component of unpaired spin on the phosphorous has implications for the competing mechanism leading to formation of formation of radical III. After the deamination reaction, the main component of the unpaired spin is located at the radical center C2 (0.69).

In order for the anionic SP to undergo dephosphorylation, the unpaired electron must be steared over from the carboxylic end towards the phosphorous. Since using a model consisting of serine phosphate alone lead to the barrierless deamination, we added in the calculations a hydronium ion (H_3O^+) to interact with the phosphate, thereby assisting in pulling the unpaired electron towards the phosphorous end. In doing so, a stable phosphoranyl anion intermediate with a local trigonal bipyramidal structure around the phosphorous atom could be found on the potential energy surface. Passing over a transition barrier of ca. 25 kcal/mol, the system then de-phosphorylated. The hydronium ion strongly localized the unpaired electron to the phosphorous (1.83 electrons) which after nuclear relaxation (formation of phosphoranyl intermediate) was reduced to 0.74, and reduced further to 0.50 at the TS, in order to be fully transferred over to the radical carbon C3 after the bond breakage.

In Fig. 14, we display the energy surfaces for the dephosphorylation reaction, computed both in vacuo and embedded in a polarized continuum. As seen, the effect of the aqueous environment on the energetics is considerable. Comparing this to the energetics of the competing reaction leading to deamination we also note that the energy gain of the initial electron uptake is very similar (ca. 27 kcal/mol in aqueous solution), as is the level of the final product (DE = −72 kcal/mol for deamination using IEF-PCM). Instead it is the existence of a barrier for the dephosphorylation as compared to the barreirless deamination that fully accounts for the observation of radical I as the dominant species. Radical II is the ionization product and leads to initial decarboxylation of SP. The calculations give at hand that this reaction—just like the deamination leading to radical I—is a barrierless process following immediately upon electron loss. Under the experimental conditions, the decarboxylated species will abstract a hydrogen atom from a neighbouring SP molecule; a situation less likely to occur in gas phase due to the distances between the different species. However, allowing the gas phase calculations to proceed after the initial decarboxylation, further degradation was observed in that the phosphate group spontaneously dissociated from the remaining fragment. Hence, in gas phase, a biomolecule like SP can be expected to undergo significant fragmentation reactions once ionized.

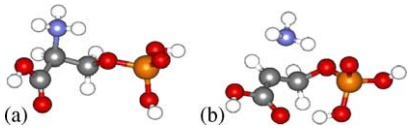

Fig. 13. (a) Optimized species prior to electron uptake and (b) after dissociate electron capture and deamination. Calculations performed at the B3LYP/6-31G(d,p) level.

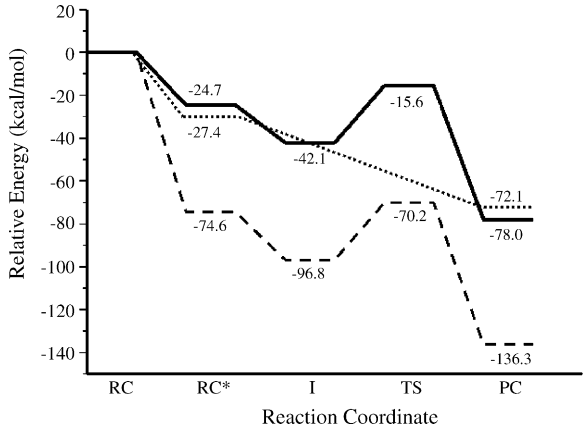

Fig. 14. Computed energy surfaces in vacuo (dashed) and in aqueous solution (solid) for the de-phosphorylation of serine phosphate after dissociative electron capture. Included is also the barrierless energy surface for deamination in aqueous solution (dotted).

5.9. Photodissociation of He_3^+

Nowadays, it is possible to study electron and molecular dynamics in real time using various experimental techniques employing intense ultra-short laser sources [406–408]. Some examples of such investigations include X-ray photoelectron spectroscopy of molecules [409,410], pump-probe ionization measurements, production of high harmonics as a source of soft X-rays [411,412], the measurement of electron–phonon interactions in thin films [413], and the estimation of the onset of Coulomb screening [414]. A technologically important and very active field of research is the application of ultra-short laser pulses to induce, control and monitor chemical reactions [415–418]. Whenever the intensity of the laser field is comparable to the molecular electronic fields, perturbative expansions break down and new processes appear, which are not fully understood from a microscopical point of view. Some examples of these novel processes are bond softening, vibrational population trapping, molecular alignment and above-threshold dissociation.

To tackle such a problems, time-dependent density functional theory (TDDFT) [226,228,419,420] appears as a valuable tool. Even with the simplest approximation to the exchange-correlation potential, the adiabatic local density approximation (ALDA), one obtains a very good compromise between computational ease and accuracy [421]. TDDFT can certainly be applied to large systems in non perturbative regimes, while providing a consistent treatment of electron correlation. As an illustrative example of the application of TDDFT on problems such as photodissociation we show the work done by Castro et al. [422] on the photodissociation of the trimers He_3^+. This work illustrates how TDDFT theory is an useful tool to study the coupling between electronic and ionic (e.g., nuclei) dynamics of many electron systems subject to strong laser fields, leading to a deeper understanding of photodissociative processes.

The He_3^+ trimer system is conceptually simple, easing interpretation: in Fig. 15 the relevant potential energy curves are depicted. TDLDA calculations of the optical response were performed varying the nuclear geometry along the given coordinate, which is the symmetric displacement of the two outer atoms along the trimer axis. The inset of the figure shows the result for the equilibrium geometry. It is clear that only one excited potential energy surface is of interest. The only relevant optical transition is the $\Sigma_g \rightarrow \Sigma_u$ at 5.0 eV. The experiments position this peak at ≈5.3 eV. This excited PES is totally repulsive, and as such photoinduced population of this state should lead to dissociation.

Haberland et al. [423] performed experiments on the photodissociation of ionized rare gas trimers including He_3^+, induced by a 10 ns laser pulse, with photon energies ranging from 1.5 to 6 eV. They utilized time-of-flight mass spectroscopy to observe the fragments. Their results support the picture of a linear trimer photo-excited to a totally repulsive state, coupled to the ground-state through a parallel transition

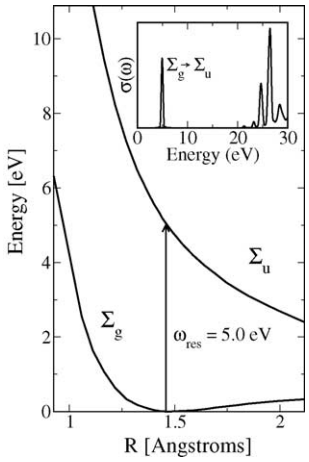

Fig. 15. Σ_g (ground state) and Σ_u potential energy surfaces. The abscissa corresponds to the simultaneous and symmetric displacement of the two outer atoms along the trimer axis. Inset: photoabsorption cross-section at equilibrium geometry. Calculations done at the TDLDA level.

moment: the two lateral atoms are expelled at high opposed velocity, whereas the central atom only gains a small velocity at either side. The positive charge generally localizes on one of the fast outer particles.

Castro et al. [422] performed a number of simulations using various sets of laser parameters, amongst whose the four samples shown in Fig. 16. Top panels depict non-resonant cases, at one-third (left) and five-thirds (right) of the resonance $\Sigma_g \rightarrow \Sigma_u$ (5 eV). In both cases the two outer atoms only oscillate slightly around the equilibrium positions. Botton panels are both resonant cases, with varying intensities. Two different dissociative channels are observed: in the left panel, a low intensity is provided, and the picture corresponds with the findings of Haberland et al. [423]—the two outer atoms gain high opposing velocities, whereas the central one remains almost unperturbed. Note that the intensity is the same as the one used in the upper panels, where no dissociation was obtained. A higher intensity was used for the simulation shown in the bottom-right panel, and in this case

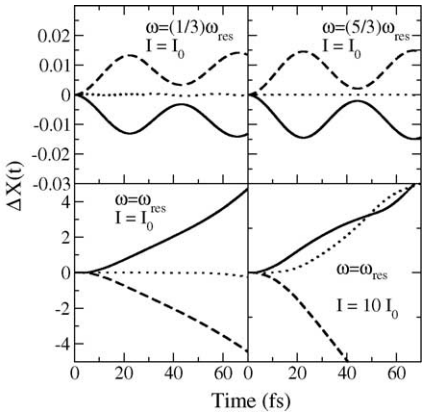

Fig. 16. Time-evolution of the three nuclear displacements (solid: top atom; dots: central atom; dashed: bottom atom) with respect to their original positions, along the trimer axis, for the frequencies and intensities given (w_{res} = 5 eV, $I_0 = 8.8 \times 10^{11}$ W/cm^2).

the trimer dissociates into a dimer and an isolated atom. Most likely, the intensity of the nanosecond laser pulse used in the experiment is low, which agrees with the symmetric dissociative picture of the bottom-left panel.

5.10. Optical properties of GFP

As another example of the applicability of TDDFT, there is the use of TDDFT to determine the optical properties of biological cromophores. The theoretical understanding of biophysical processes is a very active field of research. Many biological processes (as vision) rely in a subtle interplay between optical absorption in the photoactive center and its coupling to internal vibrational modes (including isomerization) and the environment (hosting proteine and solvent). In certain cases, when the cromophore is isolated from the solvent environment by the protein structure, the gas-phase studies of the optical properties of the cromophore can be specially relevant to understand the biophysics at the basis of the biological process. As an example of this, we have the Green Flourescent Protein (GFP). This protein has become an unique tool in molecular biology because of its flourescent properties and inertness when attached to other proteins [424]. The cromophore is formed by Ser65, Tyr66 and Gly67. Ser65 is chemically modified, such that the cromophore consist of two consecutive rings, the phenol-type ring of Tyr66 and an imidazolinone heterocyle formed by the backbone of Tyr66, the carbonyl carbon of Ser65 and the nitrogen of the backbone of Gly67 (see Fig. 17). The tyroxyl hydroxil group is part of a complex hydrogen bond network that depending on the environment favours its protonated (neutral) or de-protonated (anionic) form [424].

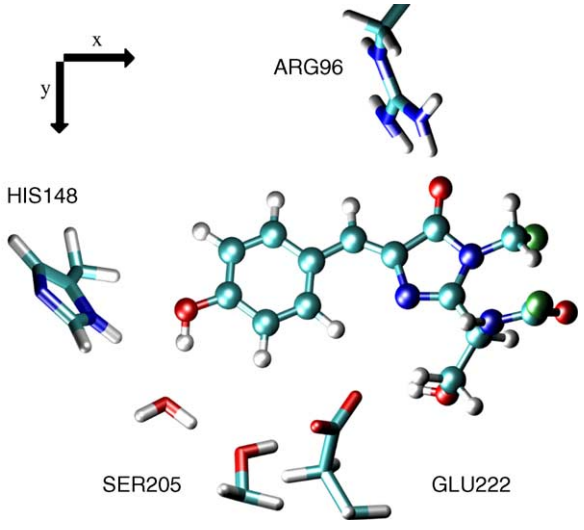

Fig. 17. AM1/MM optimized structure of the cromophore inside the 1GFL protein. The closest charge residues, His148 (which is considered in its protonated form), Arg96 (positively charged) and Glu222 (negatively charged) are also shown. The anionic cromophore structure corresponds to the proton of Tyr66 removed and passed to Glu222 using a water molecule and Ser205 as a proton bridge.

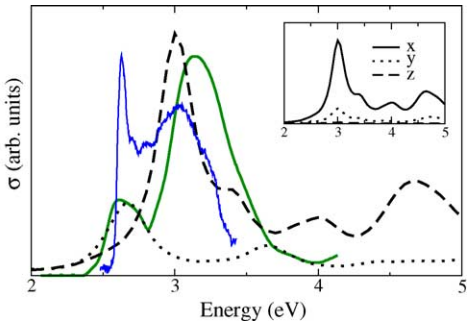

Fig. 18. The computed photo-absorption cross-section, σ, compared to the experimental measurement. The dashed line corresponds to the neutral chromphore, the dotted line to the anionic, whereas the blue and green curves are the experimental results taken from refs. [427] and [425,426] , respectively. For comparative purposes, we divided the anionic results by 4 with respect to the neutral results. Inset: decomposition of the computed spectra of the neutral chromophore in the three directions, showing the inherent anisotropy of the GFP molecule.

The optical absorption spectrum of the wild type (wt)-GFP, measured at 1.6 K shows two main resonances at 2.63 and 3.05 eV [425,426] that are attributed to two thermodynamically stable protonation states of the chromophore (neutral and anionic charge states, respectively). Only recently the optical absorption of the GFP anion chromophore has been measured in vaccuo [427]. They observed a main peak at 2.59 eV in very close agreement with the peak assigned to the anionic configuration in wt-GFP. It is clear that the photophysics and functioning of the GFP protein is governed by a complicated equilibrium between the neutral and anionic states of the cromophore. In the present example, we illustrate the work of Marques et al. [428] that shows how calculations of the GFP in vacuo using time-dependent density functional theory [419,420,429,430] to treat electron–nuclei dynamics of the photoreceptor yield useful insight into the biophysics of these important class of cromophores.

The GFP structures were prepared according to X-ray data relaxed using mixed quantum mechanical/molecular mechanics hamiltonian (QM/MM) [431], which allows the geometry optimization of structures described quantum mechanically embedded in a protein with many degrees of freedom which are efficiently treated by means of classical mechanics. Details of the calculation can be found in ref. [428]. The final structure with the closest aminoacids in the protein is depicted in Fig. 17. The anionic form of the cromophore is prepared from deprotonation of the Tyr66 and protonation of Glu222. The proton transfer is mediated through a water molecule and Ser205. The role of the protein backbone is important for the structural relaxation of the anionic form. The main changes as compare to the neutral occur at the relative orientation of the Tyr66-ring plane with respect to the five membered imidazolinone plane. In the neutral form the two ring planes are found to be slightly displaced from the planarity by 14.0°. However, in the anionic form the two rings are almost totaly coplanar (dihedral of −0.9°).

The computed optical spectra of the neutral and anionic cromophores are given in Fig. 18, together with the experi-

mental spectrum of the wt-GFP. The calculated spectra shown is averaged over the three spatial directions (shown in the inset of Fig. 18). Light polarized along the "*x*"-direction in the plot is responsible for the lowest optical transition of GFP that corresponds to a π–π^* transition between the HOMO and LUMO orbitals of both neutral and anionic forms. The molecule is nearly transparent for visible light polarised along the other two orthogonal directions. GFP turn out to be a rather anisotropic molecule in the visible and it is important for enhancing the photodynamics in well oriented GFP samples. The π–π^* transition (HOMO–LUMO) computed as difference of single-particle eigenvalues are 2.19 and 1.57 eV, for the neutral and anionic structures, respectively. A common practise is using those excitations as the physical ones and compare directly with experiments.

This leads to bad agreement with the measured excitations, however in TDDFT the difference of one-particle eigenvalues is renormalised by coulomb and exchange-correlation interactions [419,420,429,430]. Once those effects are included in the calculated spectra the main excitation peaks for the neutral and anionic forms moves to 3.02 and 2.7 eV, respectively, in good agreement with the measured peaks at 3.08 and 2.63 eV [425,426]. These π–π^* excitations are not longer pure HOMO–LUMO transitions and do include contributions from virtual particle–hole excitations involving the close lying states. The oscillator strength is larger in the anionic than in the neutral. A quantitative description of the spectra of wt-GFP both in excitation energy and intensity is obtained once we assume a ∼3:1 ratio in the concentration of the neutral/anionic forms; this ratio is close the estimated experimental ratio of 80% neutral and 20% anionic [424]. The measured peaks can be clearly assigned to either the neutral or anionic forms of the GFP. The agreement between the calculated spectra and measured one is excellent. These calculations give further support to the predominance of the neutral and anionic forms in wt-GFP in agreement the analysis of the infrared spectra [432,433], giving compiling evidence of the proton shuttle mechanism between the protonated and de-protonated forms of the chromophore through corresponding charging states of the Glu222 residue where the proton-shuttle ends. These results prove the predictive power of the TDDFT approach. However, we emphasize that the fact that the computed absorption spectra of the chromopore resembles very well the measured spectra points to an efficient electrostatic shielding of the chromophore by the rigid β-barrel structure of the protein. This makes the comparison between in vacuo and in vivo justified [427].

5.11. Surface hopping and reactivity: the overall reaction rate coefficient

For this last example, we have chosen a few selected cases where a complete kinetic study has been carried out. Thus, we will be able to compare the computed the overall rate coefficient with the results obtained from the corresponding experimental measurements.

The reaction of CH radicals with nitrogen molecules to give hydrogen cyanide and nitrogen atoms:

$$CH(^2\Pi) + N_2 \rightarrow HCN + N(^4S) \quad (241)$$

has received great attention from experimentalists because of its relevance in combustion chemistry. From the theoretical side it is also a very interesting reaction, since it is spin-forbidden and in principle several different mechanisms could be proposed. In addition, the rate constant has not been fully characterized for most important temperatures by the experimental works. Therefore, it is not surprising that several theoretical works [434–438] have addressed this reaction, mainly to determine the energetics for the possible involved species and to depict a reasonable mechanism for this process. It has been established that the essential features of the dominant channel for this reaction can be represented by a mechanism which is shown in Fig. 19. In such mechanism the reactants initially give rise to a cyclic (C_{2v}-symmetric) complex on the doublet potential surface (a barrier of ca. 10.8 kcal/mol should be surmounted). Intersystem crossing may take place from this minimum, resulting also in a C_{2v}-symmetric (which has a Y-shape and is not cyclic) structure on the quartet surface, which evolves toward the final products. The spin–orbit coupling element between the doublet and quartet surfaces is estimated to be 8.0 cm^{-1} at the CASSCF(9,9)/6-311G(d,p) level [438]. Finally, a transition state on the quartet surface (lying about 22 kcal/mol above the reactants) lead to the products.

Another possible mechanism follows a dative channel, with the formation of a HCNN doublet species (C_s-symmetry) which could lead to quartet species. Nevertheless, although a truly MECP could not be characterized for this path, the spin–orbit coupling element is estimated to be around 5.1 cm^{-1}, and a high exit barrier (ca. 37 kcal/mol) is involved for the formation of the final products. Therefore, the authors [438] conclude that the dative intersystem-crossing channel is not expected to be able to compete with the C_{2v} intersystem-crossing channel shown in Fig. 19.

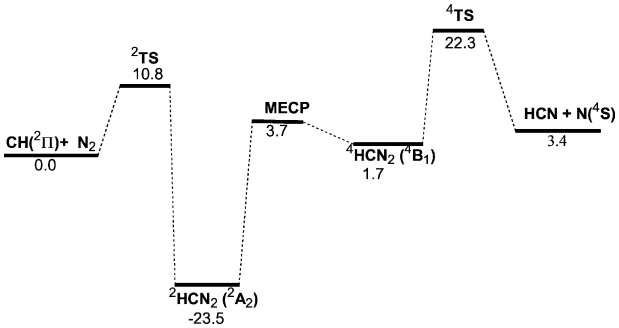

Fig. 19. Schematic representation of the energy profile for the $CH(^2\Pi) + N_2 \rightarrow HCN + N(^4S)$ reaction, adapted from refs. [437,438]. Relative energies correspond to G2M(RCC) including B3LYP zero-point energies, as explained in ref. [438].

Based on this mechanism Cui et al. [439] have carried out a detailed kinetic study of the $CH + N_2$ reaction. A one-dimensional model was constructed to consider the spin-forbidden transition probability, which in this case was solved with distorted wave approximation. The absolute values for the transition probabilities were found to be very small (on the order of 10^{-4}), showing that the reaction is highly diabatic. Finally the thermal reaction constant $k(T)$ was evaluated, obtaining a result which is two orders of magnitude lower than the experimental measurement. An empirical RRKM study [440] has shown that, in order to obtain a reasonable agreement with the experimental measurements, empirical vibrational frequencies at the MECP must be scaled by a factor of 2 and also a much larger surface hopping probability (0.04) must be considered. As pointed out by Cui et al. such an empirical approach is not a real solution to the problem. The disagreement between the ab initio thermal rate constant and the experimental results in this case probably comes from the treatment of the multidimensional dynamics. The authors point that perhaps assuming that the spin-forbidden transition takes place with uniform probability on the seam is not completely adequate in this case.

The reaction of sulphur cations with acetylene:

$$S^+(^4S) + C_2H_2 \rightarrow SC_2H^+(^3\Sigma) + H \quad (242)$$

has also received a great deal of attention, mainly as a consequence of its possible role in interstellar chemistry as a source of sulphur–carbon compounds in space. Several experimental studies [441–443], employing different techniques, agree in that the reaction is exothermic and very fast and that the main product is SC_2H^+ with minor quantities (about 20%) of $SC_2H_2^+$ being also formed, whereas production of SC_2^+ is not observed. In particular, the SIFDT study of Zakouril et al. [443] suggests that the reaction takes place through a long-lived complex lying about 117 kcal/mol below the reactants. Apparently one could propose a relatively simple mechanism for this reaction, since the global process is spin-allowed and should take place on a $(SC_2H_2)^+$ quartet surface. Nevertheless, a theoretical study of the quartet potential surface [444] shows only a partial agreement with the experimental results. Calculations at both G2 and CCSD(T) levels predict that the reaction is exothermic and apparently there is no net energy barrier, since all transition states lie below the reactant, in agreement with a fast reaction. However, the intermediates formed on the quartet surface are not very stable (the most stable one lies only about 40 kcal/mol below the reactants), in disagreement with the SIFDT observation.

This discrepancy suggests that quite likely the doublet surface could play an active role in the mechanism. Barrientos et al. [444] found that on the doublet surface the possible intermediates were much more stable than on the quartet surface, and particularly one of them lies about 110 kcal/mol below the reactants. Furthermore, a preliminary estimation of the propensity for intersystem crossing in this system was carried out. At the crossing point the spin–orbit coupling element was computed to be around 86 and 91 cm^{-1}, respectively when the S^+ cation approaches the acetylene molecule in C_{2v} and C_s symmetries. Employing these values Barrientos et al. finally found probabilities for surface hopping of 0.015–0.048 on the C_{2v} surface and of 0.063–0.187 on the C_s surface. Since the $\sigma(C_s)$ attack of sulphur cations is favored over the $\pi(C_{2v})$ approach, it is found that the spin-crossing mechanism could be relevant in this reaction.

A detailed computational study of the reaction of sulphur cations with acetylene, including the possibility of surface hopping from the quartet to the doublet surface, has been carried out [249]. The essential features of the proposed mechanism are depicted in Fig. 20, where only the more relevant species on the quartet and doublet surfaces are represented. Two different crossing points (MECPs) between the quartet and doublet surfaces were characterized, connecting, respectively, the *cis*/*trans* $SCHCH^+$ isomers on the quartet surface with a doublet cyclic $SC_2H_2^+$ structure and the vinylidene-type $SCCH_2^+$ isomer on the doublet surface. A computational study of the kinetics of the reactions, under a wide range of temperatures and bath gas densities, has been carried out employing essentially the mechanism shown in Fig. 20. A good agreement is obtained between the computed rate coefficient at 300 K (in the range 1.2×10^{-9} to 1.57×10^{-9} s^{-1} cm^3 mol^{-1}) and the experimental results obtained from the SIFT and FT-ICR studies (9.5×10^{-10} and 9.8×10^{-10} s^{-1} cm^3 mol^{-1}, respectively). In addition, the branching ratios show that the major product is SC_2H^+, with non-negligible amounts of secondary products, mainly the vinylidene-type doublet structure, $SCCH_2^+$. Furthermore, a comparison between the microcanonical rate coefficients for the competing non-adiabatic (taking place through surface hopping between the quartet and doublet surfaces) and adiabatic (involving only the quartet surface) channels has been carried out. It is found that at temperatures (or internal energies of the initially-formed complex) that are relevant for the thermal reaction the non-adiabatic channel is by far the most efficient one. This is not surprising since, at shown in Fig. 20, both MECPs lie much lower in energy than the transition state on the quartet surface. Only at very high temperatures (energies) the adiabatic channel becomes more competitive.

To summarize, only the introduction of surface hopping in the mechanism explains the essential features revealed by the experimental studies. Therefore, the reaction of sulphur cations with acetylene is a clear example of the importance of spin-forbidden steps even in processes that are globally spin-allowed.

The recombination of carbon monoxide with iron polycarbonyls:

$$[Fe(CO)_4] + CO \rightarrow [Fe(CO)_5] \quad (243)$$

exhibits different behaviors depending on the electronic structure of the involved species. For example, experimen-

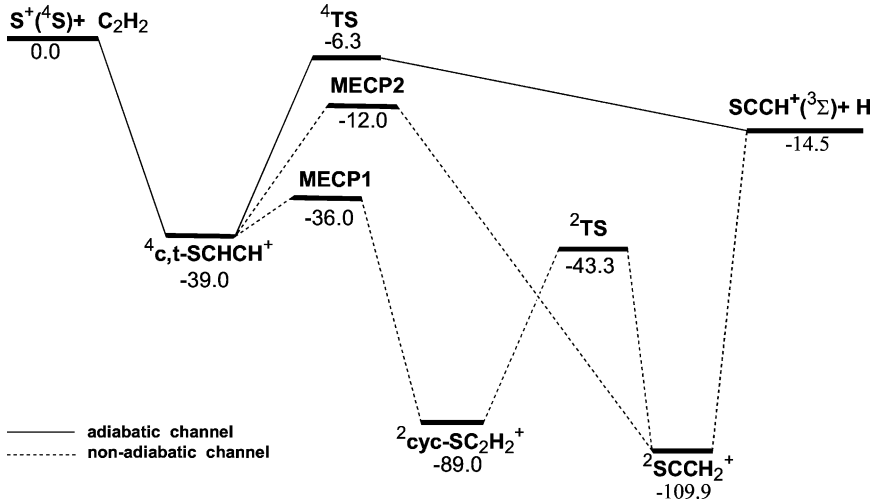

Fig. 20. Schematic representation of the mechanism for the $S + (^4S) + C_2H_2 \rightarrow SC_2H^+(^3\Sigma) + H$ reaction, adapted from refs. [249,444]. Relative energies (in kcal/mol) correspond to the G2(P) level.

tal studies [445,446] have shown that the reaction:

$$[Fe(CO)_3] + CO \rightarrow [Fe(CO)_4] \quad (244)$$

is rather fast ($k = 2.2 \times 10^{-11}\ s^{-1}\ cm^3\ mol^{-1}$), whereas the analogous reaction [243] takes place at a much slower rate ($k = 5.2 \times 10^{-14}\ s^{-1}\ cm^3\ mol^{-1}$). The reason for the difference in the rate coefficients is that reaction [244] is spin-allowed, whereas reaction [243] is spin-forbidden. Both $[Fe(CO)_3]$ and $[Fe(CO)_4]$ are unsaturated species with triplet ground state, whereas $[Fe(CO)_5]$ is a singlet. A recent study [447] has tried to model this spin-forbidden reaction computing its rate coefficient. In fact it is claimed by the authors that such study is the first computation from first principles of a spin-forbidden reaction involving a transition metal compound, and this seems to be the case. The proposed mechanism for the reaction is in fact very simple, and is shown in Fig. 21. The reaction takes place in one step involving one spin-crossing from the triplet to the singlet surface. The singlet state of $[Fe(CO)_4]$ lies too high in energy as to play a significant role in the reaction at temperatures relevant for the thermal reaction. Based on this mechanism the authors point out that there are two reasons for the slow rate coefficient observed experimentally. First there is a true barrier (although rather small), whereas in other cases the potential energy surface for the approach of both fragments is purely attractive (and the loose-transition state is obtained variationally). In second place there must be a surface hopping which takes place with a reduced probability.

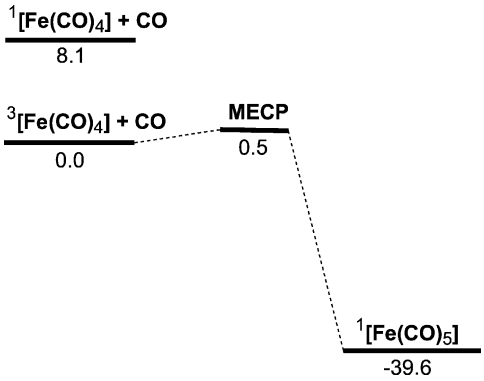

Fig. 21. Schematic representation of the mechanism for $[Fe(CO)_4] + CO \rightarrow [Fe(CO)_5]$ reaction, adapted from ref. [447]. Relative energies are given in kcal/mol.

Spin–orbit coupling, computed at the CASSCF(12,12) level, is computed to be about 66 cm^{-1} in this case. The probability of surface hopping was computed employing both Landau-Zener and Delos-Thorson models, obtaining rather similar results in both cases. The rate coefficient was computed at different temperatures. In this case a non-adiabatic version of the standard transition state theory can be applied [447]. The computed rate coefficient at 300 K is $k = 8.8 \times 10^{-15}\ s^{-1}\ cm^3\ mol^{-1}$, about six times lower than the experimental measure ($k = 5.2 \times 10^{-14}\ s^{-1}\ cm^3\ mol^{-1}$). Although only a semi-quantitative agreement is finally obtained, the result should not be considered discouraging. In fact, as the authors discussed, an inevitable number of uncertainties remain and one should consider as reasonable an agreement within an order of magnitude. There are several factors that have a high influence on the rate coefficient: the relative energy of the MECP (an increment of just 0.5 kcal/mol in its relative energy halves the rate coefficient at 300 K); the spin–orbit coupling element (doubling H_{SO} produces a rate coefficient four times larger); some of the normal modes have very low frequencies, and the harmonic approximation might not be appropriate. Nevertheless, the most significant result obtained in the computational study of the $[Fe(CO)_4] + CO \rightarrow [Fe(CO)_5]$ reaction is that the computed rate coefficient is much smaller than the gas-collision rate, and significantly lower than those measured for other spin-allowed reactions involving similar reactants.

The difficulties in estimating the rate coefficient even for an apparently simple case illustrates that the description of the kinetics for a spin-forbidden process is far from being an easy issue. But also it is clear that, even if only a semi-quantitative agreement can be finally reached, this type of studies might help in order to fully understand the chemistry underlying different processes in the gas phase.

Acknowledgments

J.M. Mercero, J.M. Matxain, X. Lopez, and J.M. Ugalde wishes to thank Eusko Jaurlaritza (Basque Government) and the Spanish Office of Scientific Research for the continuing financial support granted over the years. L.A. Eriksson kindly acknowledges the Swedish Research Council for support, and the Euskal Herriko Unibertsitatea for a visiting fellowship.

References

[1] G.C. Hall, J. Mol. Struct. (Theochem.) 234 (1991) 13.
[2] W.L. Hase, W. Koch, Int. J. Mass Spectrom. 201 (2000) ix.
[3] J.A. Pople, Nobel Lectures (1998) 246.
[4] E.C. Scerri, Found. Chem. 6 (2004) 93.
[5] H. Schwarz, Chem. Commun. (2003) 1321.
[6] J. Schummer, HYLE 10 (2004) 3.
[7] R.L. Stein, HYLE 10 (2004) 5.
[8] W. Heitler, F. London, Z. Phys. 44 (1927) 455.
[9] L. Pauling, J. Am. Chem. Soc. 53 (1931) 1367.
[10] J.C. Slater, Phys. Rev. 37 (1931) 481.
[11] J.H. van Vleck, J. Chem. Phys. 1 (1933) 177.
[12] F.W. Bobrowicz, W.A. Goddard III, in: H.F. Shaefer III (Ed.), Methods of Electronic Structure Theory, Plenum Press, New York, 1977, p. 79.
[13] F. Hund, Z. Phys. 51 (1928) 759.
[14] R.S. Mulliken, Phys. Rev. 32 (1928) 186, 761.
[15] J.C. Slater, Phys. Rev. 41 (1932) 255.
[16] H.C. Longuet-Higgins, Proc. Phys. Soc. 60 (1948) 270.
[17] C.C.J. Roothaan, Rev. Mod. Phys. 23 (1951) 69.
[18] C. Froese-Fischer, T. Brage, P. Jönsson, Computational Atomic Structure, The Institute of Physics Publishing, London, UK, 1997, p. 57.
[19] L. Laaksonen, P. Pyykkö, D. Sundholm, Comp. Phys. Rep. 4 (1986) 313.
[20] E.A. McCollough Jr., Comp. Phys. Rep. 4 (1986) 265.
[21] T. Helgaker, P. Jørgensen, J. Olsen, Molecular Electronic Structure Theory, Wiley, West Sussex, England, 2000.
[22] J.M. García de la Vega, B. Miguel, in: J. Fernádez-Rico, J.M. García de la Vega (Eds.), Temas ac-tuales de Quimíca Cuantíca, Ediciones de la Universidad Autónoma de Madrid, Madrid, 1997, p. 27.
[23] S.T. Epstein, The Variation Method in Quantum Chemistry, Academic Press, New York, 1974.
[24] H. Schwarz, Angew. Chem. Int. Ed. 42 (2003) 4442.
[25] P.A.M. Dirac, The Principles of Quantum Mechanics, fourth ed., Oxford University Press, Oxford, UK, 1958, p. 18.
[26] A. Szabo, N.S. Ostlund, Modern Quantum Chemistry. Introduction to Advanced Electronic Structure Theory, MacMillan Publishing Co., New York, 1982.
[27] R. Carbo, A General SCF Theory, Springer Verlag, Berlin, 1978.
[28] D.J. Thouless, The Quantum Mechanics of Many-Body Systems, Academic Press, London, 1964, p. 24.
[29] P.O. Löwdin, Rev. Mod. Phys. 35 (1963) 496.
[30] B.D. Dunietz, M. Head-Gordon, J. Phys. Chem. A 107 (2003) 9160.
[31] J. Marañón, J. Mol. Struct. (Theochem.) 621 (2003) 1.
[32] N.C. Handy, A.J. Cohen, Mol. Phys. 99 (2001) 403.
[33] A.J. Cohen, N.C. Handy, Mol. Phys. 99 (2001) 607.
[34] P.O. Löwdin, Phys. Rev. 97 (1955) 1474.
[35] J. Čížek, Adv. Chem. Phys. 14 (1964) 35.
[36] J. Čížek, J. Chem. Phys. 45 (1966) 4256.
[37] J. Paldus, J. Čížek, I. Shavitt, Phys. Rev. A 5 (1972) 50.
[38] J. Paldus, J. Čížek, in: D.W. Smith, W.B. McRae (Eds.), Energy, Structure and Reactivity, Wiley, New York, 1973.
[39] G.D. Purvis III, R.J. Bartlett, J. Chem. Phys. 76 (1982) 1910.
[40] W.D. Laidig, G.D. Purvis III, R.J. Bartlett, J. Chem. Phys. 89 (1985) 2161.
[41] M. Rittby, R.J. Bartlett, J. Phys. Chem. 92 (1988) 3033.
[42] J. Noga, R.J. Bartlett, J. Chem. Phys. 86 (1987) 7041.
[43] J. Noga, R.J. Bartlett, J. Chem. Phys. 89 (1988) 3041.
[44] C. Sosa, J. Noga, R.J. Bartlett, J. Chem. Phys. 88 (1988) 5947.
[45] J.D. Watts, J. Noga, R.J. Bartlett, J. Chem. Phys. 93 (1990) 6104.
[46] G. Scuseria, H.F. Schaefer III, Chem. Phys. Lett. 152 (1988) 382.
[47] K. Ragavachari, G.W. Trucks, J.A. Pople, M. Head-Gordon, Chem. Phys. Lett. 157 (1989) 479.
[48] R.J. Bartlett, J.D. Watts, S.A. Kucharski, J. Noga, Chem. Phys. Lett. 165 (1990) 513.
[49] M. Urban, J. Noga, S.J. Cole, R.J. Bartlett, J. Chem. Phys. 83 (1985) 4041.
[50] Y.S. Lee, S.A. Kucharski, R.J. Bartlett, J. Chem. Phys. 81 (1984) 5906.
[51] S.A. Kucharski, R.J. Bartlett, J. Chem. Phys. 97 (1992) 4282.
[52] R.J. Bartlett, J.F. Stanton, in: K.B. Lipkowitz, D.B. Boyd (Eds.), Reviews in Computational Chemistry, VCH, New York, 1994.
[53] P. Piecuch, K. Kowalski, in: J. Lesczynski (Ed.), Computational Chemistry: Review of Current Trends, World Scientific, Singapore, 2000.
[54] R.J. Bartlett, J. Phys. Chem. 93 (1989) 1697.
[55] S.A. Kucharski, M. Wloch, M. Musial, R.J. Bartlett, J. Phys. Chem. 115 (2001) 8263.
[56] C. Möller, M.S. Plesset, Phys. Rev. 46 (1934) 618.
[57] E. Schödinger, Ann. Phys. 80 (1926) 437.
[58] R.J. Jastrow, Phys. Rev. 95 (1955) 1479.
[59] C.M. Umrigar, M.P. Nightingale, K.J. Runge, J. Chem. Phys. 99 (1993) 2865.
[60] H. Eckstein, W. Schattke, Physica A 216 (1995) 151.
[61] H. Eckstein, W. Schattke, M. Reigrotzki, R. Redmer, Phys. Rev. B 54 (1996) 5512.
[62] S. Fahy, in: M.P. Nightingale, C.J. Umrigar (Eds.), Quantum Monte Carlo Methods in Chemistry and Physics, Vol. 525 of NATO Advanced-Institute of Series C: Mathematical and Physical Sciences, Kluwer Academic, Dordrecth, 1999, p. 101.
[63] C. Filippi, S. Fahy, J. Chem. Phys. 112 (2000) 3523.
[64] J.C. Grossman, L. Mitas, Phys. Rev. Lett. 74 (1995) 1323.
[65] J.C. Grossman, L. Mitas, Phys. Rev. Lett. 79 (1997) 4353.
[66] P.R.C. Kent, R.Q. Hood, M.D. Towler, R.J. Needs, G. Rajagopal, Phys. Rev. B 57 (1998) 15293.
[67] Y. Kwon, D.M. Ceperley, R.M. Martin, Phys. Rev. B 58 (1998) 6800.
[68] Y. Kwon, D.M. Ceperley, R.M. Martin, Phys. Rev. B 48 (1993) 12037.
[69] Y. Kwon, D.M. Ceperley, R.M. Martin, Phys. Rev. B 50 (1994) 1684.
[70] Y. Kwon, D.M. Ceperley, R.M. Martin, Phys. Rev. B 53 (1996) 7376.
[71] H.J. Flad, M. Caffarel, A. Savin, in: W.A. Lester Jr. (Ed.), Recent Advances in Computational Chemistry, vol. 2, World Scientific, Singapore, 1997, p. 73.
[72] D.M. Ceperley, J. Stat. Phys. 43 (1996) 815.

[73] J.B. Anderson, J. Chem. Phys. 63 (1975) 1499.
[74] D.M. Ceperley, B.J. Alder, Phys. Rev. Lett. 45 (1980) 566.
[75] W.M.C. Foulkes, L. Mitas, R.J. Needs, G. Rajagopal, Rev. Mod. Phys. 73 (2001) 33.
[76] P.J. Reynolds, D.M. Ceperley, B.J. Alder, W.A. Lester Jr., J. Chem. Phys. 77 (1982) 5593.
[77] J.B. Anderson, J. Chem. Phys. 65 (1976) 4121.
[78] J.W. Moskowitz, K.E. Schmidt, M.A. Lee, M.H. Kalos, J. Chem. Phys. 77 (1982) 349.
[79] R.C. Grimm, R.G. Storer, J. Comput. Phys. 7 (1971) 134.
[80] D.M. Ceperley, M.H. Kalos, Monte Carlo Methods in Statistical Physics, second ed., Springer, Berlin, 1979, p. 145.
[81] D.M. Ceperley, J. Stat. Phys. 43 (1986) 815.
[82] B.L. Hammond, W.A. Lester Jr., P.J. Reynolds, Monte Carlo Methods in Ab Initio Quantum Chemistry, World Scientific, Singapore, 1994.
[83] L. Mitas, E.L. Shirley, D.M. Ceperley, J. Chem. Phys. 95 (1991) 3467.
[84] Y. Lee, P.R.C. Kent, M.D. Towler, R.J. Needs, G. Rajagopal, Phys. Rev. B 62 (2000) 13347.
[85] C.W. Greeff, W.A. Lester Jr., J. Chem. Phys. 109 (1998) 1607.
[86] L.H. Thomas, Proc. Camb. Phil. Soc. 23 (1926) 542.
[87] E. Fermi, Zeits. für. Phys 48 (1928) 73.
[88] M. Alcamí, O. Mó, M. Yáñez, Mass Sprectrom. Rev. 20 (2001) 195.
[89] W. Kohn, L. Sham, Phys. Rev. A 140 (1965) 1133.
[90] R.G. Parr, W. Yang, Density Functional Theory of Atoms and Molecules, Oxford University Press, New York, 1989.
[91] E.S. Kryachko, E.V. Ludeña, Energy Density Functional Theory of Atoms and Molecules, Kluwer Academic Publishres, Dordrecht, The Netherlands, 1990.
[92] P.M.W. Gill, B.G. Johnson, J.A. Pople, Chem. Phys. Lett. 197 (1992) 499.
[93] B.G. Johnson, P.M.W. Gill, J.A. Pople, J. Chem. Phys. 98 (1993) 5612.
[94] M.N. Glukhovtsev, R.D. Nach, C.J. Nagel, J. Phys. Chem. 101 (1997) 316.
[95] C.D. Sherrill, M. Lee, M. Head-Gordon, Chem. Phys. Lett. 302 (1999) 435.
[96] M. Alcamí, A.I. Gonzalez, O. Mó, M. Yáñez, Chem. Phys. Lett. 307 (1999) 244.
[97] C.J. Barden, J.C. Rienstra-Kiracofe, H.F. Schaefer III, J. Chem. Phys. 113 (2000) 690.
[98] T. Nakajima, T. Tsuneda, H. Nakano, H. Hirao, J. Theor. Comp. Chem. 1 (2002) 109.
[99] Q.S. Zhao, R.C. Morrison, R.G. Parr, Phys. Rev. A 50 (1994) 2138.
[100] P.R.T. Schipper, O.V. Gritsenko, E.J. Baerends, Phys. Rev. A 57 (1998) 1729.
[101] D.J. Tozer, N.C. Handy, Mol. Phys. 101 (2003) 17.
[102] D. Cremer, Mol. Phys. 99 (2001) 1899.
[103] P.O. Löwdin, Adv. Chem. Phys. 2 (1959) 207.
[104] P. Hohenberg, W. Kohn, Phys. Rev. B 136 (1964) 864.
[105] E.J. Baerends, O.V. Gritsenko, J. Phys. Chem. A 101 (1997) 5383.
[106] R. Stowasser, R. Hoffmann, J. Am. Chem. Soc. 121 (1999) 3414.
[107] V. Polo, E. Kraka, D. Cremer, Mol. Phys. 100 (2002) 1771.
[108] J.P. Perdew, A. Zunger, Phys. Rev. B 23 (1981) 5048.
[109] J. Garza, J.A. Nichols, D.A. Dixon, J. Phys. Chem. 112 (2000) 7880.
[110] E. Zaremba, W. Kohn, J. Phys. Rev. B 13 (1976) 2270.
[111] K. Rapcewicz, N.W. Ashcroft, Phys. Rev. B 44 (1991) 4032.
[112] J.M. Pérez-Jordá, A.D. Becke, Chem. Phys. Lett. 233 (1995) 134.
[113] S.J.A. Gisbergen, J.G. Snijders, E.J. Baerends, J. Phys. Chem. 103 (1995) 9347.
[114] Y. Andersson, D.C. Langreth, B.I. Lundqvist, Phys. Rev. Lett. 76 (1996) 102.
[115] J.F. Dobson, B.P. Dinte, Phys. Rev. Lett. 76 (1996) 1780.
[116] W. Kohn, Y. Meir, D.E. Makarov, Phys. Rev. Lett. 80 (1998) 4153.
[117] J.F. Dobson, J. Wang, Phys. Rev. Lett. 82 (1999) 2123.
[118] E. Engel, A. Höck, R.M. Dreizler, Phys. Rev. A 61 (2000) 032502.
[119] H. Iikura, T. Tsuneda, K. Hirao, J. Chem. Phys. 115 (2001) 3540.
[120] T. Leininger, H. Stöll, A. Savin, Chem. Phys. Lett. 275 (1997) 151.
[121] R.D. Adamson, J.P. Dombroski, P.M.W. Gill, J. Comput. Chem. 20 (1999) 921.
[122] P.Y. Ayala, G.E. Scuseria, J. Chem. Phys. 110 (1999) 3660.
[123] G.E. Scuseria, P.Y. Ayala, J. Chem. Phys. 111 (1999) 8330.
[124] J.P.W. McDouall, Mol. Phys. 101 (2003) 361.
[125] E. Valderrama, J.M. Mercero, J.M. Ugalde, J. Phys. B 34 (2001) 275.
[126] G.C. Lie, E. Clementi, J. Chem. Phys. 60 (1974) 1275.
[127] G.C. Lie, E. Clementi, J. Chem. Phys. 60 (1974) 1288.
[128] A.J. Cohen, T. Tantirungrotechai, Chem. Phys. Lett. 299 (1999) 465.
[129] A.J. Cohen, N.C. Handy, Chem. Phys. Lett. 316 (2000) 160.
[130] R.F.W. Bader, Atoms in Molecules. A Quantum Theory, Clarendon Press, Oxford, UK, 1990.
[131] T. Kato, Commun. Pure Appl. Math. 10 (1957) 151.
[132] E. Steiner, J. Chem. Phys. 39 (1963) 2365.
[133] V.H. Smith Jr., Chem. Phys. Lett. 9 (1971) 365.
[134] I. Silanes, J.M. Ugalde, R.J. Boyd, J. Mol. Struct. (Theochem) 527 (2000) 27.
[135] N.D. Mermin, Phys. Rev. A 137 (1965) 1441.
[136] A.K. Rajagopal, J. Callaway, Phys. Rev. B 7 (19731912).
[137] M. Levy, Proc. Natl. Acad. Sci. U.S.A. 76 (1979) 6062.
[138] M. Levy, Phys. Rev. A 26 (1982) 1200.
[139] R.G. Parr, Ann. Rev. Phys. Chem. 34 (1983) 631.
[140] R.G. Parr, M.L.R.A. Donnely, W.E. Palke, J. Chem. Phys. 68 (1978) 3801.
[141] R.G. Parr, R.G. Pearson, J. Am. Chem. Soc. 105 (1983) 7512.
[142] R.G. Parr, W. Yang, J. Am. Chem. Soc. 106 (1984) 4049.
[143] R.G. Parr, W. Yang, Ann. Rev. Phys. Chem. 46 (1995) 701.
[144] G. Klopman, in: G. Klopman (Ed.), Chemical Reactivity and Reaction Paths, John Wiley & Sons, New York, 1974, Chapter 5.
[145] R.G. Pearson, J. Am. Chem. Soc. 107 (1985) 6901.
[146] R.G. Parr, Z. Zhou, Acc. Chem. Res. 26 (1993) 252.
[147] K. Fukui, Science 218 (1982) 747.
[148] K.D. Sen, C.R. Cannon (Eds.), Reviews of Modern Quantum Chemistry. A Celebration of the Contributions of Robert G. Parr, vol. 2, World Scientific, Singapore, 2002.
[149] R. Vargas, A. Cedillo, J. Garza, M. Galvan, in: K.D. Sen, G. Dalmas (Eds.), Reviews of Modern Quantum Chemistry. A Celebration of the Contributions of Robert G. Parr, World Scientific, Singapore, 2002, p. 936.
[150] M.H. Cohen, M.V. Ganduglia-Pirovano, J. Kudrnosvky, J. Chem. Phys. 101 (1994) 8988.
[151] M.H. Cohen, M.V. Ganduglia-Pirovano, J. Kudrnosvky, J. Chem. Phys. 103 (1995) 3543.
[152] B.G. Baekelandt, J. Chem. Phys. 105 (1996) 4664.
[153] T.L. Gilbert, Phys. Rev. B 12 (1975) 2111.
[154] A.K. Rajagopal, Adv. Chem. Phys. 41 (1980) 59.
[155] J.F. Janak, Phys. Rev. B 18 (1978) 7165.
[156] M. Harris, P. Ballone, Chem. Phys. Lett. 303 (1999) 420.
[157] S.B. Trickey, Phys. Rev. Lett. 56 (1986) 881.
[158] P.H. Acioli, J. Jellinek, Phys. Rev. Lett. 89 (2002) 213402.
[159] J. Jellinek, P.H. Acioli, J. Phys. Chem. A 106 (2002) 10919.
[160] J. Jellinek, P.H. Acioli, J. Phys. Chem. A 107 (2003) 1670.
[161] J. Jellinek, P.H. Acioli, J. Chem. Phys. 118 (2003) 7783.
[162] J. Jellinek, P.H. Acioli, in: N. Russo, D.R. Salahub, M. Witko (Eds.), NATO-ASI Series in Metal–Ligand Interaction in Molecular-, Nano-, Micro, and Macro-systems in Complex Environments, Kluwer, New York, USA, 2003, p. 121.
[163] R. McWeeny, Rev. Mod. Phys. 32 (1960) 335.
[164] J. Harris, R.O. Jones, J. Phys. F. 4 (1974) 1170.
[165] D.C. Langreth, J.P. Perdew, Solid State Commun. 17 (1975) 1425.
[166] D.C. Langreth, J.P. Perdew, Phys. Rev. B 15 (1977) 2884.

[167] D.C. Langreth, J.P. Perdew, Phys. Rev. Lett. 76 (1996) 3186.
[168] J.M. Mercero, E. Valderrama, J.M. Ugalde, in: N. Russo, D.R. Salahub, M. Witko (Eds.), NATO-ASI Series in Metal–Ligand Interaction in Molecular-, Nano-, Micro, and Macro-systems in Complex Environments, Kluwer, New York, USA, 2003, p. 205.
[169] O. Gunnarsson, B.I. Lundqvist, Phys. Rev. B 13 (1976) 4274.
[170] N.T. Maitra, K. Burke, in: J. Cioslowski (Ed.), Many-Electron Densities and Reduced Density Matrices, Kluwer Academic/Plenum Publishers, New York, 2000, p. 183.
[171] R.A. Bonham, M. Fink, High Energy Electron Scattering, Van Nostrand-Reinhold, New York, 1974.
[172] W. Schülke, in: G. Brown, D.E. Moncton (Eds.), Handbook of Synchroton Radiation, vol. 3, Elsevier Science Publishers, Amsterdam, The Netherlands, 1991, p. 565.
[173] J.P. Perdew, A. Savin, K. Burke, Phys. Rev. A 51 (1995) 4531.
[174] J.P. Perdew, M. Ernzerhof, K. Burke, A. Savin, Int. J. Quantum Chem. 61 (1997) 197.
[175] A.J. Thakkar, V.H. Smith Jr., J. Phys. B 11 (1978) 3803.
[176] A.J. Thakkar, A.N. Tripathi, V.H. Smith Jr., Phys. Rev. A 29 (1984) 1108.
[177] J.M. Ugalde, C. Sarasola, Phys. Rev. A 49 (1994) 3081.
[178] E. Valderrama, X. Fradera, J.M. Ugalde, Phys. Rev. A 64 (2001) 044501.
[179] E. Valderrama, X. Fradera, I. Silanes, J.M. Ugalde, R.J. Boyd, in: K.D. Sen (Ed.), Reviews of Modern Quantum Chemistry. A Celebration of the Contributions of Robert G. Parr, World Scientific, Singapore, 2002, p. 577.
[180] A.S. Hyman, S.I. Yaniger, J.F. Liebman, Int. J. Quantum Chem. 14 (1978) 757.
[181] N. Watanabe, S. Ten-no, S. Iwata, Y. Udagawa, in: K.D. Sen (Ed.), Reviews of Modern Quantum Chemistry. A Celebration of the Contributions of Robert G. Parr, World Scientific, Singapore, 2002, p. 553.
[182] K. Burke, J.P. Perdew, M. Ernzerhof, J. Phys. Chem. 109 (1998) 3760.
[183] J.C. Slater, Phys. Rev. 81 (1951) 385.
[184] S.H. Vosko, L. Wilk, M. Nusair, Can. J. Phys. 58 (1980) 1200.
[185] J.P. Dahl, J. Avery, Local Denisty Approximations in Quantum Chemistry and Solid State Physics, Plenum Press, New York, 1984.
[186] M. Levy, J.P. Perdew, Phys. Rev. A 32 (1985) 2010.
[187] J.P. Perdew, R.G. Parr, M. Levy, J.L. Balduz, Phys. Rev. Lett. 49 (1982) 1691.
[188] T. Bally, G.N. Sastry, J. Phys. Chem. A 101 (1997) 7923.
[189] M. Rasolt, H.L. Davis, Phys. Lett. A 86 (1981) 45.
[190] M. Rasolt, D.J.W. Geldart, Phys. Rev. B 34 (1986) 1325.
[191] F. Herman, J.P. van Dyke, I.B. Ortenburger, Phys. Rev. Lett. 22 (1969) 807.
[192] L.J. Sham, in: P.M. Marcus, J.F. Janak, A.R. Williams (Eds.), Computational Methods in Band Theory, Plenum Press, New York, 1971, p. 458.
[193] A.D. Becke, Int. J. Quantum Chem. 23 (1983) 1915.
[194] K. Schwartz, F. Herman, J. Phys. (France) 33 (1972) C3-C277.
[195] K. Schwartz, Chem. Phys. 7 (1975) 94.
[196] S.K. Ma, K.A. Brueckner, Phys. Rev. 165 (1968) 18.
[197] J.P. Perdew, Phys. Rev. B 33 (1986) 8822.
[198] J.P. Perdew, W. Yang, Phys. Rev. B 33 (1986) 8800.
[199] A.D. Becke, J. Chem. Phys. 84 (1986) 4524.
[200] A.D. Becke, Phys. Rev. A 38 (1988) 3098.
[201] Y. Tal, Phys. Rev. A 18 (1978) 1781.
[202] E. Clementi, C. Roetti, At. Data Nucl. Data Tables 14 (1974) 174.
[203] C. Lee, W. Yang, R.G. Parr, Phys. Rev. B 37 (1988) 785.
[204] R. Colle, O. Salvetti, Theor. Chim. Acta 37 (1975) 4135.
[205] M. Brack, B.K. Jennings, Y.H. Chu, Phys. Lett. B 65 (1976) 1.
[206] B. Grammaticos, A. Voros, Ann. Phys. 123 (1979) 359.
[207] D.C. Langreth, M.J. Mehl, Phys. Rev. B 28 (1983) 1809.
[208] J.P. Perdew, in: P. Ziesche, H. Eschrig (Eds.), Electronic Structure of Solids '91, Akademie Verlag, Berlin, 1991, p. 11.
[209] J.P. Perdew, K. Burke, W. Yang, Phys. Rev. B 54 (1996) 16533.
[210] J.P. Perdew, K. Burke, W. Yang, Phys. Rev. B 57 (1998) 14999.
[211] E.H. Lieb, S. Oxford, Int. J. Quantum Chem. 24 (1981) 243.
[212] S. Kurth, J.P. Perdew, P. Blaha, Int. J. Quantum Chem. 75 (1999) 889.
[213] J.D. Talman, W.F. Shadwick, Phys. Rev. A 14 (1976) 36.
[214] E. Engel, R.M. Dreizler, J. Comput. Chem. 20 (1999) 31.
[215] T. Grabo, T. Kreibich, S. Kurth, E. Gross, in: V.I. Anisimov (Ed.), Strong Coulomb Correlations in Electronic Structure Calculations: Beyond the Local Density Approximation, Gordon and Breach, New York, 1999, p. 203.
[216] S. Kiimmel, J.P. Perdew, Phys. Rev. Lett. 90 (2003) 043004.
[217] A.D. Becke, J. Chem. Phys. 98 (1993) 1372.
[218] A.D. Becke, J. Chem. Phys. 98 (1993) 5648.
[219] P.J. Stephens, F.J. Devlin, C.F. Chabalowski, M.J. Frisch, J. Phys. Chem. 98 (1994) 11623.
[220] M.J. Frisch, G.W. Trucks, H.B. Schlegel, P.M.W. Gill, B.G. Johnson, M.W. Wong, J.B. Foresman, M.A. Robb, M. Head-Gordon, E.S. Replogle, R. Gomperts, J.L. Andres, K. Raghavachari, J.S. Binkley, C. Gon-zales, R.L. Martin, D.J. Fox, D.L. Defrees, J. Baker, J.J.P. Stewart, J.A. Pople, Gaussian 92, Gaussian, Inc., Pittsburgh, PA, 1993.
[221] W. Klopper, K. Bak, P. Jørgensen, J. Olsen, T. Helgaker, J. Phys. B 32 (1999) R103.
[222] M.J. Frisch, G.W. Trucks, H.B. Schlegel, G.E. Scuseria, M.A. Robb, J.R. Cheeseman, J.A. Montgomery Jr., T. Vreven, K.N. Kudin, J.C. Burant, J.M. Millam, S.S. Iyengar, J. Tomasi, V. Barone, B. Mennucci, M. Cossi, G. Scalmani, N. Rega, G.A. Petersson, H. Nakatsuji, M. Hada, M. Ehara, K. Toyota, R. Fukuda, J. Hasegawa, M. Ishida, T. Naka-jima, Y. Honda, O. Kitao, H. Nakai, M. Klene, X. Li, J.E. Knox, H.P. Hratchian, J.B. Cross, C. Adamo, J. Jaramillo, R. Gomperts, R.E. Stratmann, O. Yazyev, A.J. Austin, R. Cammi, C. Pomelli, J.W. Ochterski, P.Y. Ayala, K. Morokuma, G.A. Voth, P. Salvador, J.J. Dannenberg, V.G. Zakrzewski, S. Dapprich, A.D. Daniels, M.C. Strain, O. Farkas, D.K. Malick, A.D. Rabuck, K. Raghavachari, J.B. Foresman, J.V. Ortiz, Q. Cui, A.G. Baboul, S. Clifford, J. Cioslowski, B.B. Stefanov, G. Liu, A. Liashenko, P. Piskorz, I. Komaromi, R.L. Martin, D.J. Fox, T. Keith, M.A. Al-Laham, C.Y. Peng, A. Nanayakkara, M. Challacombe, P.M.W. Gill, B. Johnson, W. Chen, M.W. Wong, C. Gonzalez, J.A. Pople, Gaussian 03, Revison A.1, Gaussian, Inc., Pittsburgh, PA, USA, 2003.
[223] J. Kong, C.A. White, A.I. Krylov, D. Sherrill, R.D. Adamson, T.R. Furlani, M.S. Lee, A.M. Lee, S.R. Gwaltney, T.R. Adams, C. Ochsenfeld, A.T.B. Gilbert, G.S. Kedziora, V.A. Rassolov, D.R. Maurice, N. Nair, Y. Shao, N.A. Besley, P.E. Maslen, J.P. Dombroski, H. Daschel, W. Zhang, P.P. Korambath, J. Baker, E.F.C. Byrd, T. Van Voorhis, M. Oumi, S. Hirata, C.-P. Hsu, N. Ishikawa, J. Florian, A. Warshel, B.G. Johnson, P.M.W. Gill, M. Head-Gordon, J.A. Pople, Q-chem 2.0: a high-performance ab initio electronic structure program package, J. Comput. Chem. 21 (16) (2000) 1532.
[224] Gamess-uk is a package of ab initio programs written by M.F. Guest, J.H. van Lenthe, J. Kendrick, K. Schoffel and P. Sherwood with contributions from R.D. Amos, R.J. Buenker, H.J.J. van Dam, M. Dupuis, N.C. Handy, I.H. Hillier, P.J. Knowles, V. Bonacic-Koutecky, W. von Niessen, R.J. Harrison, A.P. Rendell, V.R. Saunders, A.J. Stone, D.J. Tozer and A.H. de Vries. The package is derived from the original GAMESS code due to M. Dupuis and D. Spangler and J. Wendoloski, NRCC Software Catalog, vol. 1, Program no. QG01 (GAMESS), 1980.
[225] M.A.L. Marques, E.K.U. Gross, Annu. Rev. Phys. Chem. 55 (2004) 427.
[226] E. Runge, E.K.U. Gross, Phys. Rev. Lett. 52 (12) (1984) 997.
[227] E.K.U. Gross, W. Kohn, in: S.B. Trickey (Ed.), Advances in Quantum Chemistry, Academic Press, San Diego, 1990, p. 255.

[228] M.A.L. Marques, E.K.U. Gross, in: C. Fiolhais, F. Nogueira, M. Marques (Eds.), A Primer in Density-Functional Theory, vol. 620, Springer, Berlin, 2003, p. 144.
[229] C. Jamorski, M.E. Casida, D.R. Salahub, J. Chem. Phys. 104 (13) (1996) 5134.
[230] M.E. Casida, C. Jamorski, K.C. Casida, D.R. Salahub, J. Chem. Phys. 108 (11) (1998) 4434.
[231] M. Petersilka, U.J. Gossmann, E.K.U. Gross, Phys. Rev. Lett. 76 (1996) 1212.
[232] T. Grabo, M. Petersilka, E.K.U. Gross, J. Mol. Struct. (Theochem) 501/502 (2000) 353.
[233] M. Petersilka, E.K.U. Gross, K. Burke, Int. J. Quantum Chem. 80 (2000) 534.
[234] A. Castro, M.A.L. Marques, J.A. Alonso, G.F. Bertsch, A. Rubio, Eur. J. Phys. D 28 (2004) 211.
[235] L. Salem, C. Rowland, Angew. Chem. Int. Eng. Ed. 11 (1972) 92.
[236] M. Klessinger, J. Michl, Excited States and Photochemistry of Organic Molecules, VCH, New York, 1995.
[237] D.R. Yarkony, Int. Rev. Phys. Chem. 11 (1992) 195.
[238] B.F. Minaev, H. Agren, EPA Newslett. 65 (1999) 7.
[239] D. Schröder, S. Shaik, H. Schwarz, Acc. Chem. Res. 33 (2000) 139.
[240] H. Schwarz, Int. J. Mass Spectrom. 237 (2004) 75.
[241] A.K. Rappe, T.H. Upton, J. Chem. Phys. 85 (1986) 4400.
[242] I. Kretzschmar, D. Schröder, H. Schwarz, C. Rue, P.B. Armentrout, J. Phys. Chem. A 102 (1998) 10060.
[243] C. Rue, P.B. Armentrout, I. Kretzschmar, D. Schröder, J.N. Harvey, H. Schwarz, J. Chem. Phys. 110 (1999) 7858.
[244] K. Yoshizawa, Y. Shiota, T. Yamabe, Organometallics 17 (1998) 2825.
[245] N. Harris, S. Shaik, D. Schröder, H. Schwarz, Helv. Chim. Acta 82 (1999) 1784.
[246] A. Fiedler, D. Schröder, W. Zummack, H. Schwarz, Inorg. Chim. Acta 259 (1997) 227.
[247] M. Filatov, S. Shaik, J. Phys. Chem. A 102 (1998) 3835.
[248] A. Irigoras, J.E. Fowler, J.M. Ugalde, J. Am. Chem. Soc. 121 (1999) 8549.
[249] M. Aschi, A. Largo, Chem. Phys. 265 (2001) 251.
[250] W.G. Richards, H.P. Trivedi, D.L. Cooper, Spin–orbit Coupling in Molecules, Clarendon Press, Oxford, 1981.
[251] B.A. Hess, C.M. Marian, S.D. Peyerimhoff, in: D.R. Yarkony (Ed.), Modern Electronic Structure Theory, World Scientific, Singapore, 1995.
[252] H.A. Bethe, E.E. Salpeter, Quantum Mechanics of One- and Two-Electron Atoms, Springer, Berlin, 1957.
[253] S.R. Langhoff, C.V. Kern, in: H.F. Schaefer Jr. (Ed.), Modern Theoretical Chemistry, Plenum, New York, 1977.
[254] S. Fraga, K.M.S. Saxena, B.W.N. Lo, At. Data. Nuc. Data Tables 3 (1971) 323.
[255] W.C. Ermler, Y.S. Lee, P.A. Christiansen, K.S. Pitzer, Chem. Phys. Lett. 81 (1981) 70.
[256] B.A. Hess, Phys. Rev. A 33 (1986) 3742.
[257] S.K. Lower, M.A. El-Sayed, Chem. Rev. 66 (1966) 199.
[258] P.W. Abegg, Mol. Phys. 30 (1975) 579.
[259] N. Turro, A. Devaquet, J. Am. Chem. Soc. 97 (1975) 3859.
[260] B.O. Roos, P.R. Taylor, P.E.M. Siegbahn, Chem. Phys. 48 (1980) 157.
[261] T.R. Furlani, H.F. King, J. Chem. Phys. 82 (1985) 5577.
[262] J.O. Jensen, D.R. Yarkony, Chem. Phys. Lett. 141 (1987) 391.
[263] L. Salem, Electrons in Chemical Reactions, Wiley, New York, 1982.
[264] J.C. Lorquet, in: T. Baer, C.Y. Ng, I. Powis (Eds.), The Structure, Energetics and Dynamics of Organic Ions, Wiley, New York, 1996.
[265] W.H. Press, B.P. Flannery, S.A. Teukolsky, W.T. Vetterling, Numerical Recipes, Cambridge University Press, New York, 1987.
[266] D.R. Yarkony, in: D.R. Yarkony (Ed.), Modern Electronic Structure Theory, World Scientific, Singapore, 1995.
[267] M.J. Bearpark, M.A. Robb, H.B. Schlegel, Chem. Phys. Lett. 223 (1994) 269.
[268] A. Faradzel, M. Dupuis, J. Comput. Chem. 12 (1991) 276.
[269] N. Koga, K. Morokuma, Chem. Phys. Lett. 119 (1985) 371.
[270] J.N. Harvey, M. Aschi, H. Schwarz, W. Koch, Theor. Chem. Acc. 99 (1998) 95.
[271] E.E. Nikitin, Adv. Quantum Chem. 5 (1970) 135.
[272] M. Desouter-Lecomte, J.C. Lorquet, J. Chem. Phys. 71 (1979) 4391.
[273] J.B. Delos, W.R. Thorson, Phys. Rev. A 6 (1972) 728.
[274] J.B. Delos, J. Chem. Phys. 59 (1973) 114.
[275] G.J. Kavarnos, N.J. Turro, Chem. Rev. 86 (1986) 401.
[276] R. Poli, J.N. Harvey, Chem. Soc. Rev. 32 (2003) 1.
[277] R. Poli, Acc. Chem. Res. 30 (1997) 495.
[278] A.A. Cole, J.C. Fettinger, D.W. Keogh, R. Poli, Inorg. Chim. Acta 240 (1995) 355.
[279] I. Cacelli, D.V. Keogh, R. Poli, A. Rizzo, J. Phys. Chem. A 101 (1997) 9801.
[280] K.M. Smith, R. Poli, J.N. Harvey, New J. Chem. 24 (2000) 77.
[281] S. Shaik, D. Danovich, A. Fiedler, D. Schröder, H. Schwarz, Helv. Chim. Acta 78 (1995) 1393.
[282] K. Yoshizawa, Y. Shiota, T. Yamabe, J. Chem. Phys. 110 (1999) 7858.
[283] K. Yoshizawa, Y. Shiota, T. Yamabe, J. Am. Chem. Soc. 121 (1999) 147.
[284] D.G. Musaev, K. Morokuma, J. Phys. Chem. 100 (1996) 11600.
[285] J.C. Green, C.N. Jardine, J. Chem. Soc. Dalton Trans. (1998) 1057.
[286] J.C. Green, J.N. Harvey, R. Poli, J. Chem. Soc. Dalton Trans. (2002) 1861.
[287] K.M. Smith, R. Poli, J.N. Harvey, Chem. Eur. J. 7 (2001) 1679.
[288] D.G. Truhlar, B.C. Garret, S.J. Klippenstein, J. Phys. Chem. 100 (1996) 12771.
[289] J. Espinosa-García, F.J. Olivares, J.C. Corchado, Chem. Phys. 183 (1994) 95.
[290] B.D. Wladkowski, K.F. Lim, W.D. Allen, J.I. Brauman, J. Am. Chem. Soc. 114 (1992) 9136.
[291] H. Wang, W.L. Hase, J. Am. Chem. Soc. 119 (1997) 3039.
[292] Z.F. Xu, S.M. Li, Y.X. Yu, Z.S. Li, C.C. Sun, J. Phys. Chem. A 103 (1999) 4910.
[293] J.B. Lipson, T.W. Beiderhase, L.T. Molina, M.J. Molina, M. Olzmann, J. Phys. Chem. A 104 (2000) 7537.
[294] H. Hou, B. Wang, Y. Gu, J. Phys. Chem. A 104 (2000) 320.
[295] J. Espinosa-Garcia, J. Phys. Chem. A 104 (2000) 7537.
[296] J.A. Miller, S.J. Klippenstein, S.H. Robertson, J. Phys. Chem. A 104 (2000) 7525.
[297] P.J. Robinson, K.A. Holbrook, Unimolecular Reactions, Wiley, New York, 1972.
[298] R.G. Gilbert, S.C. Smith, Theory of Unimolecular and Recombination Reactions, Blackwell Scientific, Oxford, 1990.
[299] J.C. Lorquet, B. Leyh-Nihant, J. Phys. Chem. 92 (1988) 4778.
[300] K. Morokuma, Q. Cui, Z. Liu, Faraday Discuss. 110 (1998) 71.
[301] M. Aschi, J.N. Harvey, Phys. Chem. Chem. Phys. 1 (1999) 555.
[302] B. Gimarc, The Qualitative Molecular Orbital Approach, Academic Press, New York, 1979.
[303] K. Jamkowski, N. Nowakowski, J. Wasilewski, Chem. Phys. Lett. 389 (2004), p 393.
[304] T. Kar, J.G. Ángyán, A.B. Shannigrahi, J. Phys. Chem. A 104 (2000) 9953.
[305] L. Hanley, J.L. Whitten, S.L. Anderson, J. Phys. Chem. 92 (1988) 5803.
[306] L. Hanley, S.L. Anderson, J. Chem. Phys. 89 (1988) 2848.
[307] P.A. Hintz, S.A. Ruatta, S.L. Anderson, J. Chem. Phys. 92 (1990) 292.
[308] P.A. Hintz, M.B. Sowa, S.A. Ruatta, S.L. Anderson, J. Chem. Phys. 94 (1991) 6446.

[309] S.A. Ruatta, P.A. Hintz, S.L. Anderson, J. Chem. Phys. 94 (1991) 2833.
[310] R. Kawai, J.H. Weare, Chem. Phys. Lett. 191 (1992) 311.
[311] A.C. Tang, Q.S. Li, C.W. Liu, J. Li, Chem. Phys. Lett. 201 (1993) 465.
[312] H. Kato, K. Yamashita, K. Morokuma, Bull. Chem. Soc. Jpn. 66 (1993) 3358.
[313] I. Boustani, Chem. Phys. Lett. 233 (1995) 273.
[314] A. Ricca, J.C.W. Bauschlicher, Chem. Phys. 208 (1996) 233.
[315] I. Boustani, Surf. Sci. 370 (1997) 355.
[316] X. Hu, F. Gu, Q. Li, Pro. Natl. Sci. 8 (1998) 57.
[317] F.L. Gu, X. Yang, A.-C. Tang, H. Jiao, P.V.R. Schleyer, J. Comput. Chem. 19 (1998) 203.
[318] I. Boustani, Chem. Phys. Lett. 240 (1995) 135.
[319] I. Boustani, A. Quandt, Europhys. Lett. 39 (1997) 527.
[320] I. Boustani, Phys. Rev. B 55 (1997) 1.
[321] I. Boustani, A. Quandt, Comput. Mater. Sci. 11 (1998) 132.
[322] J.E. Fowler, J.M. Ugalde, J. Phys. Chem. A 104 (2000) 397.
[323] J. Aihara, J. Phys. Chem. A 105 (2001) 5486.
[324] J.M. Lehn, Rep. Prog. Phys. 67 (2004) 249.
[325] C.E. Dykstra, J.M. Lisy, in: R.J. Bartlett (Ed.), Comparison of ab initio Quantum Chemistry with Experiment for small Molecules, Reidel, Dordrech, The Netherlands, 1985, p. 245.
[326] S. Scheiner, Hydrogen Bonding. A Theoretical Perspective, Oxford University Press, New York, USA, 1997, p. 124.
[327] A. Halkier, W. Klopper, T. Helgaker, P. Jørgensen, P.R. Taylor, J. Phys. Chem. 111 (1999) 9157.
[328] J.R. Reimers, R.O. Watts, M.L. Klein, Chem. Phys. 64 (1982) 95.
[329] M.J. Fernandéz-Berridi, J.J. Iruin, L. Irusta, J.M. Mercero, J.M. Ugalde, J. Phys. Chem. A 106 (2002) 4187.
[330] R. Langner, G. Zundel, J. Chem. Soc. Faraday Trans. 91 (1995) 3831.
[331] M.W. Wong, Chem. Phys. Lett. 256 (1996) 391.
[332] H. Matsuura, H. Yoshida, M. Hieda, S. Yamanaka, T. Harada, K. Shin-ya, K. Ohno, J. Am. Chem. Soc. 125 (2003) 13910.
[333] J. Oomens, D.T. Moore, G. von Helden, F. Meijer, R.C. Dunbar, J. Am. Chem. Soc. 126 (2004) 724.
[334] C. Adamo, V. Barone, Chem. Phys. Lett. 274 (1997) 242.
[335] C. Adamo, V. Barone, J. Chem. Phys. 108 (1998) 664.
[336] R.C. Dunbar, J. Phys. Chem. A 106 (2002) 7328.
[337] R.C. Dunbar, J. Phys. Chem. A 106 (2002) 9809.
[338] A. Karpfen, J. Phys. Chem. A 104 (2001) 6871.
[339] A. Garcia, J.M. Elorza, J.M. Ugalde, J. Phys. Chem. A 102 (1998) 8974.
[340] A. Garcia, J.M. Elorza, J.M. Ugalde, J. Mol. Struct. (Theochem) 501 (2000) 207.
[341] O.K. Poleshchuk, A.C. Legon, Z. Naturforsch. 57a (2002) 537.
[342] R.A. Aziz, M.J. Slaman, J. Chem. Phys. 72 (1989) 5062.
[343] P.K. Wawrzyniak, J. Panek, Z. Latajkaa, J. Lundell, J. Mol. Struct. 691 (2004) 115.
[344] S. Simon, M. Duran, J. Dannenberg, J. Chem. Phys. 105 (1996) 11024.
[345] J. Ireta, J. Neugebauer, M. Scheffler, J. Phys. Chem. A 108 (2004) 5692.
[346] E.R. Johnson, R.A. Wolkow, G.A. DiLabio, Chem. Phys. Lett. 394 (2004) 334.
[347] Y. Zhao, D.G. Truhlar, J. Phys. Chem. A 108 (2004) 6908.
[348] J.M. Pérez-Jordá, E. San-Fabián, A. Pérez-Jimenéz, J. Phys. Chem. 110 (19991916).
[349] E.J. Meijer, M. Sprik, J. Phys. Chem. 105 (1996) 8684.
[350] S. Tsuzuki, H.P. Lüthi, J. Phys. Chem. 114 (2001) 3949.
[351] M.C. Salazar, J.L. Paz, A.J. Hernandez, C. Man-zanares, E.V. Ludeña, Theor. Chem. Acc. 106 (2001) 218.
[352] X. Wu, M.C. Vargas, S. Nayak, V. Lotrich, G. Scoles, J. Phys. Chem. 115 (2001) 8748.
[353] H. Rydberg, N. Jacobson, P.H. Nad, S. Simak, B.I. Lunqvist, D.C. Langreth, Surf. Sci. 532–535 (2003) 606.
[354] C. Douketis, G. Scoles, S. Marchetti, M. Zen, A.J. Thakkar, J. Phys. Chem. 76 (1982) 3057.
[355] C. Mavroyannis, M.J. Stephen, Mol. Phys. 5 (1962) 629.
[356] U. Zimmerli, M. Parrinello, P. Koumoutsakos, J. Chem. Phys. 120 (2004) 2693.
[357] Q. Wu, W. Yang, J. Chem. Phys. 116 (2002) 515.
[358] A. Bondi, J. Chem. Phys. 68 (1964) 441.
[359] T.A. Halgren, J. Am. Chem. Soc. 114 (1992) 7827.
[360] T.J. Kealy, P.L. Pauson, Nature 168 (1951) 1039.
[361] A. Irigoras, J.M. Mercero, I. Silanes, J.M. Ugalde, J. Am. Chem. Soc. 123 (2001) 5040.
[362] A.W. Haaland, Top. Curr. Chem. 53 (1975) 1.
[363] H.P. Lüthi, J. Ammeter, J. Almlöf, K. Korsell, Chem. Phys. Lett. 69 (1980) 540.
[364] W. Klopper, H.P. Lüthi, Chem. Phys. Lett. 262 (1996) 546.
[365] C. Park, J. Almlöf, J. Chem. Phys. 95 (1991) 1829.
[366] K. Pierloot, B.J. Persson, B.O. Roos, J. Phys. Chem. 99 (1995) 3465.
[367] H. Koch, P. Jørgensen, T. Helgaker, J. Chem. Phys. 104 (1996) 9528.
[368] C. Corliss, J. Sugar, J. Phys. Chem. Ref. Data 11 (1982) 135.
[369] M.J. Mayor-López, J. Weber, Chem. Phys. Lett. 281 (1997) 226.
[370] E.P.L. Hunter, S.G. Lias, J. Phys. Chem. Ref. Data 27 (1998) 413.
[371] M. Mayor-López, H.P. Lüthi, H. Koch, P.Y. Morgatini, J. Weber, J. Chem. Phys. 113 (2000) 8009.
[372] M. Scheibitz, R.F. Winter, M. Bolte, H.-W. Lerner, M. Wagner, Angew. Chem. Int. Ed. 42 (2003) 924.
[373] W. von Niessen, J. Schirmer, L.S. Cederbaum, Comp. Phys. Rep. 1 (1984) 57.
[374] X. Li, A.E. Kuznetsov, H.F. Zhang, A.I. Boldyrev, L.-S. Wang, Science 291 (2001) 859.
[375] D. Schröder, A. Fiedler, M.F. Ryan, H. Schwarz, J. Phys. Chem. 98 (1994) 64.
[376] D.E. Clemmer, Y.-M. Chen, F.A. Khan, P.B. Armentrout, J. Phys. Chem. 98 (1994) 6522.
[377] D. Schröder, H. Schwarz, D.E. Clemmer, Y.-M. Chen, P.B. Armentrout, V.I.B.D. Böhme, Int. J. Mass Spectrom. Ion Processes 161 (1997) 175.
[378] A. Fiedler, D. Schröder, S. Shaik, H. Schwarz, J. Am. Chem. Soc. 116 (1994) 10734.
[379] D. Danovich, S. Shaik, J. Am. Chem. Soc. 119 (1997) 1773.
[380] M. Filatov, S. Shaik, J. Phys. Chem. A 102 (1998) 3835.
[381] A. Irigoras, J.E. Fowler, J.M. Ugalde, J. Am. Chem. Soc. 121 (1999) 8549.
[382] D.M. Ceperley, B.J. Alder, Phys. Rev. Lett. 45 (1980) 566.
[383] W.M.C. Foulkes, L. Mitas, R.J. Needs, G. Rajagopal, Rev. Mod. Phys. 73 (2001) 33.
[384] A.J. Williamson, S.D. Kenny, G. Rajagopal, A.J. James, R.J. Needs, L.M. Fraser, W.M.C. Foulkes, P. Maccullum, Phys. Rev. B 53 (1996) 9640.
[385] M. Dolg, U. Wedig, H. Stoll, H. Preuss, J. Chem. Phys. 86 (1987) 866.
[386] L. Mitas, Phys. Rev. A 49 (1994) 4411.
[387] J.S. Krishnan, J.S. Binkley, P.V.R. Seeger, J.A. Pople, J. Chem. Phys. 72 (1980) 650.
[388] M.M. Hurley, P.A. Christiansen, J. Chem. Phys. 86 (1987) 1069.
[389] B.L. Hammond, P.J. Reynolds, W.A. Lester Jr., J. Chem. Phys. 87 (1987) 1130.
[390] C.J. Umrigar, K.G. Wilson, J.W. Wilkins, Phys. Rev. Lett 60 (1988) 1719.
[391] P.R.C. Kent, R.J. Needs, G. Rajagopal, Phys. Rev. B 59 (1999) 12344.
[392] R.J. Needs, G. Rajagopal, M.D. Towler, P.R.C. Kent, A.J. Williamson, CASINO version 1. 0 User's Manual, University of Cambridge, Cambridge, 2000.

[393] P.R.C. Kent, M.D. Towler, R.J. Needs, G. Rajagopal, Phys. Rev. B 62 (2000) 15394.
[394] I. Ovcharenko, A. Aspuru-Guzik, W.A. Lester Jr., J. Chem. Phys. 114 (2001) 7790.
[395] P.V.R. Schleyer, C. Maerker, A. Dransfeld, H. Jiao, N.J.V.E. Hommes, J. Am. Chem. Soc. 118 (1996) 6317.
[396] P.V.R. Schleyer, H. Jiao, N.J.V.E. Hommes, V.G. Malking, O.L. Malkina, J. Am. Chem. Soc. 119 (1997) 12669.
[397] C.F. Guerra, J.G. Snijders, G. te Velde, E.J. Baerends, Theor. Chem. Acc. 99 (1998) 391.
[398] F. Liu, M.R. Press, S.N. Khanna, P. Jena, Phys. Rev. Lett. 59 (1987) 2562.
[399] R. Pis, J.A. Alonso, Chem. Phys. Lett. 332 (2000) 481.
[400] R. Pis, J.A. Alonso, J.M. Matxain, J.M. Ugalde, Chem. Phys. Lett. 372 (2003) 82.
[401] A. Sanderud, E. Sagstuen, J. Phys. Chem. 100 (1996) 9545.
[402] S.D. Wetmore, L.A. Eriksson, R.J. Boyd, in: L.A. Eriksson (Ed.), Theoretical Biochemistry—Processes and Properties of Biological Systems, vol. 9, Elsevier, Amsterdam, 2001.
[403] F. Ban, J.W. Gauld, S.D. Wetmore, R.J. Boyd, in: A. Lund, M. Shoitani (Eds.), EPR of Free Radicals in Solids—Trends in Methods and Applications, vol. 10A, Kluwer Academic, Dordrecht, 2003.
[404] B. Engels, L.A. Eriksson, S. Lunell, Adv. Quantum Chem. 27 (1996) 297.
[405] J. Lipfert, J. Llano, L.A. Eriksson, J. Phys. Chem. B 108 (2004) 8036.
[406] T. Brabec, F. Krausz, Rev. Mod. Phys. 72 (2000) 545.
[407] M. Drescher, M. Hentschel, R. Kienberger, G. Tempea, C. Spielmann, G.A. Reider, P.B. Corkum, F. Krausz, Science 291 (20011923).
[408] M. Hentschel, R. Kienberger, C. Spielmann, G.A. Reider, N. Milosevic, T. Brabec, P. Corkum, M.D.U. Heinzmann, F. Krausz, Nature 414 (2001) 509.
[409] L.N. Glandorf, M. Scheer, M. Krishnamurthy, J.W. Odom, S.R. Leone, Phys. Rev. A 62 (2000) 023812.
[410] L.N. Glandorf, M. Scheer, D.A. Samuels, A.M. Mulhisen, E.R. Grant, X. Yang, V.M. Bierbaum, S.R. Leone, Phys. Rev. Lett 87 (2001) 193002.
[411] Z. Chang, A. Rundquist, H. Wang, M.M. Murnane, H.C. Kapteyn, Phys. Rev. Lett. 79 (1997) 2967.
[412] C. Spielmann, N.H. Burnett, S. Sartania, R. Koppitsch, M. Schnurer, C. Kan, M. Lenzner, P. Wobrauschek, F. Krausz, Science 278 (1997) 661.
[413] M. Probst, R. Haight, Appl. Phys. Lett. 71 (1997) 202.
[414] R. Huber, F. Tauser, A. Brodschelm, M. Bichler, G. Ab-streiter, A. Leitenstorfer, Nature 414 (2001) 286.
[415] C.M. Dion, S. Chelkowski, A.D. Bandrauk, H. Humeda, Y. Fujimura, J. Chem. Phys. 105 (1996) 9083.
[416] R.W. Shoenlein, L.A. Peteanu, R.A. Mathies, C.V. Shank, Science 254 (1991) 412.
[417] A. Assion, T. Baumert, U. Weichmann, G. Gerber, Phys. Rev. Lett. 86 (2001) 5695.
[418] K. Yamanouchi, Science 295 (2002) 1659.
[419] E.K.U. Gross, F.J. Dobson, M. Petersilka, Density Functional Theory, Springer, New York, 1996.
[420] G. Onida, L. Reining, A. Rubio, Rev. Mod. Phys. 74 (2002) 601.
[421] M.A.L. Marques, A. Castro, A. Rubio, J. Chem. Phys. 115 (2001) 3006.
[422] A. Castro, M.A.L. Marques, J.A. Alonso, G. Bertsch, A. Rubio, Eur. Phys. J. 28 (2004) 211.
[423] H. Haberland, A. Holfmann, B.V. Issendorff, J. Chem. Phys. 103 (1995) 3450.
[424] K.F. Sullivan, S.A. Key, Green Fluorescent Proteins, Academic Press, San Diego, 1999.
[425] T.M.H. Creemers, A.J. Lock, V. Subramaniam, T.M. Jovin, S. Völker, Nat. Struct. Biol. 6 (1999) 557.
[426] T.M.H. Creemers, A.J. Lock, V. Subramaniam, T.M. Jovin, S. Völker, Proc. Natl. Acad. Sci. U.S.A. 97 (2000) 2974.
[427] S.B. Nielsen, A. Lapierre, J.U. Andersen, U.V. Ped-ersen, S. Tomita, L.H. Andersen, Phys. Rev. Lett. 87 (2001) 228102.
[428] M.A.L. Marques, X. López, D. Varsano, A. Castro, A. Rubio, Phys. Rev. Lett. 90 (2003) 258101.
[429] E.K.U. Gross, W. Kohn, Phys. Rev. Lett. 55 (1985) 2850.
[430] E.K.U. Gross, W. Kohn, Phys. Rev. Lett. 57 (1986) 923(E).
[431] M.J. Field, P.A. Bash, M. Karplus, J. Comput. Chem. 111 (1990) 700.
[432] H.Y. Yoo, J.A. Boatz, V. Helms, J.A. McCammon, P.W. Langhoff, J. Phys. Chem. B 105 (2001) 2850.
[433] V. Tozzini, R. Nifosi, J. Phys. Chem. B 105 (2001) 5797.
[434] M.R. Manaa, D.R. Yarkony, J. Chem. Phys. 95 (1991) 1808.
[435] J.M.L. Martin, P.R. Taylor, Chem. Phys. Lett. 209 (1993) 143.
[436] S.P. Walch, Chem. Phys. Lett. 208 (1993) 214.
[437] T. Seideman, S.P. Walch, J. Chem. Phys. 101 (1994) 3656.
[438] Q. Cui, K. Morokuma, Theor. Chem. Acc. 102 (1999) 127.
[439] Q. Cui, K. Morokuma, J.M. Bowman, S.J. Klippen-stein, J. Chem. Phys. 110 (1999) 9469.
[440] A.S. Rodgers, G.P. Smith, Chem. Phys. Lett. 253 (1996) 313.
[441] V.G. Anicich, W.T. Huntress, Astrophys. J. 62 (1986) 553.
[442] D. Smith, N.G. Adams, K. Giles, E. Herbst, Astron. Astrophys. 200 (1988) 191.
[443] P. Zakouril, J. Glosik, V. Skalsky, W. Lindinger, J. Phys. Chem. 99 (1995) 15890.
[444] C. Barrientos, P. Redondo, A. Largo, Chem. Phys. Lett. 306 (1999) 168.
[445] T.A. Seder, J. Ouderkirk, E. Weitz, J. Chem. Phys. 85 (1986) 197.
[446] R.J. Ryther, E. Weitz, J. Phys. Chem. 95 (1991) 9841.
[447] J.N. Harvey, M. Aschi, Faraday Discuss. 124 (2003) 129.